Solidification Processing, Thermo-Mechanical Treatment and Structure - Property Correlation of an Al-Zn-Mg-TiO$_2$ Particulate Composite

A thesis submitted for the award of the degree of

Doctor of Philosophy
in Engineering & Technology
of the University of Kerala

By

P. K. Balasubramanian

Under the supervision and guidance of

Prof. P. K. Rohatgi	Dr. K. G. Sathyanarayana & Dr. B. C. Pai
University of Wisconsin-Milwaukee	Regional Research Laboratory
USA	Thiruvananthapuram

Faculty of Engineering & Technology
University of Kerala
Thiruvananthapuram

DEDICATION

This thesis is dedicated to

i) my beloved niece Miss Latha K Meenakshi who was the real spirit behind my work and who passed away on Sept. 28, 1990 &

ii) my eldest brother Sri K . K . Rama Iyer who brought me up during my school years but passed away on July 1, 1991.
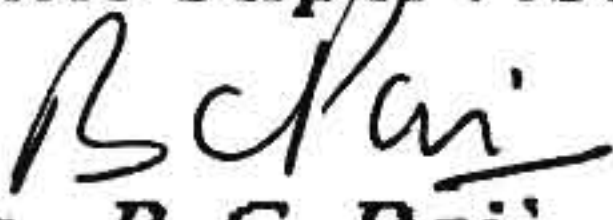
CERTIFICATE

We certify that:

(i) Sri P.K.Balasubramanian who is working as a research student under our guidance has completed the minimum period of research work as per rules and that he is eligible to submit his thesis for the PhD degree under the faculty of Engineering and Technology.

(ii) The candidate is submitting his thesis for the first time.

(iii) The thesis of the candidate is a record of bonafide research carried out by him.

signatures of the supervising teachers

Place: Trivandrum   i)   Dr. B. C. Pai
Date. Dec 27, 1991

Place: ii) Dr. K. G. Sathyanarayana
Date.

Place: Milwaukee, WI   iii) Dr. P. K. Rohatgi
Date. Oct 14, 1991

ACKNOWLEDGEMENTS

ACKNOWLEDGEMENTS

mention here, for their patience and support in completing this work.

The investigator gratefully thank Director, VSSC for his kind permission to carry out the work and submit the thesis.

DECLARATION

I P.K. Balasubramanian hereby declare that no part of this thesis has previously formed the basis for the award to me of any Degree, Diploma, Associateship, Fellowship or any other similar titles of any University or Society.

Vikram Sarabhai Space Centre
Thiruvananthapuram 695 022
Dated : 31st December 1991.

P.K.Balasubramanian
Special Materials Division

ABSTRACT

ABSTRACT

Metal-Matrix Composites (MMCs) have been investigated since the early 1960s, with the main emphasis then being the high potential structural properties engineered to specific applications. Both the fibre and particulate reinforced MMCs exhibited substantial improvements in stiffness and strength over the un-reinforced alloys. However, due to high cost of fibres coupled with the complication of dispersing them in the alloy, attention has been diverted to more cost effective reinforcements and near net shape technology. This has resulted in the development of MMCs with inexpensive particulates as the effective dispersoids. Furthermore, these MMCs have demonstrated isotropic properties and hence significant improvements in performance. However, scant attention has been paid in the literature to the methodology and process parameters related to the optimum use of the available techniques, in the synthesis and characterisation of ceramic and particulate reinforced wrought Al-Zn-Mg alloys.

The present research involves a study of :

1. Synthesis of wrought Al-Zn-Mg-TiO_2 particulate composite with special emphasis on wettability, casting routes and the suitability of incorporation of TiO_2 in wrought aluminium alloy.

2. Various parameters affecting the secondary processing of composites such as forging, extrusion and rolling.

3. Room temperature and elevated temperature mechanical properties and other physical properties.

Both Rheocasting (RC) and Liquid Metallurgy (LM) casting routes were used to synthesise the composites. During synthesis by either process, it was observed that, there was an exothermic reaction between Mg and TiO_2. This exothermic reaction raised the temperature of the melt by 50 K in RC route and 80 K in LM route, keeping the melt temperature sufficiently high for a longer time to facilitate simultaneous addition of other dispersoids as well. Reaction zones were observed around the dispersoids and the thickness of the zones were measured as 3 μm in LM cast billets and 1μm in RC billets. The reaction products were analysed to be rutile grade TiO_2 and Magnesium dititanate ($MgTi_2O_5$).

Application of RC route was found to be better than LM route since RC route resulted in better distribution of the dispersoids with refined and equiaxed cells. The cross section of the RC billet exhibited 85% of the area to be of chill zone with very fine grains and 15% of the area to be of equiaxed grains with no columnar grains in the structure. Whereas, LM billets exhibited 64% chill zone, 27% columnar grains and 9% equiaxed grains. About 94% of the particle agglomerates in RC billets were of size below 50 μm with the average particle size 14.54 μm as against about 64% of the agglomerates in LM cast billets were of size above 50 μm, with average particle size 86.6 μm.

The secondary process involving forging resulted in opening up of the particle clusters and subsequent pull out, ending up with surface cracks. This suggested that the particles are poorly bonded in the matrix. This observation is in good agreement with the reported data on Al / ceramic composites. However, extrusion process appeared to be more promising with practically no defects in the extruded products. The tensile strength of the solid extruded rods in T6 heat treated condition, was upto 300 MPa, comparable to the theoretical prediction of 340 MPa. The percentage elongation was 14% and comparable to that of the base alloy.

Both hot rolling and cold rolling experiments were conducted on the composite and the base alloy. Composite exhibited good hot workability comparable to that of the base alloy. Cold workability was found to be much superior to the composite . Composite has been cold rolled to a foil of thickness 0.1 mm without even an intermittent annealing. This was possible by the continuous de-agglomeration of the weakly bonded particulates and the reduction in the flow stress beyond 75% reduction in thickness. The particulates got aligned parallel to the direction of rolling . Maximum strength level of 540 MPa was observed at 75% cold reduction. This was 60% higher than the theoretical prediction and about 22% higher than that of the base alloy in the same condition. This increment in strength was primarily due to the particle-dislocation interactions, formation of dislocation tangles and formation of sub-grains. Further cold work beyond 75% however decreased

the strength level due to relaxation of dislocation tangles. Mechanical properties of the cold rolled sheets in heat treated condition (333 MPa) was very close to the theoretical prediction (340 MPa). The high temperature tensile strength of the composite at the test temperature of 473 K was significantly high showing about 210 MPa, more than 100% above that of the base alloy at the same test temperature. Young's Modulus and density of the composite and the base alloy are comparable.

CONTENTS

CONTENTS

LIST OF TABLES

LIST OF TABLES

LIST OF FIGURES

LIST OF FIGURES

PUBLICATIONS

TECHNICAL PUBLICATIONS of the Investigator

I. PUBLICATIONS FROM THE PRESENT WORK.

1. Forging Charecteristics of Al-Zn-Mg wrought Alloy Composite containing 5 wt% TiO2 Dispersions, P.K.Balasubramanian, P.S.Rao, K.G.Sivadasan, K.G.Sathyanarayana, B.C.Pai and P.K.Rohatgi, Journal of Materials Science Letters, UK, Vol.8, (1939), 799-801.

2. Synthesis of cast Al-Zn-Mg-TiO2 particulate Composite using Liquid Metallurgy and Rheocasting, P.K.Balasubramanian, P.S.Rao, B.C.Pai, K.G.Sathyanarayana and P.K.Rohatgi, Proc. Conference on Solidifications of Metal Matrix Composites II, TMS, USA (1989), 181-189.

3. Casting and Extrusion Charecteristics of an Al-Zn-Mg Wrought Alloy Composite containing 5 wt% TiO2 Dispersions, P.K.Balasubramanian, P.S.Rao, K.G.Sathyanarayana, B.C.Pai and P.K.Rohatgi, Composite Science & Technology,U.K.,Vol.30 (1990), 245-259.

4. Particle-Matrix interactions during the synthesis of Al-Zn-Mg-TiO2 particulate composite, Proc. of INCAL 91 India, Vol.II (1991), 777-780.

II .PUBLICATIONS RELATED TO THE PRESENT WORK

1. Development of stress corrosion resistant high strength aluminium alloy by thermo - mechanical treatment, P.K.Balasubramanian & B.K.Sarkar, Trans. IIM, Vol.30, (1977), 172-176.

2. Development of high strength aluminium alloy for aerospace applications, P.K.Balsubramanian & B.K.Sarkar, Trans.IIM, Vol 31, (1978), 417-419.

3. Development of aluminium alloy for liquid fueled rocket engines, P.K.Balasubramanian & B.K.Sarkar, Trans. IIM, Vol 32, (1979), 170-171.

4. Extrusion studies on high strength aluminium alloys, P.K.Balasubramanian, Proc. International conf. on deformations, Ranchi, (1983).

5. Extrusion Studies on Al-Zn-Mg-Cu-Zr alloys, P.K.Balasubramanian, Materials Science & Technology, London, Vol.1, (June 1985), 470-474.

III. OTHER PUBLICATIONS ON ALUMINIUM ALLOYS BY THE INVESTIGATOR

1. Aluminium alloys for cryogenic applications in space technology, Proc. FNSC, Lucknow, 1980 & Indian cryogenic journal, (Dec 1983).

2. High strength aluminium aloys for space applications-past, present & future, P.K.Balasubramanian, Proc. seminar on Aluminium for electrical, electronics and aerospace applications, Trivandrum, (1984), 27-36.

3. Ring Rolling Experimentation on High Strength Aluminium Alloys, P.K.Balasubramanian, P.Balakrishnan, R.Jayaraman and K.V.Nagarajan, Presented in the International Conference on Aluminium (INCAL 85) Vol.11 New-Delhi (1985) 317-326 and Published in Trans.of Ind.Inst.of Metals, Vol.40, No.2, (April 1987), 170-171.

4. Forming Charecteristics of AA 2219 Al alloys, P.K.Balasubramanian, R.Ganesan, and K.V.Nagarajan, Presented in Seminar on Modern Trends in Metal Forming Technology, Hyderabad, 1986, and Published in the Journal of Inst. of Engineers (I), Vol.68, Part ME 4, (Jan 1988), 112-114.

5. Delivered an Invited talk on "Corrosion Aspects of Metallic Failures in Space Systems", at the Seminar on Failure of Engineering Materials , IIM, Trivandrum, (1987).

6. Developmental Studies on AA 2219 Al alloys, P.K.Balasubramanian, Aluminium India, (March 1988), 3-6.

7. Cold Spinning Studies on AA 2219 Al alloy Sheets, P.K.Balasubramanian, P.Balakrishnan, P.S.Rao, K.G.Sivadasan and K.V.Nagarajan, Presented in the IIM Seminar, Trivandrum, and Published in the Jourmnal of Inst. of Engineers(India),MM 1,Vol.70,(Sept 1989),25-27.

8. Cryogenic Temperature characterisation of AA 2219 Al alloy, P.K.Balasubramanian, and P.S.Rao, Accepted for publication in Indian Cryogenic Journal,Vol.14 (1989).

9. Extrusion and Wire Drawing Studies on AA 2219 Al alloy, P.K.Balasubramanian, K.G.Sivadasan and P.S.Rao, Accepted for publication in the International Journal of Metals, Materials and Processes, (1989), 309-318.

10. Aluminium Alloys for Space Applications - Criteria for Indigenisation, P.K.Balasubramanian, Invited paper in Minerals & Metals Review, (August 1989), 91-95.

11. Electron Beam Welding Studies on AA 2219 Al alloy Sheets, P.K.Balasubramanian, K.G.Sivadasan, P.S.Rao and V.Ramachandra, International Journal of Joining Sciences, UK, Vol.1,No.1,(1991), 29-35.

12. Studies on the Effect of Heat Treatment Variables on the Mechanical Properties of AA 2014 Aluminium Alloy, P.K.Balasubramanian, K.G.Sivadasan and P.S.Rao, Trans. IIM, (April,1991).

13. AA 2219 Aluminium alloy- State of the art in India, Proc. of INCAL 91, Bangalore, Vol.I (1991), 243-246.

14. Effect of thermo-mechanical treatment on residual stresses in AA 2014 aluminium alloy forgings,Proc. of INCAL-91 Bangalore,Vol.II, (1991), 637-640.

15. Advanced aluminium alloys for cryogenic applications in space launch vehicles, seminar on light structural materials, IIM, Trivandrum (1991).

INTRODUCTION

INTRODUCTION

Metal-Matrix Composites (MMC) have been investigated since the early 1960s with the impetus at that time being the high potential structural properties that would be achievable with materials engineered to specific applications. Both particulate and fibre reinforced MMCs, feature substantial improvements in stiffness and strength over unreinforced alloys. However, due to the high cost of fibres coupled with complications in dispersing them in the alloy, the emphasis of the 1980s came towards cost effective reinforcements and near net shape technology This has resulted in the development of MMC with inexpensive particulates as the effective dispersoids.

Furthermore, these particulate dispersed composites have demonstrated isotropic properties and hence significant improvements in performance. However, scant attention has been paid in the literature to the methodology and process parameters related to the optimum use of the available techniques, especially in the characterisation of ceramic particulate reinforced wrought Al-Zn-Mg alloys. The present research has undertaken the study of :-

1. Synthesising MMCs with special emphasis on wettability, casting routes and the suitability of incorporation of TiO_2 in a wrought Al-Zn-Mg alloy.

1

2. Various parameters affecting the secondary processing of the composite such as forging, extrusion and rolling, and

3. Structure-property correlation .

Chapter I gives a detailed literature survey from publications and reports on metal-matrix composite systems. Efforts have been made to include the technology of solidification synthesis, wettability, particulate dispersion, various casting routes and a survey on various Aluminium - matrix composites, high strength aluminium alloys and the basic properties of TiO_2. Scope of the present investigation is also listed in this chapter.

Chapter II deals with experimental methods and materials. Materials include basically Al-Zn-Mg alloy and TiO_2 particulate powders. Experimental methods include processing aspects such as primary processing of the composite, homogenisation, secondary processing such as forging, extrusion, heat treatment, rolling and thermomechanical treatment: and the analytical and testing aspects such as chemical characterisation, study of macro and microstructures through optical metallography, scanning electron microscopy (SEM), EDAX analysis, Transmission Electron microscopy (TEM), X-Ray diffraction (XRD), microhardness testing, mechanical properties evaluation ,both at room temperature and high temperatures and determination of Youngs modulus and other physical properties..

2

Chapter III deals with the results and discussions of the above processing, testing and analytical aspects. Results and discussions are combined to have an effective understanding and to avoid duplications in the text.

Conclusions drawn from these experiments and the scope for further studies are listed in chapter IV and V respectively.

CHAPTER I

LITERATURE SURVEY

1.1 Introduction.

Metal-matrix Composites essentially consist of metal matrices with additions of hard insoluble and non-reacting constituents as reinforcements. MMCs combine metallic properties (ductility and toughness) with properties of ceramics (high strength and high modulus) leading to greater strength in shear and compression, and higher service temperature capabilities. These properties have made MMCs very attractive candidate materials for aerospace, automotive and numerous other applications. Interest in MMCs has increased over the last 5 years as a result of availability of relatively inexpensive reinforcements and the development of various processing routes which result in reproducible microstructures and properties (1). The attractive physical and mechanical properties that can be obtained with MMCs such as high specific modulus, strength and thermal stability have been documented extensively (2-8) .

The family of particulate reinforced MMCs include dispersion strengthened (DS) alloys and cermets. DS alloys consist of metal matrices with addition of hard insoluble particle constituents with sizes of the order of a micrometer and in small proportions, typically below 5 Vol.%. A cermet is a mixture of ceramics and metals. Its structure is composed of ceramic grains bonded in a metal matrix. The volume fraction of the metal matrix may be upto 30% (9). The bonding between the metal and the ceramics results from their mutual or

partial solubility or from elemental additions that are partially soluble in both (10). Therefore the ultimate properties of the MMCs basically depend on the selection of the reinforcement and the matrix material.

I.2 Materials selection

I.2.1 Reinforcement Selection

Selection criteria for the reinforcements include the following properties:-

* Elastic modulus

* Tensile strength

* Density

* Melting temperature

* Thermal stability

* Coefficient of thermal expansion (CTE)

* Size and shape

* Compatibility with matrix and

* Cost .

Some selected properties of commonly used ceramic reinforcements are shown in Table I. The structural efficiency of the particulate reinforced MMCs is a function of density, elastic modulus and tensile strength of the reinforcing phases. The chemical stability and compatibility of the reinforcement with the matrilx material are important not only for the end application but also during material fabrication.

TABLE-I

Characteristics of Particulate Dispersoids used
for reinforcing in Aluminium matrix composites:-

Particle	Size μM	Amount vol%	Density gm/cc	U T S MPa	E GPa	Ref.
Graphite	15-500	1-8	1.6-2.2	20000	910	63,83,84,175
SiC	0.5-120	3-20	3.2	3000	480	31-34,175
SiO$_2$	5-53	5	2.3	4700	70	39
MgO	40	10	2.7-3.6	41	317	9,33
Zircon	40	0-30	4.9	--	--	40
Al$_2$O$_3$	3-340	3-30	3.97	8000	460	30-34,175
TiC	46	15	4.9	--	320	32
BN	46	15	2.25	180	100-500	32
Si$_3$N$_4$	40-46	10	3.2	3000-6000	360	32
ZrO$_2$	5-180	4	5.65-6.15	140	210	129
TiO$_2$	5-80	4	3.9-4.3	56	-	129,150
B$_4$C	40-340	-	2.5	6500	480	176

1.2.2. **Matrix Selection**

Where as for room temperature applications, any higher
strength aluminium alloys can be utilized as matrices, the
use of MMCs for high temperature applications necessitates
the presence of thermodynamically stable dispersoids. The
requirement has been achieved by using an alloy-dispersoid
system in which elemental stability, solid state diffusivity
and interfacial energies are minimized, thereby minimising
coarsening and interfacial reactions (11). The requirement of
low density with high thermal conductivity have made Al and
Mg aloys, the commonly used matrices. Regarding alloy
additions, earlier studies (12,13) have shown that , low
additions result in MMCs with attractive combinations of
strength, ductility and toughness. Aluminium alloys which
have already been used as matrices for reinforcing various
particulates are shown in Table II.

7

TABLE - II

PROPERTIES OF MATRIX ALLOYS EXTENSIVELY USED IN THE SYNTHESIS OF Al MATRIX COMPOSITES

ALLOY	CHEMISTRY	COND.	UTS MPa	YS MPa	%E
1100	Commercial aluminium	H18	165	150	5
2014	4.5Cu-Mg-Mn-Si	T6	480	410	13
2024	4.3Cu-Mg-Mn	T8	480	450	6
2124	4Cu-Mg-Mn	&8	490	440	8
3003	1.2Mn	H18	200	185	4
5083	4.5Mg-Mn	H343	360	280	8
6061	1Mg-Si	T6	310	275	12
6351	1Si-Mg-Mn	T6	300	255	14
7075	5.5Zn-2.5Mg-1.6Cu	T6	570	500	11
7178	6.8Zn-2.8Mg-2Cu	T6	558	490	10

1.3 Synthesis of Composite

A variety of processing techniques have evolved for synthesising of composites over the last two decades in an effort to optimise the structure and properties of particulate reinforced MMCs (14,15). The processing methods can be grouped, according to the temperature of the metallic matrix during processing, into three catagories :
(i) liquid phase process, (ii) solid state process and (iii) two phase (solid-liquid) process.

Solid phase processing basically includes powder metallurgy (PM) techniques and high energy rate (HER) processing. PM process involves blending of powders with particulates and consolidation by either hot extrusion or hot rolling. These methods have been successfully applied to a large number of metal/ceramic combinations (16-20). The results show that PM processed Al-SiC MMCs possess higher overall strength levels relative to those corresponding to the equivalent material processed by a liquid phase process, the elongation values however are low in powder processed composites.

HER process involves consolidation of a metal-ceramic mixture through the application of a mechanical or electrical high energy. Al-SiC MMCs have been successfully consolidated by this process (21) but the process is still in experimental stage.

8

Liquid phase processing is a well established process and incorporates ceramic particles into a molten matrix using various proprietary techniques followed by mixing and casting of the resulting MMC. Extensive studies have been made on the various aspects of liquid phase processing and good part of its discussion is included in a later section of this chapter.

Two phase processing includes Osprey deposition (OS), Rheocasting (RC) and Variable co-deposition of multi phase materials (VCM). In the OS process (22,23), the reinforcement particulates are introduced into the stream of molten alloy which is subsequently atomised by jets of inert gas. The MMC powder is further consolidated by PM process.

In RC process, the ceramic particulates are added into a metallic alloy matrix at a temperature within the solid-liquid range of the alloy, followed by vigorous agitation to form a low viscosity slurry and the resulting MMC is cast by conventional methods. RC method offers several advantages and the details are given in a later section of this chapter.

VCM processing is a recent technology successfully applied for SiC reinforced Al-Li alloy composite system (24). During VCM processing, the matrix material is disintegrated into fine dispersion of droplets using high velocity gas jets. Simultaneously, particulates are also injected into the atomised spray which contain only limited amount of volume

9

fraction of liquid. Hence, contact time and thermal exposure of the particulates with the partially solidified matrix are minimised and interfacial reactions can be controlled. The processed MMC powder will have to be consolidated by PM process.

Considering the merits and demerits in applicability of the above processing tehniques, liquid phase process and rheocasting process have certain definite advantages over other processes. Considerable amount of work has been reported (25-42) over the last 3 decades in the area of synthesising Al based MMCs by these solidification routes.The various technical aspects of these two processing methods are dealt with , at a greater length, in the following sections.

1.4 Matrix-Ceramic Interface

The characteristics of the interface formed between the matrix and the ceramic reinforcement determine the load transfer and the crack resistance of the MMCs during deformation. Systematic studies of metal ceramic interfaces were initiated in the early 1960s (43). It is now widely accepted that in order to maximise interface bond strength in MMCs, it is necessary to promote wetting, control chemical interactions and minimise oxide formation. The interaction may be in the form of mechanical locking or chemical bonding between the matrix and the reinforcement.

The wettability of a solid by a liquid is indicated by the 'contact angle θ ' defined in Fig.1. This angle is related to the three surface tensions Γsg, Γsl and Γlg of the interfaces solid-gas, solid-liquid and liquid-gas, respectively, by the well known Young's Equation (44) shown below.

$$\Gamma lg \times cos\theta = \Gamma sg - \Gamma sl \qquad (1)$$

A liquid is said to wet a solid surface when $cos\theta \gg o$, i.e. when $\Gamma sg \gg \Gamma sl$. The driving force Df for wetting may thus be defined (45) as:

$$Df = \Gamma sg - \Gamma sl \qquad (2)$$

when $Df \geq \Gamma lg$, $\theta = 0$ and the liquid spreads spontaneously on the solid surface.

11
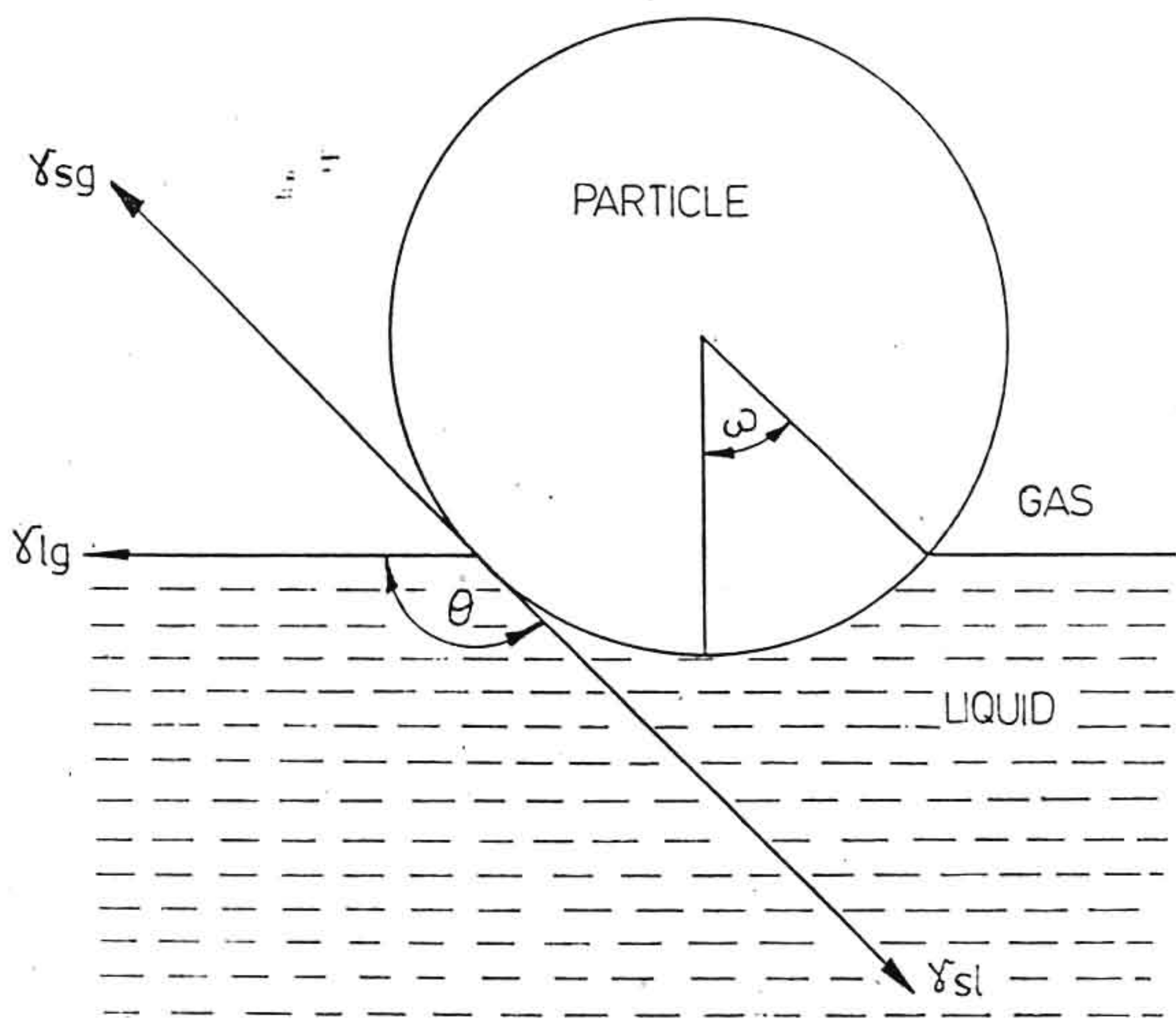
FIG. 1. DEFINITION OF ANGLE OF IMMERSION, ω, CONTACT ANGLE, θ & SURFACE TENSION

Fig.2 shows the overall energy change for a 250 micron size graphite spheroid at increasing degrees of angle of immersion 'W'in an Al melt (42). The two curves in this figure correspond to two contact angles : $\theta = 157°$ (non-wettable) and $\theta = 60°$ (wettable), the total free energy change being negative in the later case ($\theta = 60°$), particles enter the melt spontaneously, which is confirmed by experiments (46). In all cases when $\theta \ll 90°$, the initial entry of the particle into the melt is energetically favourable.

Wettability of a reinforcement by a metal is measured by the amount of work required by the metal to engulf the fibre or particulate reinforcement (7). On a quantitative basis, this resistance is measured by the pressure drop at the infiltration front when the metal is entering a fibrous or particulate preform. When that pressure is negative, the metal is said to wet the particle and slowly infiltrate the preform spontaneously, a process often called "wicking". When wetting is not spontaneous, pressure must be applied and the magnitude of this pressure (capillary pressure) depends on the wettability of the system. A simple calculation (47) gives the minimum pressure (P) required as:

$$P = \frac{A \times Vf (\Gamma sl - \Gamma sg)}{df (1 - Vf)} \qquad (3)$$

where df is the diameter and Vf the volume fraction of the reinforcing phase. A is a constant which is '6' for spherical particles and '4' for cylindrical fibres (47)

12
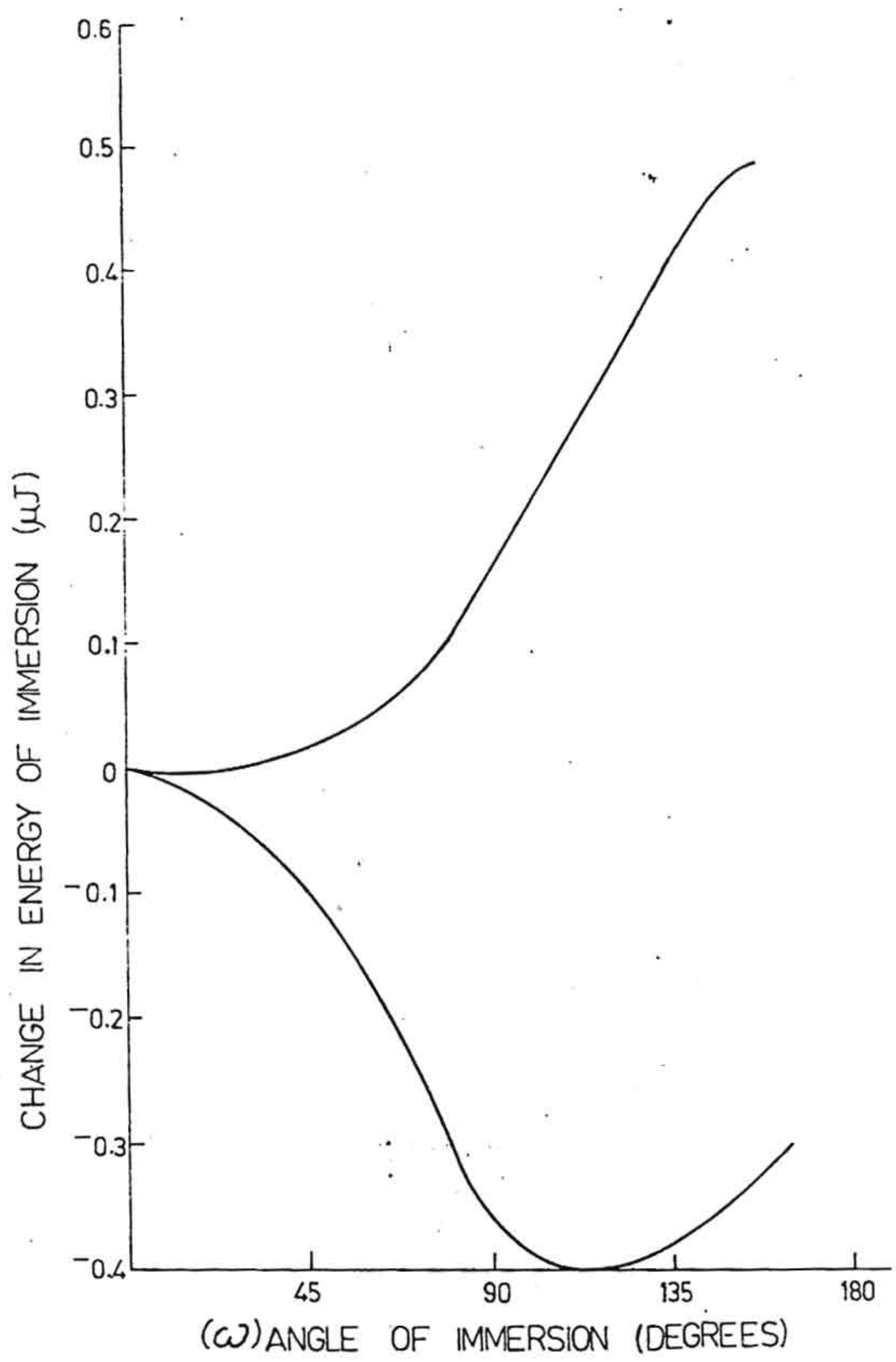
FIG. 2. ENERGY CHANGE Vs. ANGLE OF IMMERSION IN Al MELT

Energetics for particle transfer to a melt demonstrate that the fundamental requirement for transfer is the wetting between the ceramic particle and the melt (42). While ceramics are generally poorly wetted by the metallic melts, their incorporation in the metal matrix can be facilitated by inducing wettability or by use of mechanical agitation like stirring or by a combination of these two techniques.

I.5. Wetting Enhancement Techniques:

With wetting angle data and chemical intuition as a guide, a large number of attempts have been made at designing solutions to the problem of the generally poor wetting of reinforcements by metals. These can be classified into three broad categories: i) reinforcement pretreatment, ii) reinforcement coating and iii) alloy modifications.

i) REINFORCEMENT PRETREATMENT;

Reinforcement pretreatment include heat treatment and ultrasonic vibration treatments. The reinforcement surface energy Γsg can be raised by changing the chemical nature of the atmosphere prior to infiltration. In particular, adsorption of oxygen or other elements from the atmosphere on the reinforcement can modify the reinforcement surface to a considerable extent. Results have been published (42,48,49) on the influence of heat treatment of alumina and graphite particles on their wettability, which improved their ease of incorporation into aluminium melts. This was attributed to desorption of adsorbed gases from the reinforcement surface during the heat treatment.

Ultrasonic vibrations (42) promote wetting of ceramics by metallic melts as a result of partial desorption of adsorbed gases (mostly hydroxyls) from the surface of particles; in addition, they supply the excess energy for melt cavitation which facilitates particle dispersion in the melt.

14

ii) **COATING OF REINFORCEMENTS** : Coating of reinforcement is the most widely explored technique for promoting wettability. Coatings can also be classified broadly into two categories (i) Coatings that react with the matrix which include metallic coatings for various reinforcements in aluminium (1,50-52) and ii) coatings that do not react with the matrix but modify the oxide layer like coating of K_2ZrF_6 which is also a fluxing agent for aluminium (53). The primary role of coatings is not always the enhancement of wetting. When reaction between reinforcement and metal is a major concern, coatings were designed to provide a diffusion barrier. Such coatings usually lower the wettability. The best solution is then the deposition of a second coating which promotes wetting. The general perception is that there are two fundamental ways of promoting wettability of reinforcements by metals such as aluminium; modification of the reinforcement or the matrix with a substance that will promote chemical reactions or disrupt the oxide layer on the metal. Presence of oxide layer otherwise prevents actual contact of the metal with the substrate and therefore inhibits wetting. Elements with greater affinity for oxygen than the solvent can preferentially concentrate at the melt/ceramic interface reducing the surface energy ΓSL and thereby improving the ceramic wettability. Similarly, elements with lower surface tension are enriched at the ceramic surface. For example, addition of Mg to an aluminium melt improves wetting because of the lower surface tension of

15

Mg (0.599 N/M) compared to that of Al (0.760 N/M) (42).

Addition of 3% Mg to Al reduces its surface tension from
0.760 to 0.620 N/M at 993 K (54). Several studies (48,55-57)
have been made on wetting and interface reactions in a
variety of melt ceramic systems involving Al melts and Al_2O_3,
zircon, graphite etc., as reinforcements. It was observed
that Al_2O_3 readily reacts with many divalent transition metal
oxides to form aluminides which are iso-structural with
spinels of composition $MgAl_2O_4$. Mineral spinel or similar
oxides promote interfacial bonding since they form strong
bonds with both metals and ceramics. The composites produced
by liquid metallurgy technique generally show excellent
bonding between the matrix and the reinforcements when
reactive elements are added to induce wettability. An
earlier study (41) indicated that Mg addition to cast
aluminium alloy resulted in a recovery of about 80% of TiO_2
dispersions. A reaction zone was reported around TiO_2
particle but not on ZrO_2 particle. Mg has also been reported
(58) to possibly reduce TiO_2 to Ti containing 2.5wt% OX. at
1273 K and at lower temperatures to Ti_3O_4 and TiO.

iii) **ALLOY MODIFICATIONS ;**

Alloying additions to the matrix have been shown to affect
the wetting angle on, and ease of infiltration into, most
reinforcement preforms. Effective additions fall into two
categories;

16

(1)   Additions   that   promote   reactions   between   the reinforcements   and   the matrix.   Examples   include: Li   in aluminium   for Al_2O_3 (45,59,60) and SiC (45) reinforcements, and   Si   in   aluminium for carbon   particulates   (61).   This tendency   agrees   well   with the wetting   angle   data,   which indicates   that,   in general,   alloying additions that   promote reactivity   between   the metal and the   substrate   lower   the wetting   angles.

(2)   Additions   to aluminium that do not   promote   reactions with   the reinforcements, but modify the   characteristics   of the   oxide   layer on the metal surface: Examples are   Mg   in aluminium with mostly all reinforcements   and Li in aluminium for   carbon (55,62).   These data also correlate with   wetting angle data, in the sense that the transition temperature from wetting   to   non-wetting   as well as   the   wetting   angle   are decreased   by these additions.   These   two   classes   broadly illustrate the chief methods that have been used in   practice to   achieve   wettability   for   fabrication   of   metal   matrix composites.   Wetting   is thus favoured by the   formation   of strong   chemical bonds at the interface.   Good wetting   often also   involves a good bond strength at the interface   in   the final   composite.   The   formation   of   these   bonds   may   be accompanied by reaction of the two bulk phases (method 1)   or mutual   dissolution   (method 2)   The   reaction   phenomena   are very   detrimental   to the composite as they   bring   about   a decrease   of   the mechanical properties.   A   compromise   must therefore be found between the contradictory requirements   of good wetting and absence of reaction.

17

1.6. Techniques of introducing particulate reinforcements

Several techniques have been developed for introducing solid particles and short fibres into molten alloys: the more commonly used of these are summarised in Table-III. The process involves mechanical introduction of particles in the melt just before casting. The techniques of synthesizing metal-matrix composites by solidification processing make use of one of the following strategies. i) Injection of powders entrained in an inert carrier gas into the melt with the help of an injection gun (63-65), the particle is transferred from the gaseous phase to the melt as the bubbles rise through the melt.

ii) Addition of particles to molten stream filling the mold.

iii) Mechanical stirring of the molten alloy with a suitable impeller to create a 'Vortex' in the melt and simultaneous addition of solid dispersoids to it (40,49,66-69), this method has been most extensively used.

iv) Forming pellets or small briquettes by co-pressing powders of base alloy and solid particles, and subsequently plunging these pellets into the melt followed by hand or mechanical stirring (38,70).

v) Using centrifugal acceleration to disperse particles in a melt (71).

18

vi) Pushing the particles into the melt by reciprocating rods

vii) Using high intensity ultrasound with or without mechanical force like injection of particles through a shot-gun while the melt is being irradiated with ultrasound (72,73).

and viii) zero gravity processing which involves utilising an ultra-high vacuum and high temperature for long periods of time (9).

1.7. Effect of suspended particle on melt fluidity:

Decrease in the fluidity of Al alloys has been observed as a result of additions of alumina (74), mica (75) and graphite (76), particles to Al alloy melts. The spiral fluidity of Al-11.8 Si alloy was reported (74) to decrease with an increase in the amount of dispersed alumina (for a given size) and decrease in the particle size (for a given wt %). Decrease in the spiral fluidity with a decrease in inter particle distance was also noticed. In addition, the casting fluidity of Al alloys containing suspended particles decreases with a decrease in temperature in a manner similar to that of the fluidity of molten alloys without any suspended particles.

The observed reduction in spiral fluidity of Al alloys containing ceramic particles could possibly be owing to changes in (i) freezing time (ii) freezing mechanism or (iii) effective viscosity of the melt. In principle, although the presence of insulating ceramic particles should lead to a slight decrease in solidification time because of the reduced quantity of heat (super heat + latent heat) to be dissipated; apparently, the decreased effective conductivity of the composite melt just compensates for this, leaving the over-all freezing time of the casting approximately the same. However, when the volume percentage of the suspended particle is greater, there may be measurable effect on solidification time.

20

Presence of alumina or graphite particles considerably refines the eutectic silicon in Al-11.8 Si alloy (42) Finer silicon provides greater surface area resulting in greater decreases in fluidity because of the greater volume of stagnant layers around particles. This rules out the role of an altered solidification mechanism in effecting fluidity changes, leaving the third factor - increase in effective viscosity owing to the presence of suspended particles - as possibly the major factor for the observed fluidity decrease. The existence of such a relationship between fluidity and viscosity for Mica-LM 11 alloy composites had previously been reported (75).

It is well known that in metallic liquids, the viscosity depends on the size and shape of the dispersoids. Flemings et al (77) have shown that the viscosity of a solid-liquid mixture of Al alloys between solidus and liquidus is higher, the finer is the size of primary solid particles at a constant volume percentage. Such results have generally been explained in terms of a higher effective volume fraction of the finer dispersed phase owing to the existence of a stagnant boundary layer around the surface of the particles. The greater increase in suspension viscosity with finer size is therefore, attributed to the larger apparent surface area of these particles.

Although the fluidity of Al alloy-ceramic particle composites decreases with the increasing amount of dispersed particles, the values of casting fluidity and spiral

21

fluidity were found to be adequate enough for making a variety of castings (74). The fluidity of Al-11.8 Si- 5.5 Al_2O_3 (60 μm size) composite poured at 1013 K was of the same order of magnitude as that of Al-11.8 Si alloy at 973 K, which is considered to be a very good casting alloy.

I.8. Casting Techniques:

A variety of casting techniques have been used to cast molten alloys containing suspended ceramic particles to obtain useful components of cast composites. Choice of casting technique and configuration of mold are important since the dispersed particles generally exhibit a tendency to float or settle because of density differences. Right from sand casting (33), permanent mold casting (25-30), centrifugal casting (78), compo-casting / Rheocasting (36) squeeze casting (38,79-81) etc., variety of casting techniques have been used for cast components. Casting techniques can broadly be divided into three classes:-

i) Liquid metal casting like sand casting, permanent mold casting, and gravity casting (without involving pressure)

ii) Squeeze casting (7,35) (involving pressure) and

iii)Slurry casting involving rheocasting / compocasting (33,35,82), where the metal is in the semi liquid state.

In all these cases, a vortex (35,37,41) is formed in the melt by means of mechanical stirring, to which the dispersoids are introduced. Liquid metal casting technique stands out as the simplest process for highly wettable particulate reinforcements. Several aluminium composites containing graphite, Al_2O_3, SiC or glass have been cast by sand casting process (33,83,84). A variety of permanent mold castings of Al-based composites have been made by Rohatgi and

23

co-workers (66,67,70,85). Centrifugally cast Al - graphite and Al-zircon composites have been developed (86) to get anti-friction and abrasion resistant surfaces respectively. These liquid metal casting techniques without involving pressure, however result in high porous castings (87,88), porosity, due either to poor infiltration or to shrinkage of the matrix during solidification. The problem of feeding matrix shrinkage during solidification can be solved by using directional solidification towards a riser in a temperature gradient or by applying very high pressure during solidification as in squeeze casting.

Squeeze casting is the technique of liquid metal working under pressure into near net shapes. This technique offers two major advantages:

(i) Pressure compensates for the poor wettability of the reinforcements and

(ii) Solidification under pressure gives the aluminium matrix a better metallurgical quality and reduces macro and micro porosity.

Rheocasting techniques provide improved wetting, and bond formation between particles and the matrix could be achieved by dispersing ceramic particles in vigorously agitated, partially solid slurries of alloys held between their liquidus and solidus temperatures. This approach takes advantage of the fact that many metallic alloys behave like a low viscosity slurry, when subjected to vigorous agitation

24

during solidification. This behaviour which has been observed for fraction solids as high as 0.5 is thought to result from the breaking of solid dendrites during stirring, into spheroidal solid particles which are then suspended in the liquid as fine grained particulates (33,89). This characteristics of numerous alloys, known as thixotropy, can be regained even after complete solidification by raising the temperature.

The slurry characteristics of the matrix during the stirring permit the addition of reinforcements during solidification. The ceramic particulates are mechanically entrapped initialy and are prevented from agglomeration by the presence of primary alloy solid particles. The particulates subsequently interact with the liquid matrix to effect bonding. Furthermore, the continuous deformation and the breaking down of the solid phases during agitation prevent particle agglomeration and settling. This method has been successfully utilised (33,90,91) to incorporate Al2O3, SiC, glass particles, TiC, and Si_3N_4 in various Al alloys like Al-Cu, Al-Cu-Mg, Al-Mg-Si and Al-Si-Fe alloys.

25

1.9. Reinforcement and Matrix Solidification:

Generally, the poor wettability between the particle and the melt, and the particle tendency to segregate as a result of density differences, results in an inhomogeneous distribution of particles in the alloy matrix. This uneven distribution is, in general, undesirable, though particles are sometimes deliberately segregated at certain locations for specific applications, such as for wear or abrasive resistance.

Desired distribution of suspended particles can be obtained by suitable control of the fluid flow and solidification parameters. This could be achieved, for example, by external forces (ultrasonic, centrifugal, electromagnetic) before and during solidification for localised segregation, or by creation of colloidal suspensions by use of specially surface treated or surface coated mutually repelling particles which would form a homogeneous dispersion in the melt. Several attempts have been made (54,92,93) to characterise statistically the distribution of dispersed ceramic particles such as graphite, zircon and shell char in cast Al alloy matrices. In general, these studies show that the maximum frequency of interparticle spacings occurs close to the average mean particle spacing, indicating fairly uniform distribution of ceramic particles. Moreover, these studies have also amply demonstrated that the distribution of interparticle spacings is reasonably uniform across different casting sections and the mean particle size is very close to

the size for maximum frequency distribution, indicating absence of any significant clustering.

The grain size in a casting is determined by the nucleation rate as well as the presence of fluid flow during solidification which results in grain multiplication (94). The nucleation rate is influenced by the cooling rate as well as by the presence of heterogenous nucleation catalysts.

The reinforcements can influence each of these processes, and hence modify the resulting grain size in the matrix. If the reinforcement surface serves as a propitious site for heterogeneous nucleation of the matrix, a much finer grain size will result, for example, TiC infiltrated with Al (95). Most commercial reinfrocements, however, do not act as heterogeneous nucleation catalysts for aluminium base alloys, since grain sizes far in excess of the reinforcement diameters have been observed in several instances, for example, Al_2O_3 (6,96), SiC (6,87) and carbon (7) reinforcements. When the reinforcement is relatively mobile within the solidifying matrix, particle-pushing effects can be important (42,97). This affects the distribution of the particles, which are generally found between individual dendrite arms in particulate reinforced composites, solidified from the liquid state (42,98). In compocast MMC, the reinforcement is found between nodules of the primary phase those were solid at the time of particle incorporation (33,82). This further increased the propensity of the

27

reinforcement to concentrate in regions of the matrix that are last to solidify and often results in non-uniform particulate distributions.

The distribution of the reinforcement, in general, is an important and unresolved issue in MMC solidification processing. The metal tends to form channels during infiltration due to poor wettability of the reinforcement and liquid metal viscosity. The reinforcement is therefore concentrated into regions of high reinforcement volume percent, surrounded by channels of unreinforced metal. For all practical purposes, one is therefore limited to fabricating a composite in which the reinforcement is packed to maximum density of approximately 30% for a narrow size distribution particulates, to prevent channelling (7). Further more, if the grain boundary energy of the reinforcement Γss is less than 2 Γsl or 2 Γsg, sintering of particles takes place which may promote particle clustering in slurry casting process that is frequently observed (82,99).

After solidifcation, large stresses can build up in the matrix due to differences in the coefficient of thermal expansion between the matrix and the reinforcement (100-103). These stresses result in higher dislocation densities in the matrix (104-109). The importance of a uniform reinforcement distribution in the composite has been demonstrated by Imai et al (110). However, actual measurements for all the systems are not yet available.

28

1.10. Aluminium Metal Matrix Composites (AMC):

Though significant improvements in properties including high temperature capability have already been established (35), the industrial development of AMC has been impeded mainly due to higher cost of fibrous reinforcement and some problems related to high temperature processing. As a result, many studies have been carried out on AMC reinforced by cost and technology effective short fibres, whiskers and particulates. Thus, a substantial amount of knowledge is now available in the literature although the classified nature of significant parts of the research by various active groups has led to some restriction in the diffusion of this knowledge to larger scientific community.

Table-I indicates the range of particles reinforced in aluminium metal matrix composites. When the first AMC were processed, particularly with particles, the choice of matrices was not usually dependent on the reinforcing elements. The alloys were considered for their processing ability like casting, forging etc. Thus, most work dealing with AMC considered Al-Si alloys (4000 series) for casting operation and Al-Cu (2000 series) and Al-Si-Mg alloys (6000 series) for powder metallurgy operations. Later developments facilitated alloy additions like Mg, Cu or Li to the matrix alloy which enabled better and stronger reinforcements by improving wettability, chemical compatibility and metallurgical characteristics (34,39,56,95,111-115). A list of matrix alloys used extensively is shown in Table II.

Similarly, the strengthening mechanism of the ceramic elements is not merely an addition of their own properties but is the conjunction of numerous effects, for example, the overstraining of the alloy lattice (106,116). Thus the effects of heat treatment are also not easy to forecast and the efficiency of one type of reinforcement can be quite different depending on the nature of the matrix (116).

Some of the recent studies (117-122) on dispersion of SiC, B_4C and Al_2O_3 in 2124, 6061 and 7475 Al alloys have indicated that the age hardening is more effective in these composite strengthening . These particle dispersoids were thought to be inert with respect to the age hardening - precipitate reactions. However, B_4C is found to effect the age hardening behaviour of 6061 Al alloy viz the composite reached peak hardness at 450 K in 3 hours instead of 10 hours for the base alloy at the same temperature of ageing. This is due to the high diffusivity path by high dislocation density of the order of 4×10^{14} /SQ.M, introduced by differential thermal expansion of the order of 10 : 1 between B_4C and the matrix. This suggested that the dislocation strengthening is a predominant effect in this composite strengthening.

McDanel (123) suggested particle dispersion effect on strengthening of these composites. Possible effects of residual stresses on tensile behaviour of the composite also are reported (124) . Average matrix residual tensile stress of 206 MPa in 30% SiC particulate dispersed 6061 Al alloy

30

composite in T6 condition with higher stresses near SiC particle was observed. Clegg (125) has analysed extensively the various strengthening mechanisms in MMC . As is apparent from the diversity of conclusions, a consensus on the effect of particle on the strength of Al -matrix composite has not yet been reached.

Only discontinuously reinforced AMC can be subjected to any plastic deformation since continuous reinforcements prevent sometimes extensive deformation on composites.(35). Furthermore, plastic forming is able to give the reinforcement a preferential orientation in which higher mechanical properties can be induced. Similarly, the applied stresses are able to reduce residual porosity. However, plastic forming is possible only if the volume fraction of the reinforcement (Vf « 25%) (116) does not too greatly reduce the failure strain. Plastic forming is performed at higher temperatures in order to facilitate matrix flow and to avoid either fracture of the reinforcement or the formation of voids at the reinforcement matrix interface. The operating conditions (35) generally used for extrusion of composites are in the range 773 K - 873 K for the temperature, 20-25 mm per minute for deformation rate and 10-20 for the extrusion ratio. The properties of several AMC studied earlier (111,126,127) are tabulated in Table-IV. It can be seen that an increase upto 30% for yield strength and upto 400% for rupture strength have been noticed for certain systems. In practice, the increase in rupture strength is

31

TABLE-IV

PROPERTIES OF ALUMINIUM MATRIX WROUGHT ALLOY COMPOSITES

Composite	UTS MPa	YS MPa	E %	E GPa	Ref.
6061-Al_2O_3 Saffil (PM)	385	290	-	91-96	35
6061-Al_2O_3 (Sq.cast)	360	260	-	92	35
2017-SiC Whiskers(PM)	410	-	-	90	35
6061-SiC Powder(PM)	450	380	-	126	35
6061-SiC Whiskers (PM)	450	420	-	98	35
2024-Al_2O_3 Powder (Liq. Forge)	350	250	3.4	-	36
2014-Al_2O_3 Powder (Liq. Forge)	340	240	5.7	-	36
2124-SiC dis-continuous fibre (PM-RST)	720	570	5.3	KC 59 MPa√M	179
5456-SiC(PM)	459	253	15	81	128

mainly due to two opposite effects: on the one hand, the
material requires a higher flow stress related to the
increasing rigidity; but on the other hand, rupture tends to
occur after a smaller deformation. It is worthy of note (35)
that no further improvements in strength occur when the
volume fraction of reinforcement is greater than 35%. A
recent report (117) also stated that particle dispersion
resulted in increased elastic modulus and work hardening rate.

Ductility is the most significant property of discontinuously
reinforced AMC, since it controls the strength and
facilitates plastic forming after billet processing.
Unfortunately, ductility decreases markedly with the content
of reinforcing elements (36), though the orientation of the
reinforcement particles does indicate a non-negligible
effect. This means that the alignment of the ceramic elements
during extrusion is the major source of anisotropy of the
ductility. However a very recent report (128) indicated that
91% reduction by hot rolling of 5083 Al-Mg alloy - 10% SiC
particle reinforced cast composite increased the percentage
elongation from 5% to 15% with no change in strength level.
This increase in elongation is reported to be attributed to
the homogenisation of the reinforcement, second phase
distribution and closure of microporosity and interparticle
voids during hot rolling.

The wear resistance of composites increases linearly with
hardness and above 5-10% volume percent of the reinforcement,

32

the hardness is a quasi-linear function of the particulate content, as observed (129) in ZrO_2 reinforced composites. Larger particles are more effective against abrasive wear than smaller ones (31,36). It was also observed that, the use of fibres rather than particles allowed to combine a good wear resistance with a higher strength (36). A general feature of the resistance to crack propagation in discontinuously reinforced AMC is a simultaneous reduction in toughness and impact resistance as the volume fraction of ceramic elements is increased (130-135). A recent study (119) indicated that fracture toughness JIC of Al-Zn-Mg-Cu alloy decreased from 31 MPa for the base alloy to 16 MPa for 15% SiCp reinforcement and to 11 MPa for 11% reinforcement. Toughness depends mainly on the size, shape and distribution of the ceramic elements since the predominant mechanism of crack propagation is related to the coalescence of voids associated with these elements (119). As a result, the direction giving rise to easier crack propagation is the direction along which the distances between ceramic elements are the smallest. Nevertheless, toughness values similar to that of the matrix can be obtained with a fibrous reinforcement provided sufficiently strong bonding at the fiber-matrix interface is achieved (134). This also enhance the fatigue resistance of AMC as observed in the case of Al_2O_3 fibers and SiC whiskers reinforced AMC (136).

Elevated temperature properties are reported (111,126,136-139) to be significantly improved by an order of 100-200%

33

relative to the unreinforced matrix in the temperature range 473 - 623 K for AMC reinforced by Al_2O_3 fibers and SiC whiskers. Although particle-reinforced AMC also behaves as fibrous composites, the creep rates are 50-100 times smaller, so that the l/d ratio is presumably a predominant factor for creep resistance as well as the fiber matrix bonding (115, 137-140).

It appears that the mismatch in the thermal expansion coefficients of the matrix and reinforcement is likely to cause damage of the fiber-matrix interface, which can significantly influence composite behaviour at elevated temperatures. Otherwise, thermal cycling is able to facilitate plastic forming, giving the composite super plastic behaviour by overstraining the matrix (140).

Discontinuously reinforced AMC exhibit significantly improved behaviour on compression, damping and pin bearing resistance (113, 126, 134, 139, 141). On the other hand, corrosion resistance is not as good in the composite as it is in the matrix, particularly in the case with graphite dispersoids (133).

The electrical and thermal conductivities are reduced by the presence of ceramic elements (111, 141) The effect is stronger the more insulating the reinforcement, for example, thermal conductivity of AMC with 30 Vol% SiC whiskers is half that of unreinforced aluminium (141) Similarly, the thermal expansion coefficients of AA 7075 aluminium alloy is halved by 30 Vol% SiC whiskers and is 50% greater than that of 7075 with 25 Vol% Al_2O_3 fibers (111).

34

1.11. High strength aluminium alloys:

J.T.Staley (142) has earlier reviewed aluminium alloy and the process developments for the aerospace industry. Al-Zn-Mg (7000 series) alloys form the highest strength aluminium alloys so far developed with alloy specifications 7075, 7178, 7475, 7001 etc. Al-Li alloy 2090 (143) has a lower specific gravity of 2.57 as against 2.80 for 7075 alloy, with 10-15% higher modulus which are the outstanding properties for space applications. However, it has a set back of lower ductility and fracture toughness.

7005 and 7039 are the prominent low strengtrh aluminium alloys in the 7000 series used for special purpose welding applications (144). The conventional ageing treatment recommended for these type of alloys are normally very long viz., 72 hours room temperature ageing followed by 24 hours at 420 K for 7005 alloys and 48 hours at 390 K for 7039 alloys. However, an earlier study (145) has recommended only 24 hours ageing treatment to achieve the optimum properties.

The high strength alloys of 7000 series contain copper also as a major alloy addition and are not recommended for welded structure applications. Considering welding as a requirement, the selection of alloy for this study was based on copper free Al-Zn-Mg alloys. Effect of Ti and Zr (146) trace additions have already been studied in improving the properties of Al-Zn-Mg alloys. Ti has strong influence in reducing the grain boundary precipitates and the width of precipitate free zones. Zr addition drastically reduces the

35

grain size resulting in better mechanical properties. The strength of these alloys, are predominently based on the GP zone formation (144) and effect of M' precipitate $MgZn_2$ is only marginal. As a result, these alloys do not retain their strength levels at higher temperatures where the zones transform to M' and subsequently to non-coherent $MgZn_2$ precipitates. Reversion of GP zones (147) is observed at about 443 K for these 7000 series aluminium alloys. The properties of Cu free Al-Zn-Mg alloys (148) viz 7005 is shown in Table V. Alloys AA 2219 and AA 2618 are good high strength high temperature alloys upto 423 K and their properties are shown in Table VI. It is observed that the properties drastically come down beyond this temperature of 423 K. The highest strength aluminium alloy 7075 has superior strength at room temperature but has only half the strength of 2219 or 2618 at 473 K. Al-Li alloys are likely to be much superior but are still under developmental stage.

TABLE V

Properties of Al-Zn-Mg Alloys

	AA 7005 (148,180)	G 74 S (159,181)
Chemistry :		
Zinc:	3.7 - 4.0	3.6 - 4.4
Magnesium:	1.0 - 1.4	1.8 - 2.2
Manganese:	0.05 - 0.50	0.25 - 0.45
Zirconium/Titanium:	0.08 - 0.20	0.50 total
Copper:	0.2 Max.	0.2 Max.
Iron:	0.4 Max.	0.3 Max.
Silicon:	0.35 Max.	0.9 Max.
Aluminium:	Balance	Balance
Mechanical Properties:		
(T6 condition,Nominal)		
UTS MPa:	350	380
Y S MPa:	270	300
% Elongation:	12	12
Physical Properties		
Young's Modulus GPa	71	72
Specific Gravity	2.78	2.79
Coefficient of thermal expansion cm/cm/K	23.5 x 10 E-6	
Thermal Conductivity cals/cm.s.K	0.29	

TABLE VI

Ultimate Tensile Strength at Higher Temperatures

of various Aluminium Alloys

(All values in MPa)

Temperature K	7005(148)	2219(180)	2618(180)	7075(180)
Room Temp.	350	460	450	580
373	300	420	440	490
423	165	340	350	220
473	97	250	220	110
533	76	200	90	80
583	--	50	50	60

1.12. Properties of TiO_2:

TiO_2 exist basically in 3 grades viz., rutile, brookite and anatase and their basic properties are shown in Table-VII (149-153).

Rutile TiO_2 is more stable whereas anatase and brookite grades exist only under specialised conditions and do not form equilibrium phase of Ti-O system (154). Specially stabilised anatase and brookite grades TiO_2 on heating converts to rutile grade (155,156). Finely ground material gives good plasticity without binders. Glenco Corporation (152) had rolled TiO_2 into microsheets of thickness upto 0.001 mm
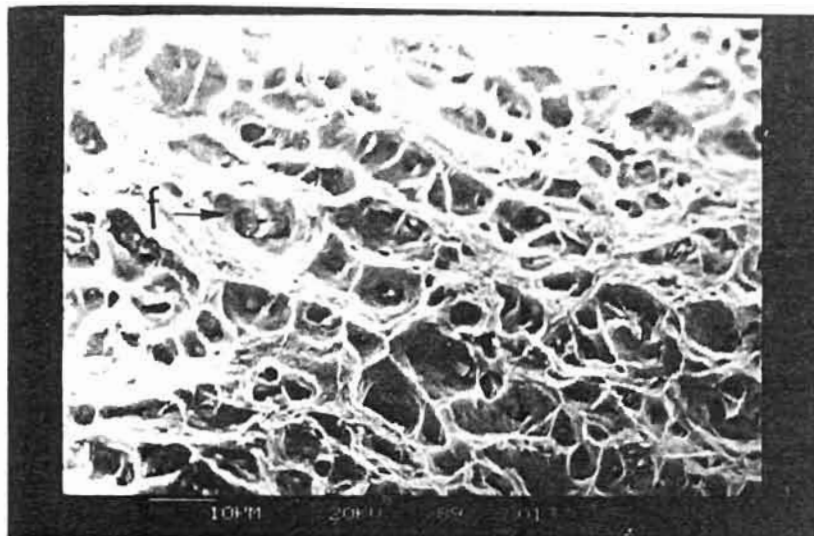
20 um

g.41 : Fractograph of tensile fracture on hot rolled
composite sheet. Reveals deep dimples and
particles inside.

6 um
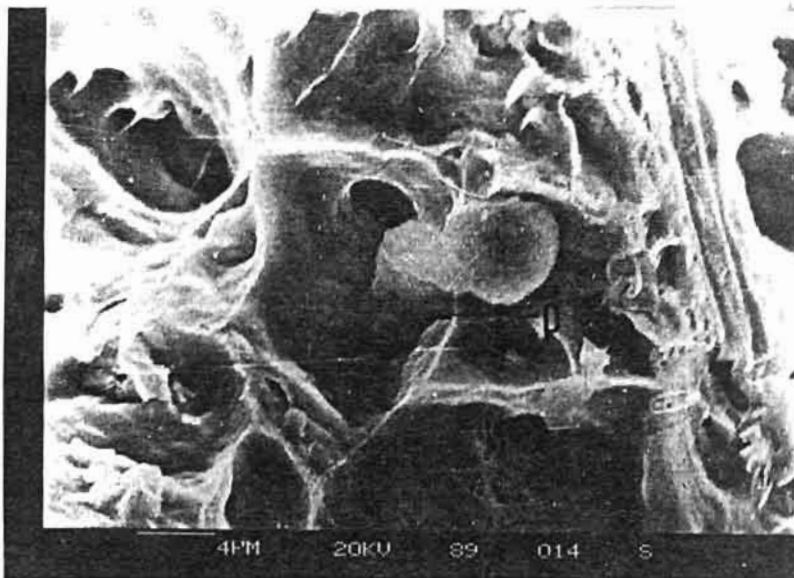
g.42 : Same as above at higher magnification. Shows a
particle, pulled out of a dimple.

1.13. Scope of the present investigation:

Considering the present day status of aluminium technology, the need exist to improve the high temperature properties of Al alloys with required ductility at room temperature for forming into shapes. Though aluminium alloy AA 2219 and AA 2618 are good high temperature alloys, their strength level reduces drastically beyond 423 K as shown in Table VI. This reduction in strength level is due to the dissolution of the hardening precipitates at higher temperatures in the alloy system. Dispersion hardening by particulate dispersoids of sub-micron size on these alloy systems should quite possibly maintain the strength level high, since these dispersoids do not dissolve in the matrix. SiC, Al_2O_3 etc. are some of the high temperature dispersoids already experimented in Al-Cu alloys. Al alloy composite 2124 reinforced with SiC has exhibited a very high strength of 720 Mpa but has very low ductility and poor formability. It is thereby felt necessary to introduce a new system of composite which will have good formability.

Based on the extensive work by the investigator in the Al-Zn-Mg system, it was decided to select the alloy system Al-Zn-Mg of composition corresponding to AA 7005 as the matrix material for the composite. This alloy has a good ductility of about 12% by way of tensile elongation as shown in Table V. TiO_2 has an unfavourable tensile strength of only 56 MPa (Table VII) and is not expected to enhance the

38

strength properties of the composite. Considering the strength value of the matrix alloy (σm) as 350 MPa and that of TiO_2 (σp) as 56 MPa, the strength of the composite (σc) is calculated using the basic rule of mixture of composite as:

$$\sigma c = \sigma m \times Vm + \sigma p \times Vp \qquad (4)$$

where Vm and Vp are the volume fractions of the matrix and the dispersoid respectively. The composite strength at 5 wt% (3.3 vol.%)TiO_2 dispersion is calculated to be about 340 MPa, 10 units less than the strength of the base alloy. TiO_2 has a higher density also. However, the favourable selection criteria for TiO_2 are its higher melting temperature, better thermal stability, spherical shape and finer size of average particle size 0.37 μm and above all, TiO_2 powder is reported to have been rolled into very thin foils and hence the composite sytstem Al-Zn-Mg-TiO_2 is expected to have good malleability (good workability on rolling) and formability. The following are the specific advantages based on the technology of composite synthesis available in the literature for selecting this composite system.

1 .Al-Zn-Mg alloy is a medium strength , weldable and heat treatable wrought aluminium alloy with high ductility and formability.

2. Mg content of the alloy is likely to lead to better wettability with the particulate dispersoid.

39

3. TiO_2 is reported to have been rolled into thin sheets without the use of any binders and the composite containing TiO_2 is also presumed to have good workability on rolling.

4. Sub-micron size TiO_2 dispersoids (average particle size- 0.37 micron) is expected to impart some amount of dispersion hardening effect in the composite system.

5. Such dispersoids are also expected to improve the high temperature properties of the system.

6. For the expected dispersion strengthening effect in this composite at room temperature, it is sufficient to introduce about 3 Vol% (5 Wt%) of the dispersoids.

Keeping the above said objectives in mind, the scope of the present study is limited to the following areas.

1. Synthesising the composite Al-Zn-Mg-5wt.% TiO_2 by both liquid metalurgy and rheocasting technique and study of the characteristics of the composite .

2. Investigation of the effect of TiO_2 on solidification, cast microstructure, dendrite arm spacing and grain size.

3. Study of the effects of particulate dispersion on forgeability, extrudability (includung solid extrusion, semi - solid extrusion and semi - liquid extrusion) and rolling (both hot rolling and cold rolling).

4. Effect of thermomechanical treatment and heat treatment on the alloy composite.

5. Evaluation of properties at various stages of processing and evaluation of properties at high temperatures.

6. Structure - property correlation at various stages of processing and analysis of the products during the composite synthesis.

CHAPTER II
EXPERIMENTAL
METHODS & MATERIALS

THE   PROCESS FLOW SHEET FOR THE COMPOSITE SYNTHESIS

IS GIVEN IN THE NEXT PAGE.

Al-Zn-Mg-TiO2 Particulate Composite

Process Flow Sheet

Raw Materials   : G74S (Al-Zn-Mg Alloy)

Anatase Grade TiO_2 Powder of APS 0.37 Microns

Consolidation   : Liquid Metallurgy technique

Rheocasting technique

Thermal Treatment   : Homogenisation

Mech. Treatment   : Forging

    Extrusion : Solid extrusion

                 Semi-solid extrusion

                 Semi-liquid extrusion

    Rolling   : Hot rolling

                 Cold rolling

Thermo-mechanical Treatment of Hot Rolled Sheet

Thermal Treatment of Extruded and Cold Rolled Products

Products   : Extrusions   : 17 mm Dia Rods

             Hot Rolled Sheets : 1 . 8 - 3 . 8 mm thickness sheets

             Cold Rolled Sheets : 0 . 10 - 1 . 4 mm thickness sheets

Analysis   : Metallography   : Optical metallography

                                  SEM

                                  TEM

         Mech. Properties : Room temperature

                              High temperature

         Phy. Properties : Young's Modulus

                              Thermal Conductivity

                              Density

11.1 Matrix Alloy and the Dispersoid used.

The basic raw materials for the synthesis of composite in this study include the commercial Al-Zn-Mg alloy G74S (AA 7005) as the matrix alloy and TiO_2 powder as the reinforcement dispersoid. G74S aluminium alloy was procured from M/s Indian Aluminium Company in homogenised and as extruded condition. This extruded bar stock was used as the matrix base alloy for reinforcing TiO_2 dispersoids. The basic properties of G74S alloy are tabulated in Table-VIII (148,157-159).

The reinforcing material TiO_2 powder was procured from M/s Travancore Titanium Products Limited, Trivandrum. The properties of the powder are given in Table-IX. The powder was subjected to particle size analysis in Micrometrics Model USA make Particle Size Analyser. The powder was dispersed in dilute sodium silicate solution and the PH of the slurry was maintained at 9.0. The testing was done at 306 K. The particle size distribution graph is shown in Fig.3. It may be observed that 95% of the particle size varied from 0.15 to 1.5 microns, with the average particle size at 0.37 microns. The size distribution varies as:

98 %	Below	1.5	microns
90 %	''	0.8	''
80 %	''	0.6	''
70 %	''	0.45	''
50 %	''	0.37	''
35 %	''	0.25	''
15 %	''	0.15	''

The powder was also subjected to x-ray diffraction studies as per annexure-2 and the results are shown in the table- IX.

TABLE-VIII

PROPERTIES OF G74S ALUMINIUM ALLOY

----

1. Source   : Indian Aluminium Company Ltd.,Alwaye.

		Range	Measured Value
2.**Chemical composition**			
(Wt.per cent) : Zn		: 3.6-4.4	4.15
Mg		: 1.8-2.2	2.12
Mn		: 0.25-0.45	0.29
Zr		: 0.08-0.20	0.15
Ti		: 0.01-0.06	0.01
Cu		: 0.10 Max.	0.06
Fe		: 0.90 Max.	0.22
Si		: 0.5 Max.	0.28
Others		: 0.05 Max.	No traces.

3. Liquidus temperature (148): 916 K

   Solidus temperature (148) : 877 K

4. Mechanical properties (158)   UTS   : 390 MPa
   (T6 condition)   0.2% YS: 340 "
                                 E   : 15%

5. Elastic Modulus (159)   : 70 GPa

TABLE-IX

Properties of TiO$_2$ Powder used in this Investigation

```
-----------------------------------------------------------------

Source             : Travancore Titanium Products Ltd.Trivandrum

Grade              : Anatase ( XRD Analysis )

Crystal
Structure          : Tetragonal (    ,,   )

Lattice
Constants (A)      : a  =  3.78

                   : c  =  9.5153

Chemical
Composition        : TiO2           : 98.5
( wt % )             Soluble Salts : 0.4
                     P2O5          : 0.42
                     Moisture      : 0.25

Particle Size
Distribution       : Average Particle Size 0.37 microns.


Colour             : Snow White.
-----------------------------------------------------------------
```

SAMPLE IDENTIFICATION : TITANIUM DIOXDE UNTREATED

DENSITY : 3.9 g/cc

PREPARTION : DISPERSED WITH SODIUM SILICATE : pH OF THE SLURRY :9.0

START DIA : 28 μm

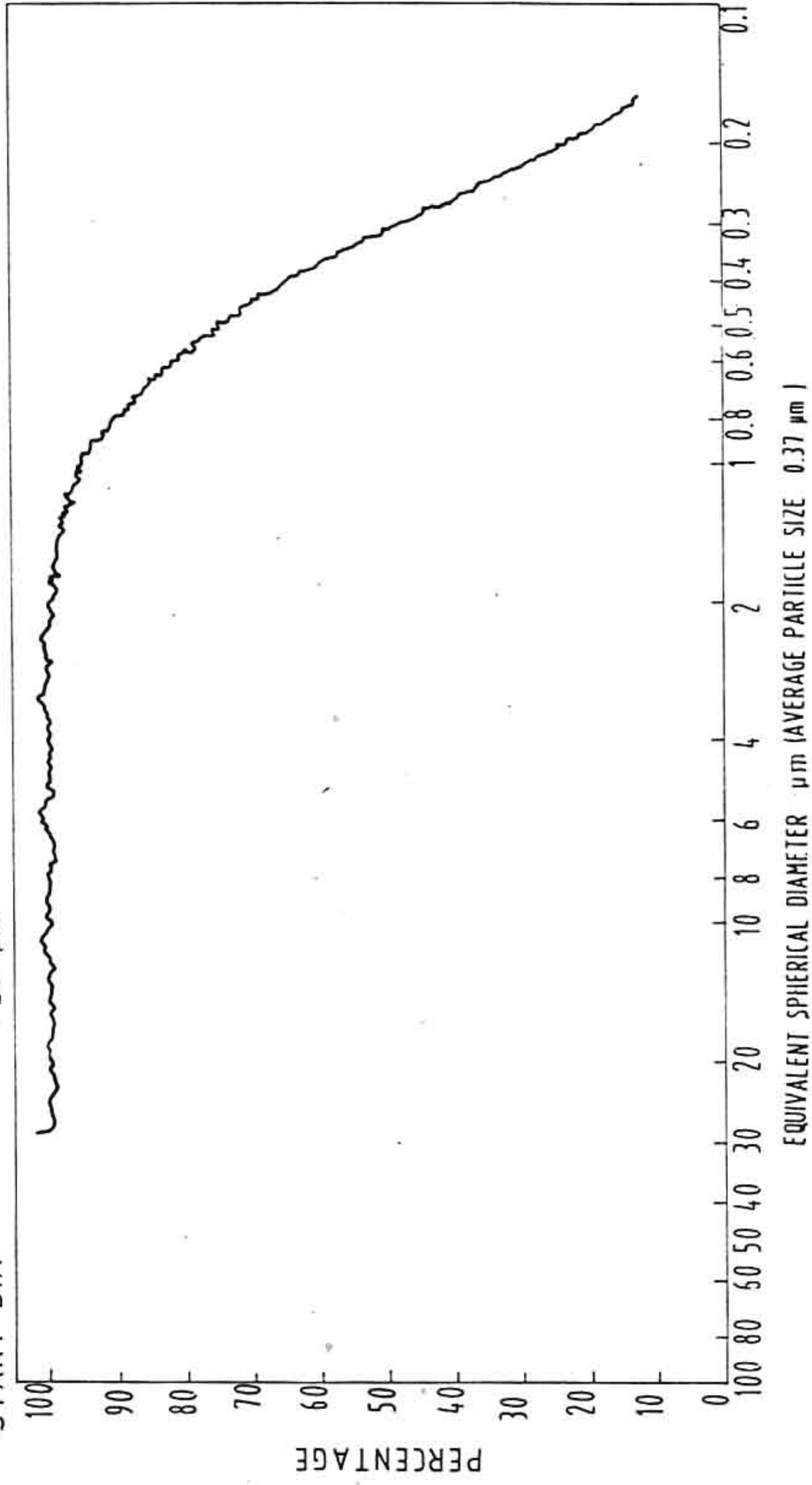EQUIVALENT SPHERICAL DIAMETER μm (AVERAGE PARTICLE SIZE 0.37 μm)

FIG. 3. PARTICLE SIZE DISTRIBUTION OF UNTREATED Ti O₂

PERCENTAGE

11.2 **Processing Methods:**

Processing of the composite include the following steps:

1. Synthesis of composite.

2. Homogenisastion.

3. Forging.

4. Extrusion.

5. Heat Treatment.

6. Rolling.

7. Tests and Evaluation

II.2.1. Synthesising the composite:

Synthesis of the composite is done by casting or solidification route. Casting is done by both liquid metallurgy (LM) and Rheocsting (RC) techniques. Typical steps involved in the process are schematically illustrated in Fig.4.

In LM technique, about 6.5 kg. of the base alloy (G74S) was thoroughly cleaned by wire brush to remove oxide and any foreign materials. About 5 wt percent (325 gms) TiO_2 powder was taken in a clay graphite crucible. The base alloy was then separately melted in a clay graphite crucible in the electric resistance pit furnace maintained at 1073 K. The crucible containing TiO_2 was also preheated at this temperature of 1073 K in the same furnace for 2 hours. When the alloy was thoroughly molten, an aluminium silicate clay coated and preheated impeller was introduced into the melt. The impeller was attached to the flexible shaft of an electric motor, of variable speed. A Vortex was formed and maintained in the melt at a mechanical agitation of 300 rpm. The preheated TiO_2 powder was then steadily added to the Vortex of the melt, using a spatula at an average rate of about 15 gms per minute. After the completion of the dispersions, the melt was isothermally held and stirred for another 30 minutes, then degassed using dry nitrogen gas, and stirred and cast into 90mm diameter x 200 mm high cylindrical billet and 100 x 100 x 200 mm length rectangular billet using preheated (573 K) permanent moulds. The pouring temperature was maintained at 993 K.

45

(a)

i: Al -750°C

ii: ADD Ti O$_2$ HOT PARTICLES 750°C

iii. DEGASSING-N$_2$

iv. HAND STIRRING

v. CASTING 720°C

LIQUID METALLURGY

(b)

i. FREEZING RANGE

ii. ADDITION OF HOT PARTICLES

iii. CASTING ABOVE SOLIDUS
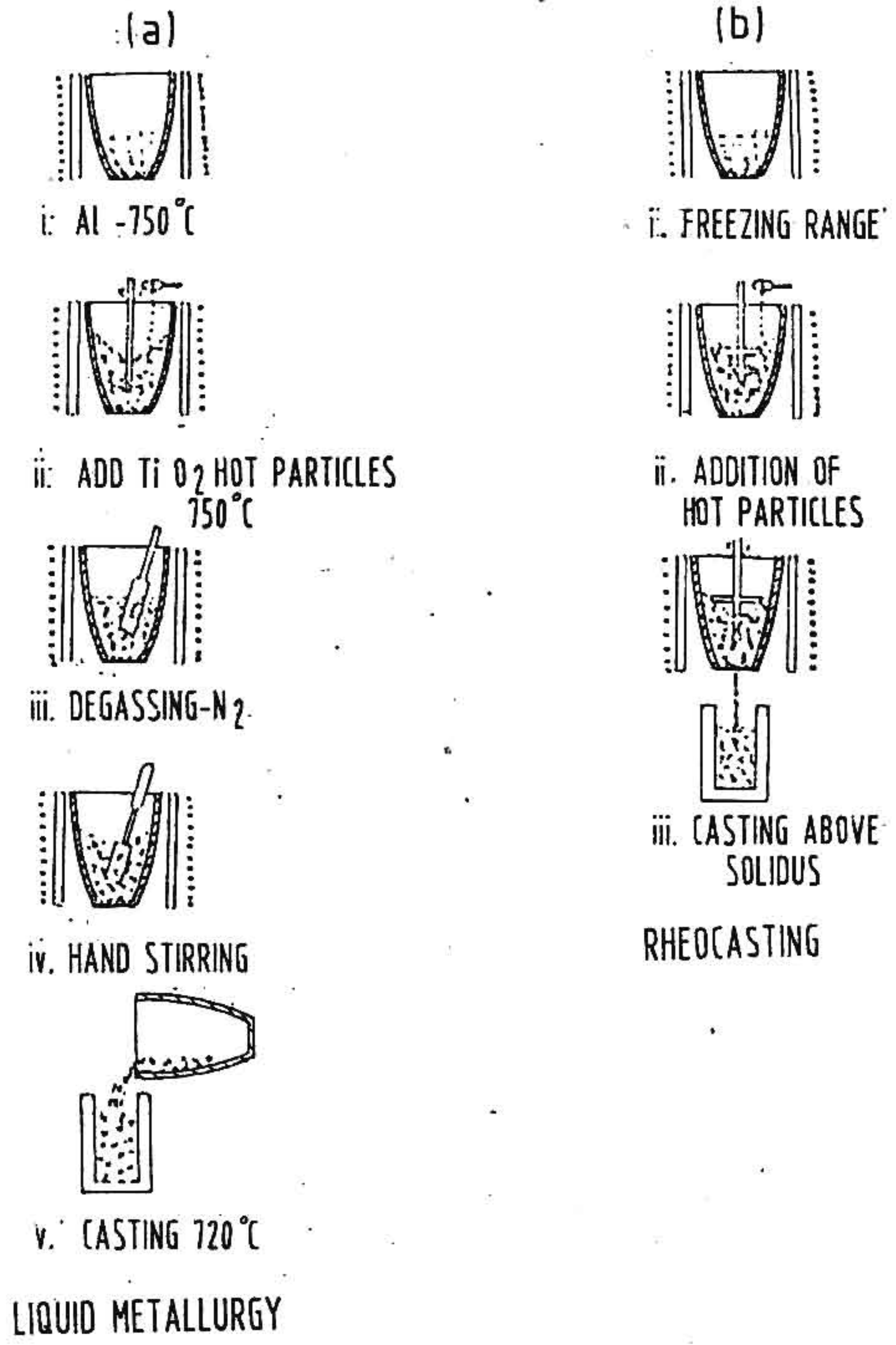
RHEOCASTING

FIG. 4. TYPICAL STEPS INVOLVED IN PREPARATION OF COMPOSITES

In RC technique, about 10 kg. of the matrix alloy was melted in the electric resistance bottom pouring furnace, known as the Rheocaster (160). The rheocaster was a locally fabricated system with 20 kg of aluminium melt capacity, working temperature of 1073 K, clay coated steel impellers and bottom pouring type. The melt was then cooled down to 893 K (freezing range 873-916 K) to a slurry form (semi-solid state). The slurry was then mechanically agitated at 400 rpm using the same impeller set up, as used in LM technique, to form the Vortex. 5 wt per cent (500 gm) of TiO_2 powder, pre-heated to 1073 K for 2 hours was then steadily added to the Vortex at an average rate of 10 gm per minute.

After complete addition of the powder, the slurry was stirred at 300 rpm for another 30 minutes and then bottom poured to preheated moulds of two sizes viz., 90 x 150 x 200 mm and 90mm diameter x 200 mm length. The pouring temperature was noted as 893 K.

11.2.2. Homogenisation:

Prior to homogenisation, the cast billets were visually examined and surface machined to remove the surface defects. The end faces were macro etched with 0.5% HF to reveal the as cast structure. Specimens were cut and subjected to microstructrual investigations. The billets were then homogenised in an air circulating furnace at 733 K for 24 hours to dissolve the eutectic at the grain boundaries and make it suitable for further mechanical processing. Billets were also subjected to scanning electron microscopic studies and x-ray diffraction analysis. The dispersoids were further extracted by chemical method (annexure-1) and subjected to x-ray diffraction analysis.

11.2.3. **Forging:**

Forging operations were carrried out using a 500 tonne capacity John Shaw model, Indian Make hydraulic press. The LM cast billets were preheated at 733 K for 2 hours in a billet heating furnace and hot forged within a close temperature range of 733 - 693 K Temperature crayons (Tempil sticks) were used to check the temperature measurements over the billets. Crayon markings evaporate at temperatures above that specified on them. Crayons with temperature specifications of 733 and 693 K were used during these operations. Forging was carried out in two steps with an intermittent annealing at 733 K for 30 minutes. 30% reduction in thickness was given in the first step. During further reduction of 20% in the second step, side cracks developed on the forging stock and the forging operation was discontinued.

A Similar effect was observed on a trial forging of the RC cast billet also.

II.2.4. Extrusion:

Extrusion was carried out using an extrusion die set up designed and fabricated indigenously to be operated by a hydraulic press of 500 tonne capacity. The extrusion container is of size 80 mm diameter x 170 mm length with the die opening of size 17 mm diameter. This extrusion reduction from 80 mm to 17 mm diameter gives an extrusion ratio of 21. The homogenised billets were machined to 78 mm diameter and extrusion was carried out using a graphite back up plate. The extrusion die assembly was preheated to 573 K using a furnace designed for the purpose prior to extrusion. The billets were subjected to 3 types of extrusion.

i) Solid extrusion(SE) wherein the LM cast billets were heated to the normal hot working temperature of 733 K for 3 hours and then extruded. The extrusion was complete at a maximum load of 500 tonnes.

ii) Semi-solid extrusion(SSE) wherein, the RC cast billets were heated just above the solidus temperature (877 K) of the matrix alloy and then extruded in the semi-solid state. A load of 300 tonnes was sufficient to complete the extrusion.

iii) Semi-liquid Extrusion(SLE) wherein the RC cast billets were initially heated in the extrusion die above the liquidus temperature of the matrix alloy (916 K) and then cooled down to about 900 K and then extruded. The extrusion was again complete within a load of 300 tonnes.

49

11.2.5. **Heat Treatment of Extruded Composite Sections:**

Heat treatment of extruded sections were carried out in line with that of the base alloy as established earlier by the investigator (145).The solution treatment was carried out by heating at 723 K for 3 hours in an electrical resistance air circulating furnace, followed by quenching in water maintained at room temperature (303 K). The sections were then preaged at 378 K for 4 hours followed by reaging at 393 K for 20 hours. Heat treated rods were subjected to microstructural analysis and evaluation of mechanical properties.

11.2.6. **ROLLING:**

RC cast billet of rectangular cross section, after homogenisation were subjected to rolling operation, using a Carl Wezel model rolling mill. The billets of thickness 90 mm were surface machined and cut into two pieces of size 35mm each, to suit the roll gap of the rolling mill. The billets were initially heated to 733 K, held for two hours and hot rolled in the temperature range of 733 K - 693 K. When the temperature dropped below 693 K the billets were subjected to intermittent annealing at 733 K for 30 minutes. The rolling load was noted as 4000 kg on the rollers. Hot rolling was done at a speed of 20 meters per minute, with a sequence as shown in Table-X.

Billets of thickness 35 mm were reduced to 3.8 mm sheets in 5 heats. Percentage reduction in each heat varied from 23% for the first heat to 46% for the last heat. The 3.8 mm sheets were further warm rolled to finish sizes of 2.6, 2.3, 2.0 and 1.8 mm thickness without any intermittent heatings. The percentage reduction varied from 63% for 2.6 mm thickness to 74% for the 1.8 mm thickness sheets. Total percentage reduction in thickness from 35 mm to 1.8 mm is 95. It was observed that the material was very malleable and the rolled surface was very smooth with no edge cracks. Mechanical properties were evaluated for 3.8 mm thickness sheets in the hot rolled condition. These sheets of 3.8 mm thickness were further subjected to various thermomechanical treatments

51

TABLE-I

Hot Rolling Operation Sequence for the composites

Steps	Starting Thickness (mm)	Soaking Temp. 733 K Time in Minutes	No of Passes at 2 mm reduction per pass.	Finish Thickness mm.	Reduction % Stage wise	Total
1	35	120	4	27	23	23
2	27	30	4	20	26	43
3	20	30	4	13	35	63
4	13	30	3	7	46	80
5	7	30	1-5	3.8	46	89
			Warm Roll Finish	2.6	63	92.5
				2.3	67	93.4
				2.0	71	94.3
				1.8	74	95

(TMT) as shown in Table XI. TMT schedules were selected based on the investigator's earlier findings (161) on the base alloy systems that final TMT enhances the mechanical properties of the alloy. Mechanical properties were evaluated after each TMT operation .

All the hot rolled sheets were then subjected to cold rolling operation without an intermittent annealing treatment, using the 4-High rolling mill. The scheme of cold rolling operations carried out is tabulated in Tables XII to XVI. Total percentage reduction on cold rolling to finish size is shown in Table XVII.

3.8 mm sheets were rolled down to 1.4 mm thickness in 10 stages (Table XII), at each stage the reduction in roll gap was not more than 0.2 mm.

2.6 mm thickness sheets were rolled to 4 finish sizes as 0.65, 0.50, 0.40 and 0.35 mm thicknesses (Table XIII) with total reduction in thickness varying from 75% to 87%.

2.3 mm thickness sheets were cold rolled to finish sizes of 0.60 and 0.20 mm thicknesses (Table XIV) with reduction percentages of 74 and 91 respectively.

2.0 mm thickness sheets were rolled to 0.70 and 0.35 mm thickness sheets with reduction percentages of 65 and 83 (Table XV).

1.8 mm sheets were rolled to 0.2, 0.15, and 0.10 mm foils with reduction percentages of 89, 92 and 94 respectively (Table XVI).

52

TABLE - XI

Heat Treatment of Hot Rolled Composite Sheets
(thickness 3.8 mm)

Solution Treatment	:	733 K / 3 Hours
	:	Water Quench
Precipitation Treatment	:a)	413 K / 36 Hours
	b)	378 K / 4 Hrs.+ 413 K / 24 Hrs
	c)	378 K / 4 Hrs.+ 393 K / 20 Hrs
	d)	378 K / 4 Hrs.+ 10% CW + 413 K / 24 Hrs.
	e)	10% CW + 378 K / 4 Hrs. + 413 K / 24 Hrs.
	f)	10% CW + 413 K / 24 Hrs.

TABLE-XII

Cold Rolling Schedule for the composites

(for Reduction in thickness from 3.8 to 1.4 mm)

Steps	Starting Thickness mm	Reduction set. mm	Rolling Load 1000 Kg	No of Repeat Passes	Finish Thickness mm	Total Reduction Percent
1	3.8	1	40-18	6	3.1	18
2	3.1	0.3	35			
		0.1	30			
		0.1	30			
		0.1	34-25	3		
		0.2	30			
		0.2	32		2.4	37
3	2.4	0.2	38-28	3		
		0.3	38-30	2	1.8	53
4	1.8	0.3	36-22	2	1.4	63

TABLE XII.1

Cold Rolling Schedule for Composites. (Reduction in thickness from 2.6 mm to 0.65, 0.50, 0.40 and 0.35 mm).

Steps	Starting thickness (mm)	Roll gap reduction (mm)	Roll Load 1000 Kg	No. of Passes	Finish thickness (mm)	Total Percentage Reduction
1	2.6	0.5	38-25	3		
		0.3	35-25	2		
		0.3	35-20	3	1.8	30
2	1.8	0.3	32	1		
		0.2	33	1		
		0.2	32	1		
		0.2	30	1	1.2	54
3	1.2	0.3	32	1		
		0.2	30	1		
		0.2	30	1	0.65	75
4	0.65	0.2	30	1	0.50	81
5	0.5	0.2	25	1	0.4	85
6	0.4	0.2	25	1	0.35	86.5

TABLE XIV

Cold Rolling Schedule for Composites.

(Reduction in thickness from 2.3 mm to 0.6 and 0.2 mm).

Steps	Starting thickness mm	Roll gap reduction mm	Roll load 1000 Kg	No of pass	Finish thickness mm	Total Percentage Reduction
1	2.3	0.5	35-25	3		
		0.3	32	1		
		0.3	32	1		
		0.3	32-30	3	1.10	52
2	1.1	0.3	33	1		
		0.3	32-20	2	0.60	74
3	0.6	0.3	33	1		
		0.2	32-25	3	0.20	91

TABLE XV

Cold Rolling Schedule for Composites.

(Reduction in thickness from 2.0 mm to 0.7 and 0.35 mm).

Steps	Starting thickness mm	Rol gap reduction mm	Roll load 1000 Kg	No of pass	Finish thickness mm	Total Percentage Reduction
1.	2.0	0.5	35-22	3		
		0.3	32	1		
		0.2	32-25	2	1.2	40
2.	1.2	0.2	30	1		
		0.2	30	1		
		0.2	30-20	2	0.7	65
3.	0.7	0.2	30	1		
		0.1	25	1		
		0.1	25-20	2	0.35	82.5

TABLE XVI

Cold Rolling Schedule for Composites.

(Reduction in thickness from 1.8 mm to Ø.2, Ø.15 and Ø.1Ø mm)

Steps	Start thickness mm	Roll gap Reduction mm	Roll load 1ØØØ Kg	No of pass	Finish thickness mm	Total percentage Reduction
1.	1.8.	Ø.3	3Ø	1		
		Ø.2	32	1		
		Ø.2	32-28	2	1.4	22
2.	1.4	Ø.2	3Ø	1		
		Ø.2	32	1		
		Ø.2	32-3Ø	2	1.Ø	44
3.	1.Ø	Ø.3	32	1		
		Ø.3	3Ø	1		
		Ø.2	3Ø-25	2	Ø.4	78
4.	Ø.4	Ø.2	3Ø-25	3	Ø.2	89
5.	Ø.2	Ø.1	28-25	2	Ø.15	92
6.	Ø.15	Ø.1	27-25	2	Ø.1Ø	94

TABLE-XVII

Total Percentage Reduction on cold rolling of composites to Finish Size

S.No.	Hot Rolled Sheet Thickness mm.	Cold Rolled Finish Thickness mm.	Reduction %
1-1	3.8	1.4	63
2-1	2.6	0.65	75
2-2	2.6	0.50	81
2-3	2.6	0.40	85
2-4	2.6	0.35	86.5
3-1	2.3	0.60	74
3-2	2.3	0.20	91
4-1	2.0	0.70	65
4-2	2.0	0.35	82.5
5-1	1.8	0.20	89
5-2	1.8	0.15	92
5-3	1.8	0.10	94

Mechanical properties of the as-cold rolled sheets were evaluated .

Cold rolled sheets were then subjected to a series of thermal treatments as listed in Table XVIII. Several possible combinations of thermal treatments were carried out to investigate the influence of the TiO_2 dispersoids on the ageing charecteristics of the alloy system. The sheets were then solution treated at 733 K for 3 hours and quenched in water, as is the case for the base alloy system. Both natural ageing and artificial ageing were carried out. Artificial ageing was carried out at 417 K in one instance and as a double ageing with preageing at 378 K followed by reageing at 393 K in the other instance. Reageing time was varied upto 40 hours, as was done earlier on the base alloy system (145). Mechanical properties were evaluated in each case.

Heat treated sheet of 0.65 mm thickness was subjected to high temperature tensile tests upto 473 K. Optical, Scanning and Transmission Electron Microscopic studies and X-Ray Diffraction analysis were conducted on various sheet samples. Physical properties like modulus of elasticity and density of the rolled sheet samples were experimentally conducted.

The matrix alloy was also initially hot rolled from 30 mm thickness down to 2.6 mm thickness (91%) with 5 intermittent heatings using the same rolling parameters as used for the

53

TABLE-XVIII

Heat treatment Schedule for Cold Rolled Composite Sheets

Solution Heat treatment   : 733 K / 3 hours

                               Water Quench

Precipitation Hardening

A. Natural Ageing   : 5 days

B. Artificial Ageing

   a) full ageing   : 417 K / 36 hours

   b) preageing   : 378 K / 4 hours +

  + reageing   b1   : 417 K / 24 hours.

           b2   : 393 K / 5 hours.

           b3   : 393 K / 10 hours

           b4   : 393 K / 15 hours

           b5   : 393 K / 20 hours

           b6   : 393 K / 30 hours

           b7   : 393 K / 40 hours

----

composites. The hot rolled sheets were further cold rolled upto 0.6 mm thickness (77%) in 10 steps with average roll gap reduction of 0.2 mm at each stage. Rolling was discontinued at 0.6 mm thickness, when cracks developed at the edges of the sheets.

II.2.7 **Tests and Evaluation:**

The scheme of tests and evaluations carried .out on this composite synthesising is given below:

1. Cast billets : Chemical analysis

Macro structure

Optical Microstructure

SEM Analysis

EDAX Analysis

XRD Analysis on the cast billet and on the dispersoid extracted from the billet

Evaluation of particle size distribution

Microhardness testing

Thermal conductivity measurements

Density measurements

2. Forgings : Optical microstructure

SEM Analysis

Fractographs

3. Extrusions : Surface feature analysis

Optical microstructure

SEM Analysis

Microhardness testing

Evaluation of particle size distribution

Mechanical properties evaluation

Fractography

Thermal conductivity measurements

Density measurements

55

4.Sheets :   Optical metallographic studies

                       TEM Studies

                       SEM Analysis

                       Room temperature mechanical testing

                       High temperature Mechanical testing

                       Determination of Youngs Modulus
                       using strain gauges

                       Fractography

                       Density measurements

11.2.7.1. Chemical analysis

Zn and Mg were analysed by gravimetric method using atomic
absorption spectophotometer of model Varian Techron AA 1275
and standards synthesised from high purity metals to
conform to the alloy specification. Zr was only a trace
addition and was confirmed by EDAX analysis. TiO_2 was
extracted from composite as detailed in Annexure 1 and
evaluated quantitatively.

11.2.7.2. Macrostructure.

Cast billets were surface turned in a lathe and polished in
'O' grit emery paper. The polished surface was then
macroetched with 5% HF solution for about a minute which
revealed a clear macrostructure of the composite.The
macrostructure was recorded by a camera using colour film.

56

II.2.7.3. Microstructure.

Specimens were prepared at various stages of processing and polished by conventional means using alumina/diamond paste in wet polishing wheels. Etching was done using Keller's reagent (2 ml of 48% HF + 3 ml of HCl + 5 ml of HNO_3 in 190 ml water) for 10 seconds. Microstructure details were analysed and recorded using MeF2 optical microscope and Stereoscan 250 MK3 model scanning electron microscope.

II.2.7.4. Microhardness testing.

Microhardness testing was used to evaluate the hardness of the dispersoids which was not possible using the conventional hardness testing techniques. Leitz miniload microhardness tester with a load of 50 gms was used for the purpose.

II.2.7.5. EDAX Analysis.

Elemental compositions of various constituents in the microstructure were qualitatively estimated using energy dispersive analysis of X-Rays (EDAX) of model EDS TN 5502, an attachment to the SEM.

II.2.7.6. Fractograph.

Fracture surfaces of the tensile tested samples were examined and fractographs were recorded using SEM.

II.2.7.7. Electron microscopy.

Jeol 100 KV JEM 100 B and Phillips 125 KV CM 12 transmission electron microscopes were used for both microstructural details and diffraction analysis. Samples for TEM were prepared by thin foil technology. Thin foils were initially prepared by chemical thinning using the acid mixture containing phosphoric acid + nitric acid + sulphuric acid. Final samples were prepared by electrolytic thinning (window method) using 10% perchloric acid ($HClO_4$) in 90% methanol (CH_3OH) at 8V and 0.15 A/sq.cm current density with stainless steel cathode. Thinning was done at a temperature of 273 K. No reactions were noticed during this thinning operation. However, partial fall out of particles was observed in some areas creating some voids in the samples.

II.2.7.8. X-Ray diffraction.

X-ray diffraction studies were made as detailed in annexure 2 using Phillips X-ray generator PW 1729 and diffractometer control PW 1710.

II.2.7.9. Mechanical properties.

Mechanical properties were evaluated by tensile testing at room temperature and at temperatures upto 583 K using 4206 model Instron testing machine. Tensile tests were made at a cross head speed of 2 mm per minute, using standard specimens shown in figure 5. -

58
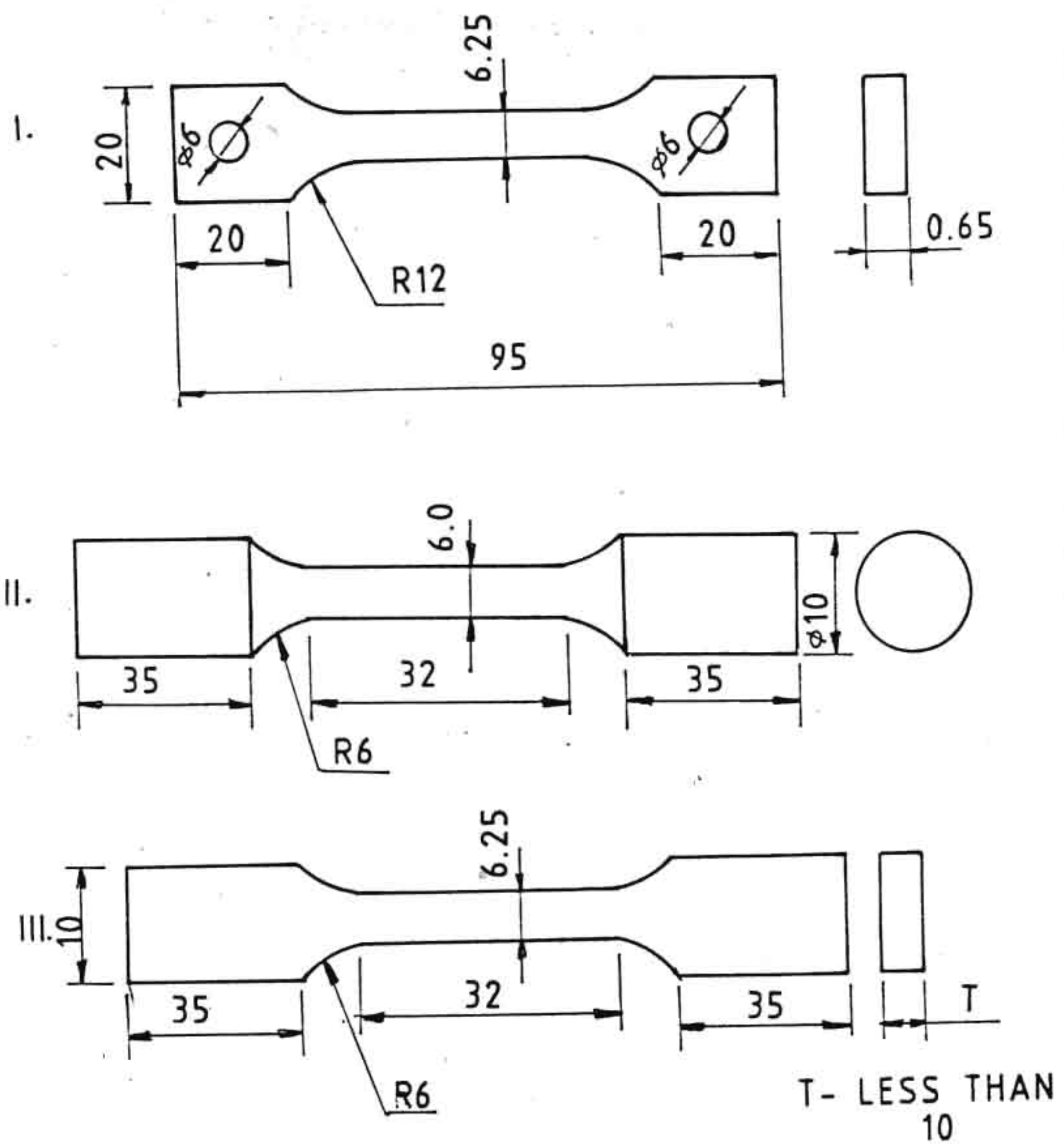
(All dimensions in mm)

I- HIGH TEMPERATURE SPECIMEN
II-ROUND SPECIMEN
III-FLAT SPECIMEN

FIG. 5. STANDARD TENSILE SPECIMENS (ASTM B 557 M)

11.2.7.10.Physical properties.

Density of the composite was determined by basic Archimedes principle. Thermal conductivity was measured by thermal comparator. Young's modulus was determined using strain gauges and Instron testing machine. The samples were cyclic loaded for 3 times within the elastic limit to stabilise the strain gauges. Loading was continued upto the fracture point in the 4th cycle. Both Young's modulus and poisson's ratio were calculated from the stress-strain data.

CHAPTER III
RESULTS & DISCUSSIONS

III.1 **Castings:**

III.1.1. **Melt Characteristics:**

The melt temperature from the molten state prior to the addition of the particulate and upto the casting stage was measured using a sheathed chromel-alumel thermocouple dipped into the melt. The results are plotted in Fig.6. It is observed that in both the casting techniques, there is an initial temperature drop (from 1033 K to 993 K for LM route and from 933 K TO 893 K for RC route)followed by an increase in temperature (from 993 K to 1073 K for LM route and from 893 K to 923 K for RC route) during the composite synthesis and final drop after the particles are dispersed. The initial temperature drop is due to the immersion of the preheated mechanical stirrer into the melt to form the vortex. It is generally understood in all aluminium alloy composites reported earlier that the temperature drop further continues with the addition of the particulates. However, in this case, it is very unusual that the temperature rises during the composite synthesis on the addition of the TiO_2 particulates. This is well understood by one of the possible exothermic chemical reaction (162) between the particulate TiO_2 and magnesium present in the base alloy.

60
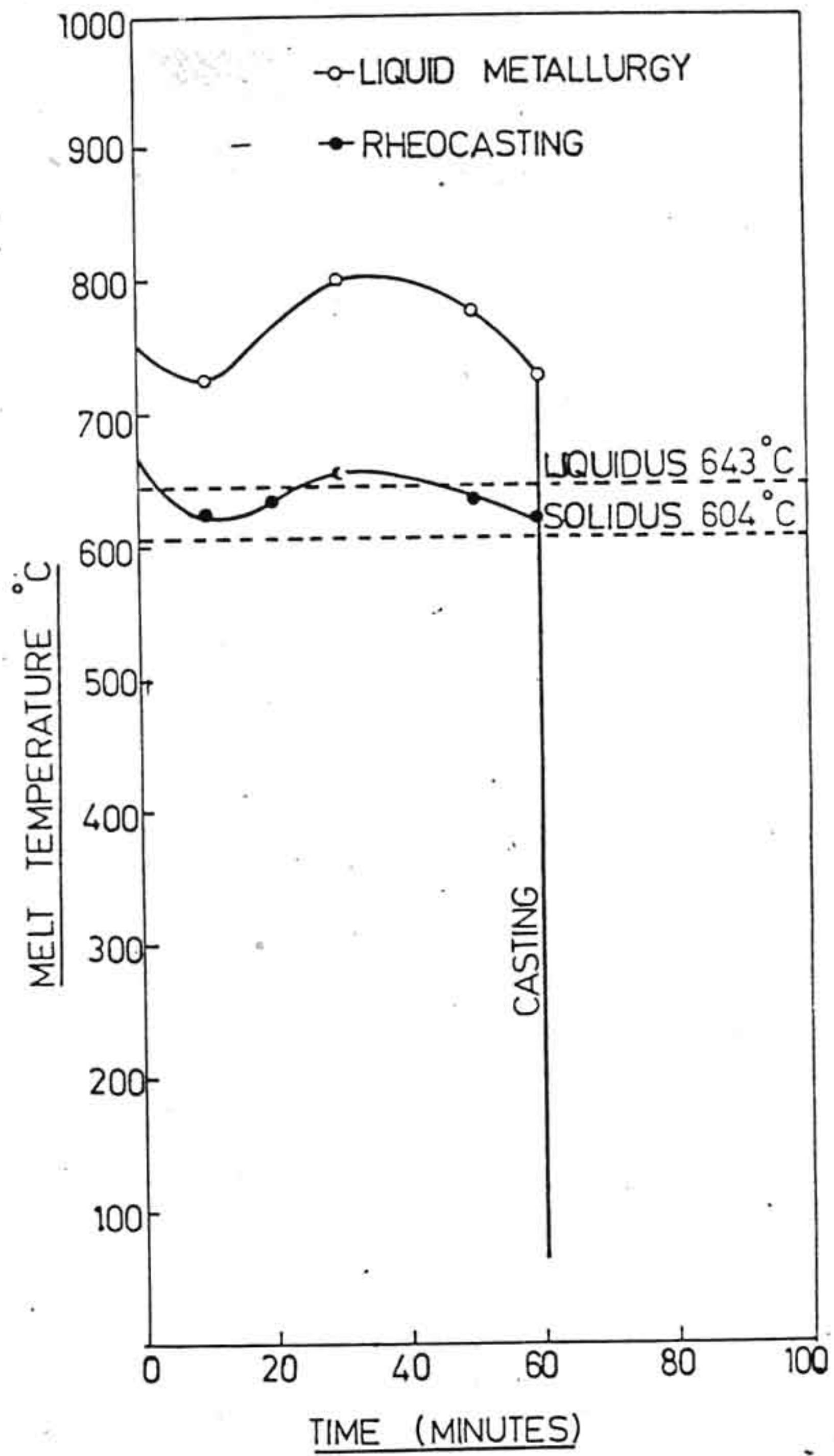
FIG. 6. TYPICAL TEMPERATURE PROFILE OF
THE COMPOSITE MELT
DURING SYNTHESIS

The possible chemical reactions are as follows :

1. Reaction between Al and TiO_2.

$4\ Al\ +\ 3\ TiO_2\ =\ 2\ Al_2O_3\ +\ 3\ Ti$, $\pounds G(1100) = -422.54\ KJ.$ -   (5)

2. Reactions between Mg and TiO_2

$Mg\ +\ 2\ TiO_2$ $=\ MgO\ +\ Ti_2O_3$, $\pounds G(1100) = -209.13KJ.$ -   (6)

$Mg\ +\ Ti_2O_3$ $=\ MgO\ +\ 2TiO$, $\pounds G(1100) = -132.82KJ.$ -   (7)

$Mg\ +\ TiO$ $=\ MgO\ +\ Ti$, $\pounds G(1100) = -47.61\ KJ.$ -   (8)
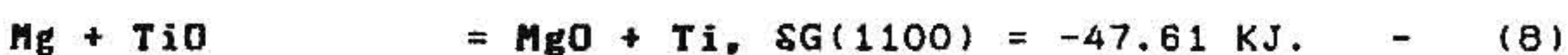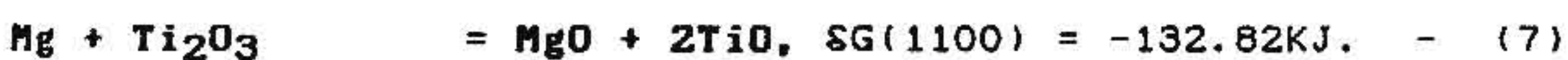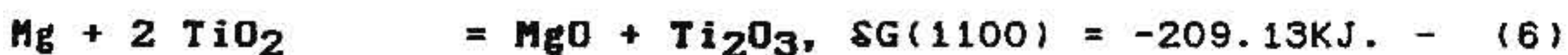
3. Reactions between MgO and TiO_2

$2MgO\ +\ TiO2\ =\ 2MgOTiO_2$, $\pounds G(1100) = -24.14\ KJ$ -   (9)

$MgO\ +\ TiO_2\ =\ MgOTiO_2$, $\pounds G(1100) = -22.90\ KJ$ -   (10)

$MgO\ +\ 2TiO_2\ =\ MgO\ 2TiO_2$, $\pounds G(1100) = -26.92\ KJ$ -   (11)
$(\ MgTi_2O_5)$
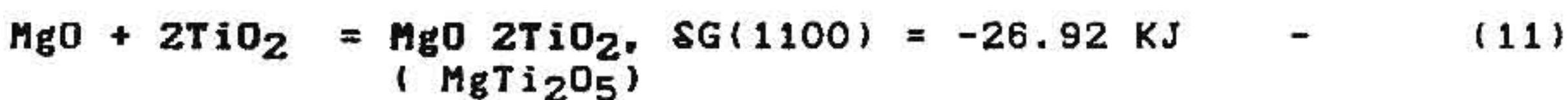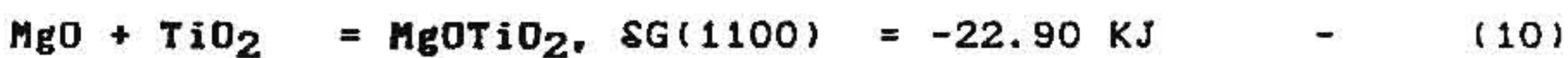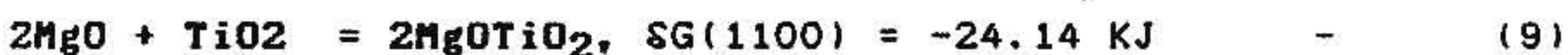
4. Reaction between Ti_2O_3 and O_2.

$2Ti_2O_3\ +\ O_2\ =\ 4\ TiO_2$ -   (12)

However, which of these reactions would be predominant during
the processing of the composite depends upon the relative
concentrations of the participating species and the kinetics
of individual reactions.

Evidence for the exothermic nature of the above reactions
were the appearance of sparks in the melt during the
additions of TiO_2 and subsequent mixing. The extent of this
effect could be seen from the temperature profile of the melt

61

(Fig.6),noting that furnace power was cut off during the dispersions. Though the temperature rise during the synthesis is evident. from the temperature profile (Fig.6), the same could not be calculated theoretically for want of sufficient thermodynamic data on the reaction systems. The rise in temperature subsided with the completion of the chemical reaction as also indicated by the absence of further sparks in the melt and the melt temperature started falling down when it was cast into the billets.

III.1.2. **Chemistry of the composite:**

Samples from both RC and LM cast composites were subjected to chemical analysis for Zn, Mg and TiO_2. Zn and Mg were analysed as 3.9% and 1.2% by weight, respectively. Insoluble dispersoids were analysed by chemical extraction method (Annexure 1) and found to be 4.7 weight %. The extracted dispersoids have shown on XRD analysis, the presence of both TiO_2 and $MgTi_2O_5$ indicating that magnesium and TiO_2 has reacted forming the magnesium dititanate ($MgTi_2O_5$) as shown in Fig.7. The quantum of reaction products is approximately calculated from the diffraction data presented in the Tables AT I and AT II of Annexure -2. These calculations reveal that practically more than 90% of TiO_2 has been converted to magnesium dititanate This confirms the reaction suggested in equation 11.The TiO_2 that is present in the extracted dispersoid is also found to be of rutile structure. The fresh TiO_2 powder was heated at 1073 K for 2 hours to stimulate the heating cycle involved during the composite synthesis and subjected to XRD analysis to observe any posible conversion of anatase grade TiO_2 to rutile structure. It was observed that the anatase grade was retained during this heating. XRD data is shown in Fig.8.

The conversion of anatase grade TiO_2 to rutile grade during this synthesis is discussed (155) in the following lines. All the 3 elements of the matrix alloy viz., Al, Zn and Mg are strong catalysts for TiO_2, forming their respective

63
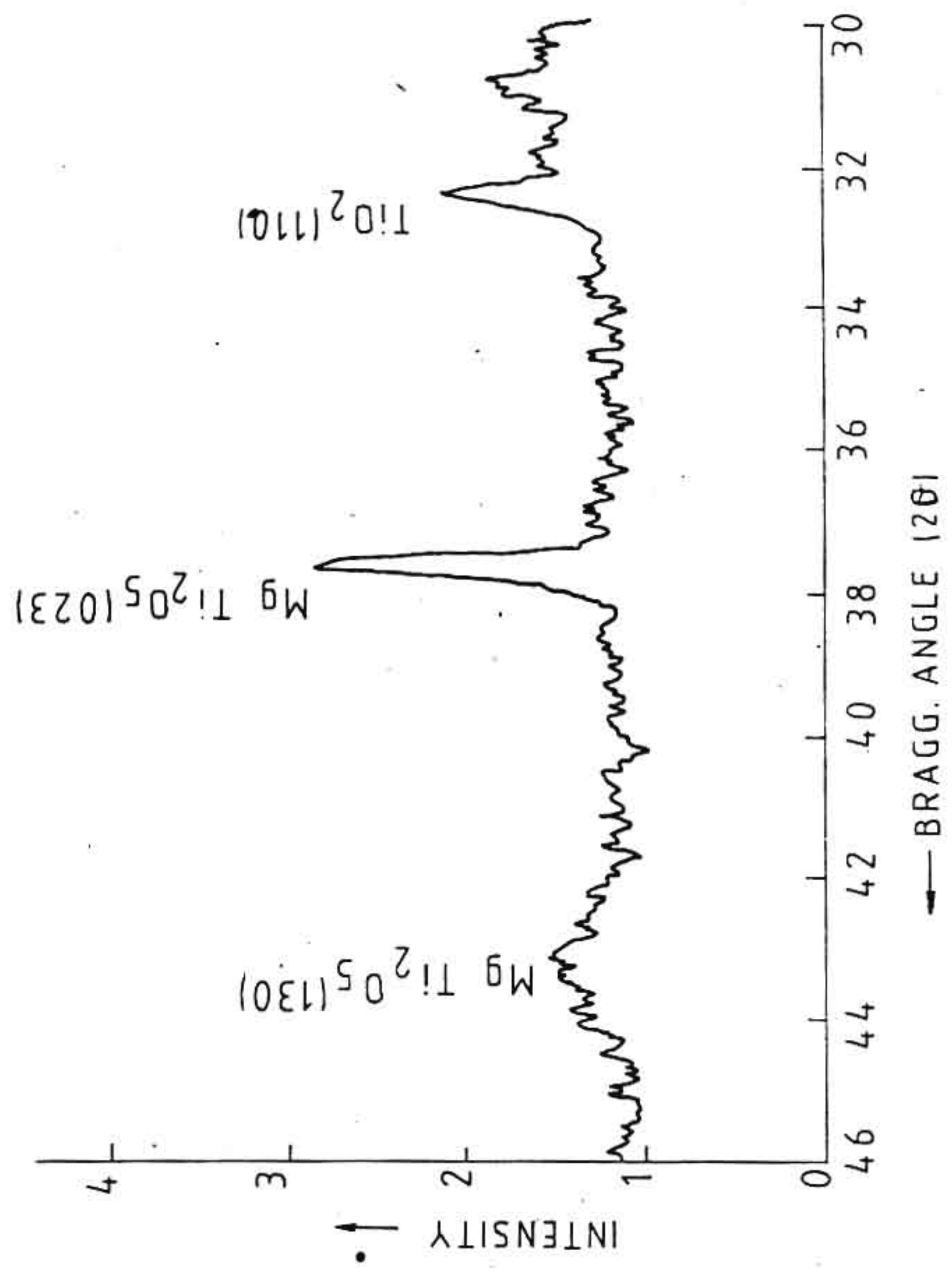
FIG.7. EXTRACTED PARTICLE-1
(XRD DATA)
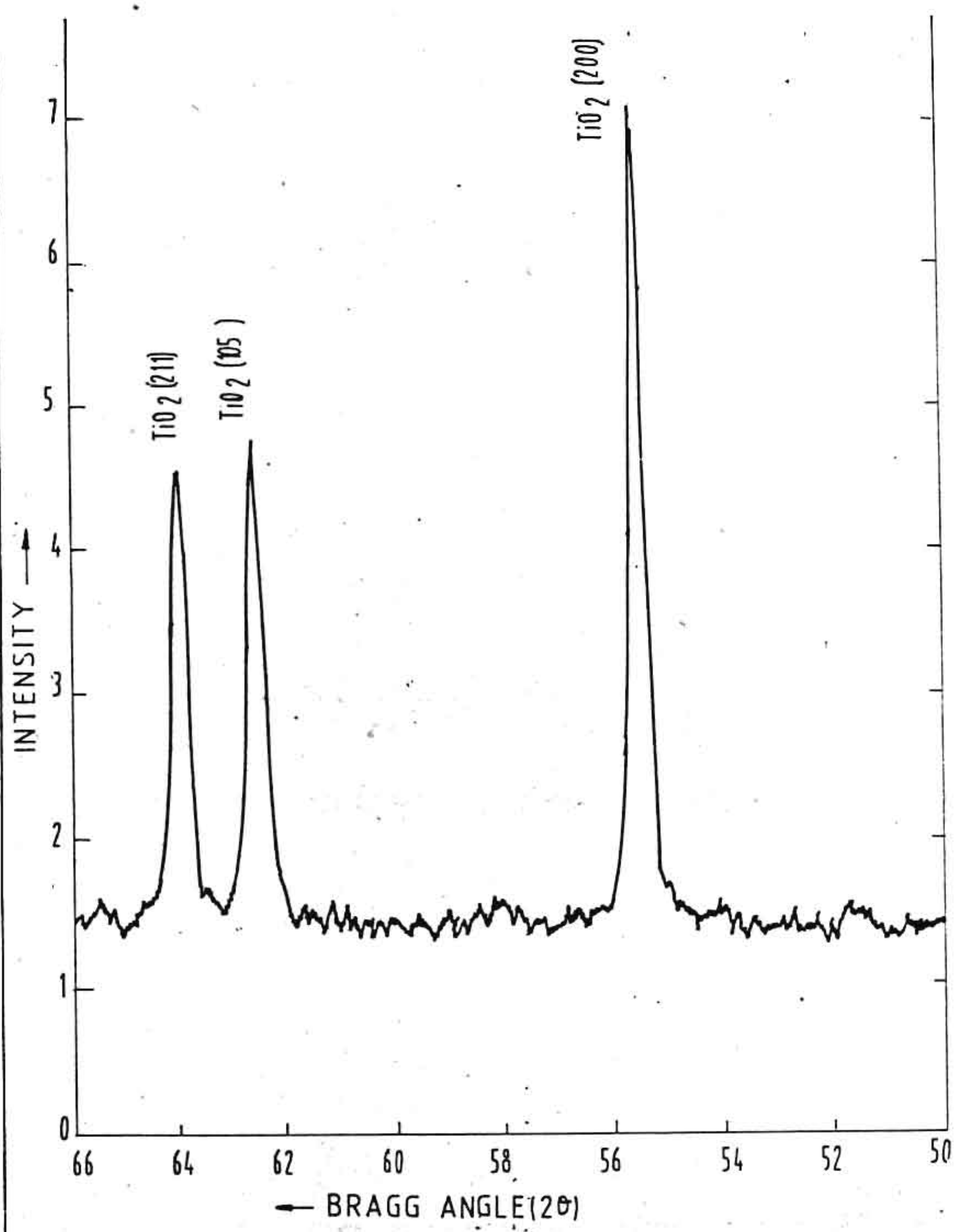
FIG. 8. TiO$_2$ MILLED STOCK -2 (XRD DATA)

Mg are strong catalysts for TiO_2, forming their respective titanates. However, the reactions are reversible, forming fresh TiO_2, which is rutile. Anatase or brookite grade exist (154) only under specialised conditions, like the presence of anatase stabilisers viz., P_2O_5 / Sb_2O_5. This explains why the anatase grade TiO_2 containing P_2O_5 did not get converted to rutile grade on heating at 1073 K. The chemically extracted TiO_2 powder from the composite exhibited charcoal black colour corresponding to rutile grade as against the snow white anatase grade TiO_2 that was added for the composite synthesis.

The presence of $MgTi_2O_5$ phase in the composite confirms the stability of the Mg titanate unlike Zn or Al titanates. Absence of aluminium titanate Al_2TiO_5 in the composite is in line with the literature (163) that aluminium titanate is stable only above 1700 K. Absence of zinc titanate in the composite shows the instability of the Zn spinel during this composite synthesis.

Absence of Ti_2O_3 in the composite though predicted by equation 6, reveals that Ti_2O_3 is also not a stable oxide and further get oxidised to stable TiO_2 during the synthesis as per rection shown in Equation 12.

Addition of TiO_2 to the base alloy has resulted in a heavy loss (43%) of Mg in the composite viz 2.12% in the base alloy got reduced to 1.2% in the composite. This loss is quite

64

marginal viz 4.15% in the base alloy reduced to 3.9% in the composite, a total loss of only 6%. This also suggests that Zn has not participated in the chemical reactions.

Considering the chemistry and reaction products of the composite, the most favourable reactions those are possible during this composite synthesis are as follows:-

$$Mg + 2\ TiO_2 = MgO + Ti_2O_3 \qquad - \qquad (6)$$

$$2Ti_2O_3 + O_2 = 4\ TiO_2 \qquad - \qquad (12)$$

$$MgO + 2\ TiO_2 = MgTi_2O_5 \qquad - \qquad (11)$$

It may be noted here (164) that Mg forms 3 titanates with TiO_2 as (i) magnesium meta-titanate ($MgTiO_3$) of rhombohedral crystal structure, (ii) magnesium ortho-titanate (Mg_2TiO_4) of cubic structure and (iii) magnesium di-titanate ($MgTi_2O_5$) of orthorhobmic structure. The XRD data has shown that the magnesium titanate in this composite system corresponds to $MgTi_2O_5$ with orthorhombic crystal structure.

III.1.3. **Distribution of TiO$_2$ particles in the castings:**

The machined outer surface of the cast composite billets prepared by both liquid metallurgy (LM) and rheocasting (RC) route on visual examination showed uniform distribution of TiO$_2$ particles throughout the surface except for some segregation near the shrinkage pipe in LM cast billet. In RC billets, such segregations were not observed.

Macrostructure (Fig.9) of the cross section of the LM cast billet of size 100 x 100 mm square reveals chill zone of size about 20 mm all around, covering about 64% of the total cross sectional area. Columnar grains of size 2 mm width and 5.8 mm length are seen immediately after the chill zone to a depth of about 15 mm towards the centre, covering an area of about 27%. The central zone of about 30 mm square, covering an area of about 9%, contained equiaxed grains of size about 3 mm diameter.

Macrostructure (Fig.10) of RC billet of cross section 90 x 150 mm revealed a larger area of chill zone, 35 mm on either side along the width and 25 mm on either side along the length, covering a cross sectional area of about 85%. The structure did not reveal any columnar grains as in the LM cast billets, and the central region of size 20 x 70 mm, covering an area of about 15%, showed equiaxed grains of average diameter 2.8 mm.

66
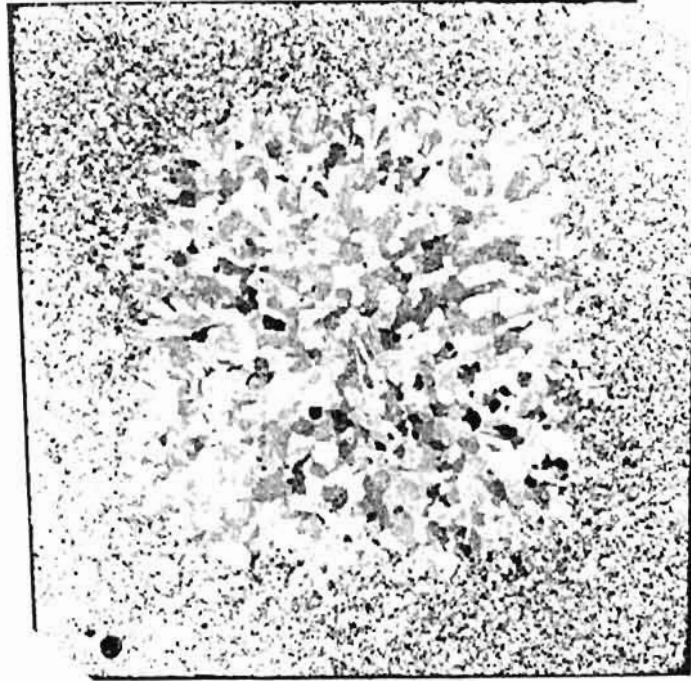
Fig. 9 : Macrostructure on the cross section of LM cast
         billet. Structure reveals peripheral chill zone,
         middle columnar grains and core equiaxed grains.
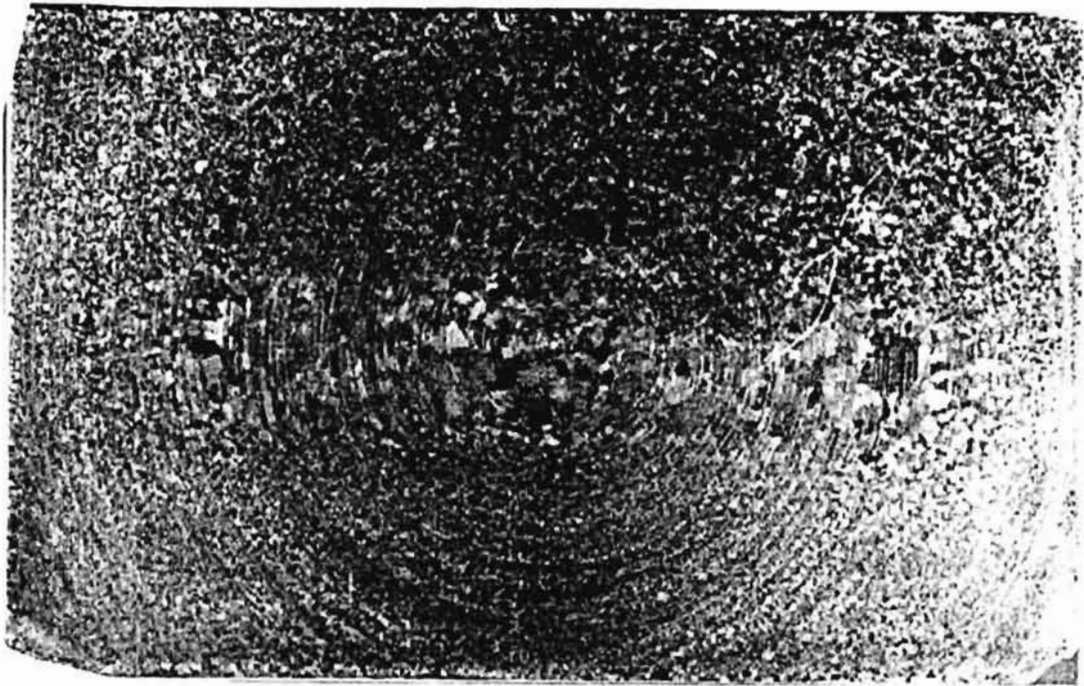
Fig. 10 : Macrostructure on the cross section of RC billet .
          Structure reveals chill zone and equiaxed grains .
          No columnar grains are seen.

From these macrostructures, it can be said that, metallurgical conditions are more favourable in the case of RC billets to obtain a structure more of fine and equiaxed grains and free of columnar grains.

The microscopic examination across the cross section of LM cast billet showed fine equiaxed chilled structure at the periphery which progressively got coarsened towards the core leading to columnar type dendrites with DAS of the order of 150 to 200 μm. In the peripheral regions the particles were distributed uniformly. (Fig.11). As the columnar / dendritic solidification sets in, the particles were found in the inter dendritic regions, and at the centre of the castings which clearly indicates particle segregation (Fig.12) as a result of particle pushing by the growing solid/liquid interface. This particle pushing has been attributed to the lower thermal conductivity and thermal diffusivity of TiO_2 compared to that of αAl (42) as discussed below.

The particles are pushed by the solidifying interfaces when

$$\left\{ \frac{Kp \cdot Cp \cdot \mathcal{S}p}{Kl \cdot Cl \cdot \mathcal{S}l} \right\}^{\frac{1}{2}} \ll 1 \quad \text{and} \quad \frac{Kp}{Kl} \ll 1 \quad - \quad (13)$$

where K, C and $\mathcal{S}$ represent thermal conductivity, specific heat and density of the particle P and liquid matrix l respectively. Using the following data for $Al-TiO_2$ system

$Cp = 0.195$ cal/gmK.　　　　$Cl = 0.258$ cal/gmK

$\mathcal{S}P = 4.26$ gm/cc　　　　$\mathcal{S}l = 2.39$ gm/cc

67
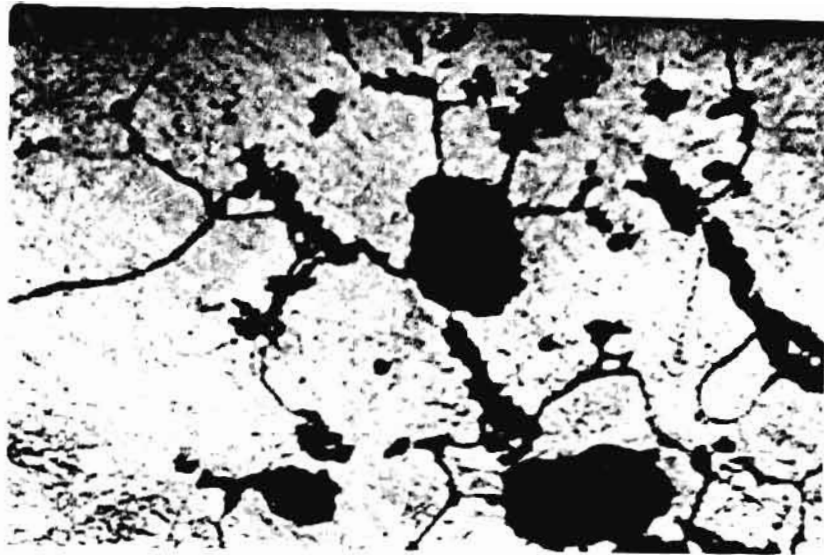
200 μm

Fig.11 : Optical microstructure of LM cast billet .
Uniform distribution of dispersoids both
in the matrix and the grain boundaries are seen.
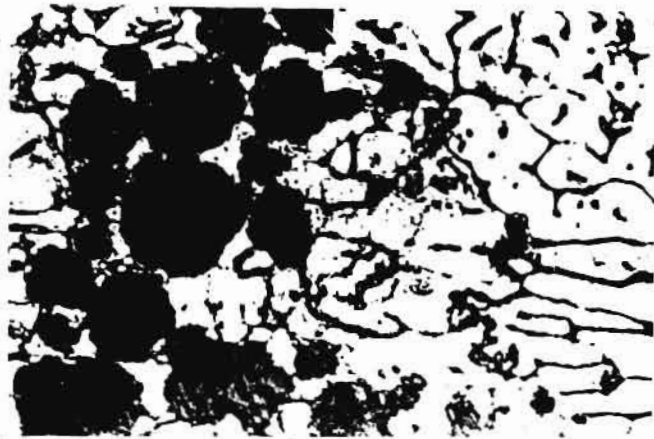
200 μm

Fig.12 : Optical microstructure of the above in the core
region. Particle segregation due to particle pushing
effect by growing dendrites is evident.

$Kp = 0.01487$ cal/cm.s.K $Kl = 0.225$ cal/cm.s.K

the above conditions yield

$$\left\{ \frac{Kp.Cp.SP}{Kl.Cl.Sl} \right\}^{\frac{1}{2}} = 0.2984 \quad i.e \quad \ll \quad 1$$

and $\frac{Kp}{Kl} = 0.06609 \quad i.e \quad \ll \quad 1$

These computations show that TiO_2 particles should be pushed by aluminium dendrites to the last freezing liquid. This is consistent with the experimental observations made here.

In RC billets more refined and equiaxed dendritic structure was observed with uniform particle distribution through the entire cross section of the billet (Fig. 13) except for the small central region where dendrites were coarser than the rest of the area. Unlike the LM cast billets where there was particle segregation at the centre by particle pushing effect, RC billets exhibited good distribution of particulates in the centre region (Fig.14). This indicates that the particles get trapped within the semi solid slurry during solidification and are not free to move around. This enhances the uniformity of the particle distribution over a large area of cross section. The dendrite arm spacing in the centre region of the RC billet is of the order of 30-50 μm, and over the rest of the area, it is very low of the order of 10-20 μm, as compared to the dendrite arm spacing of 150-200 μm for LM cast billet and 200 μm for the LM cast base alloy (Fig.15). This indicates that rheocasting
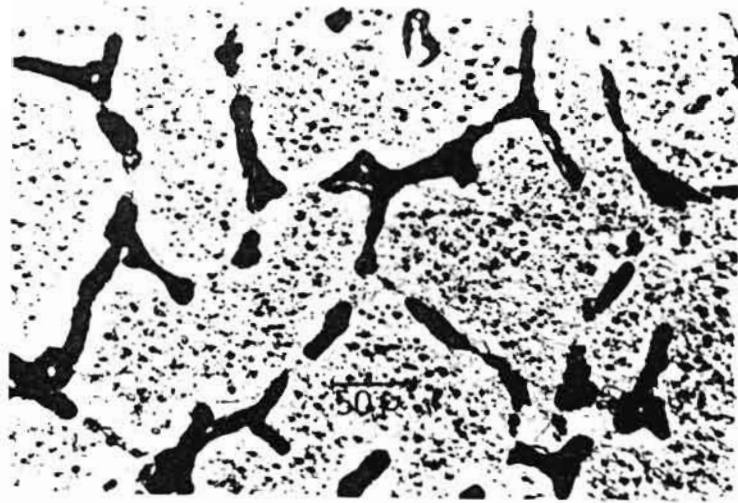
68
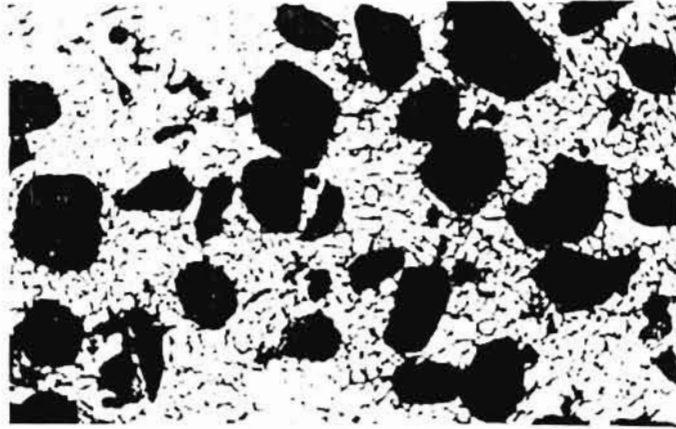
100 μm

Fig.13 : Optical microstructure of RC billet. Region towards
·surface. Structure revelas fine matrix grains and
uniform distribution of dispersoids.
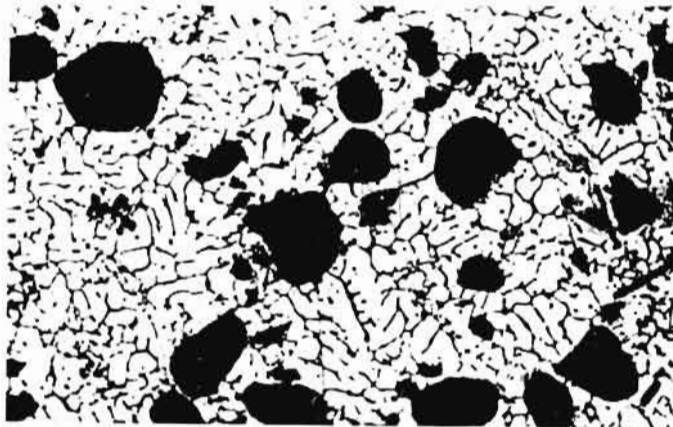
100 μm

Fig.14 : Optical microstructure of the above at the core
region. Equiaxed grains and good distribution of
dispersoids are seen.

100 μm

Fig.15 : Optical microstructure of the matrix alloy
(G74S) in the LM cast condition. Indicates
eutectic grain boundaries typical of cast structure.

has a very pronounced effect to refine the grain structure and that the TiO_2 particles has only marginal influence on grain refinement in the cast structure, as no significant refinement was observed in LM cast billets. Grain refinement by TiO_2 could be expected only if they were probably finely and separately dispersed in the melt. Since in both LM and RC billets, the particles are in agglomerated form, no grain refinement has been observed by the dispersoids. Grain refinement by rheocasting is a process characteristics which has been explained (12) in the following lines. as metals and alloys freeze, the primary dendrites normally grow and intermesh with each other, so that, as soon as a relatively small fraction (about 20%) of the melt has frozen, viscosity increases sharply, and flow ceases practically. If, however, the dendrites are broken up by vigorously agitating the melt during solidification, as is done in rheocasting, reasonable fluidity persists until the solid content reaches as much as 60%. Each broken piece of dendrite becomes a separate crystal and very fine grain size can be achieved without the use of grain refiners.

11.1.4. <u>Agglomeration</u> <u>of</u> <u>the</u> <u>particles</u>:

The average particle size (APS) of TiO_2 in the as received condition was about 0.37 μm. Heating the particles to about 1073 K was found to be essential to remove any adsorbed moisture and gases and further to improve the wettability. This heating has however resulted in agglomeration of the particles. The preheated particles were subjected to particle size analysis using the same instrument and method that was used to evaluate the size of the untreated particles. The particle size distribution is noted below and the distribution graph is shown in Fig. 16.

```
98 %        : Below 28 microns
95 %        :   ''    18   ''
90 %        :   ''    15   ''
80 %        :   ''    11   ''
70 %        :   ''    7.5  ''
60 %        :   ''    4    ''
50 %        :   ''    1.8  ''
40 %        :   ''    1.1  ''
30 %        :   ''    0.8  ''
20 %        :   ''    0.6  ''
10 %        :   ''    0.4  ''
 5 %        :   ''    0.3  ''
```

It may be observed that the size variation is much larger ranging from o.3 to 28 μm with the average particle size at 1.8 μm as against the size variation of 0.15 to 1.0 μm for the untreated particles. It may also be noted that the magnetic stirring involved in the process of particle size analysis is likely to break down the weakly agglomerated particles of the treated powder. This is to say that the average size of the treated particles that was used in the

70

SAMPLE IDENTIFICATION : TITANIUM DIOXDE TREATED

DENSITY : 3.9 g/cc
PREPARATION : DISPERSED WITH SODIUM SILICATE : pH OF THE SLURRY: 9.0
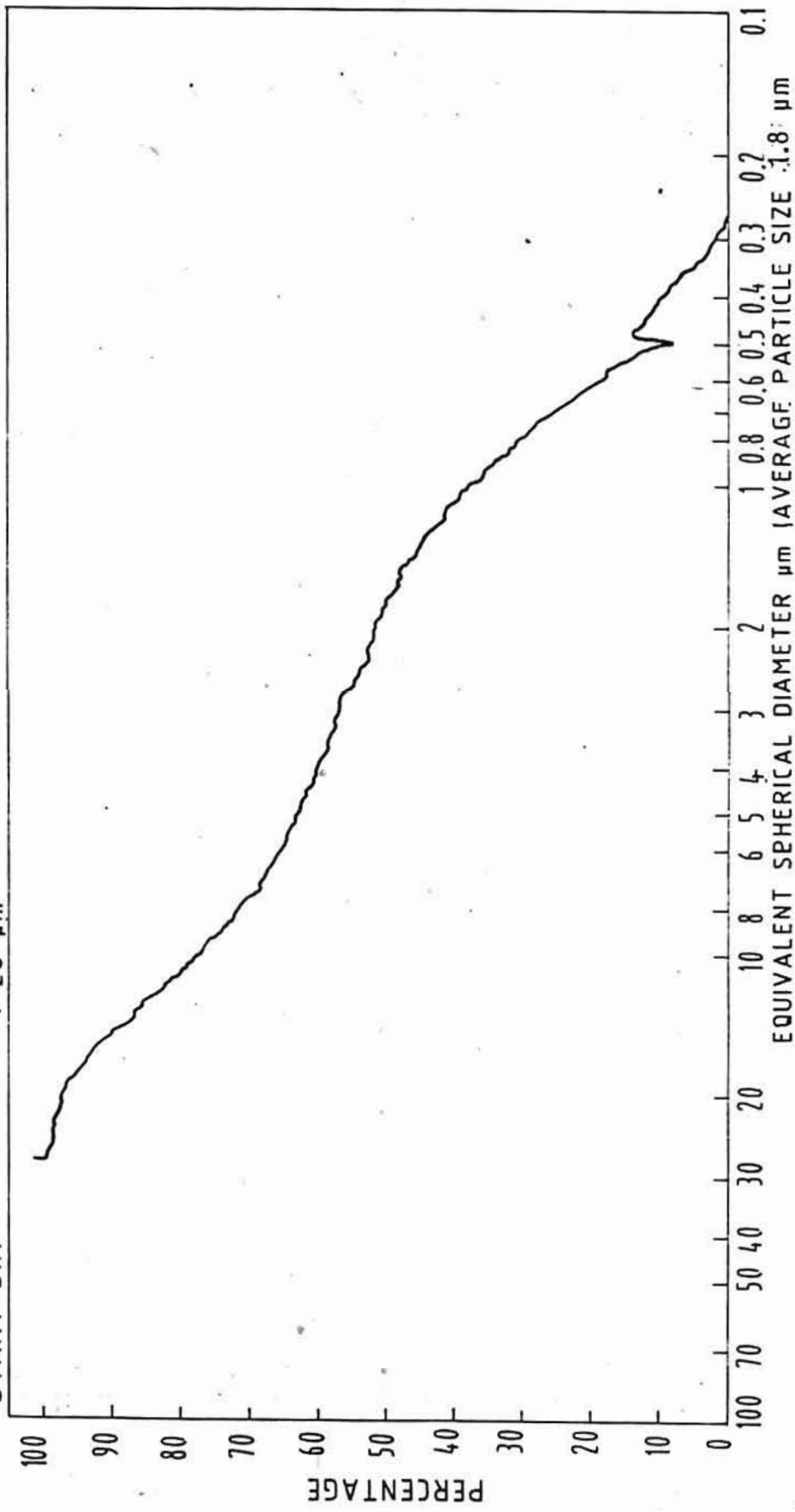START DIA : 28 μm

FIG. 16. PARTICLE SIZE DISTRIBUTION OF TREATED Ti O2

EQUIVALENT SPHERICAL DIAMETER μm (AVERAGE PARTICLE SIZE 1.8 μm

PERCENTAGE

composite synthesis without any further processing like
magnetic stirring would be definitely larger than the size of
the powder that was subjected to particle size analysis after
the magnetic stirring.

By optical metallography techniques, the size distribution of
TiO_2 particles was estimated for both RC and LM cast
composite billets. A typical distribution of the TiO_2
agglomerates in the RC and LM cast route composite billets
has been shown in Fig.17. In RC composites, the agglomerate
sizes ranged upto 150 μm with the average particle size
14.54 μm. The size distribution of the particles is given
below.

About 13%	below 5 micron
48%	between 5 and 10 microns
13%	between 10 and 15 microns
10%	between 15 and 20 microns
7%	between 20 and 30 microns
5%	between 30 and 50 microns
3%	between 50 and 100 microns and
1 %	above 100 microns.

For LM composites, the particle agglomerate size varied upto
250 μm with the average particle size 86.6 μm. The size
distribution of the particles is given below.

About 8%	below 30 microns
12%	between 30 and 40 microns
16%	between 40 and 50 microns
38%	between 50 and 100 microns and
26%	above 100 microns.

71
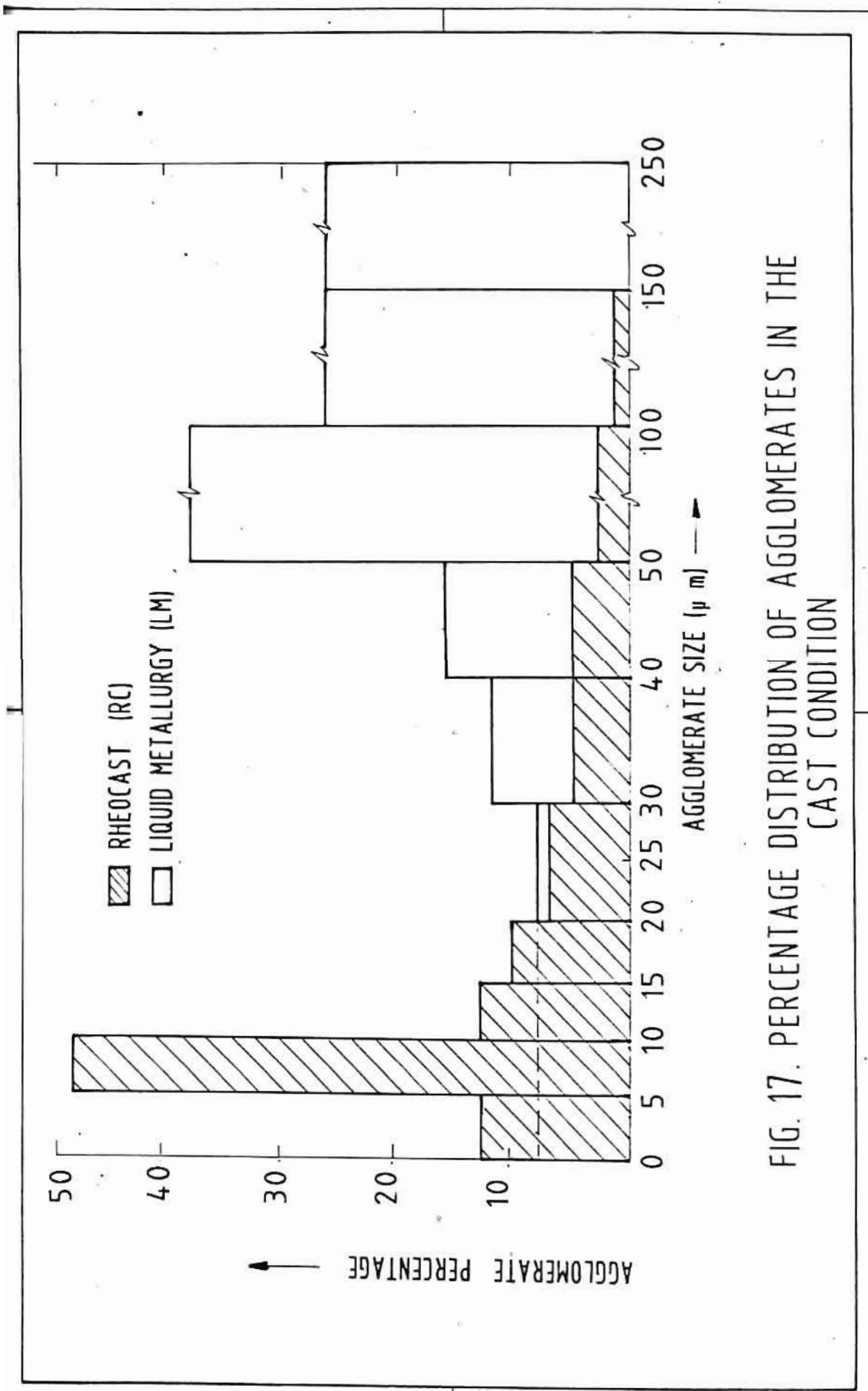
FIG. 17. PERCENTAGE DISTRIBUTION OF AGGLOMERATES IN THE CAST CONDITION

The results clearly indicate that the particles do agglomerate in both the types of casting processes and that the agglomerate sizes are much smaller in RC billet (82% less than 20 μm) than in LM billet (64% more than 50 μm) : that is to say , rheocasting technique is certainly superior to disperse fine particles in the composite, or else, as reported in earlier studies (140) particles of size less than 50 μm are difficult to be dispersed by LM technique without larger agglomerations. The distinct advantage of rheocasting route to disperse particles of size less than 50 μm size can be attributed to the following:

(i). Since RC casting is done in a two phase region (solid-liquid), the particulates remain in liquid phase separated by solid phase within the slurry. This minimises the possibility of too many particles coming together to form any agglomerates.

(ii) The relatively higher viscosity of the melt slurry enables higher shear transfer during dispersion and subsequent mixing, whereby the particles even in the smaller agglomerates can get separated individually or into finer agglomerates. (iii). Since the primary solid is comparatively softer it can flow along with particles and prevent the separated particles to come in contact with each other, thus avoiding reagglomeration. (iv). The moving solid phases of the solid slurry can also break certain agglomerates , which are weakly bonded, by impingement action, and

(v) The higher viscosity of the slurry also prevents the gravity induced segregation during unstirred conditions.

72

III.1.5. Particle matrix interactions:

SEM observation of particle matrix interface of the composite exhibited reaction products for both LM and RC billets. The reaction zone was observed to be of thickness about 3 μm for LM cast billet (Fig. 18) and that for RC billets was found to be only about 1 μm thickness (Fig. 19 and 20). This is possibly due to the lower dispersion temperature viz., only about 923 K maximum for RC process as against above 1023 K for LM process.

Extensive EDAX analysis was carried out in the composite samples to ascertain the elemental distribution over the particle, particle segregations, reaction zones, adjacent to the particles and over the matrix material. The intensity chart of the elements are shown in Figures 21 to 23. Elemental distribution over the smallest particle agglomerate (Fig. 21) reveal preferential Ti peaks possibly corresponding to TiO_2 with low peaks for Mg and Al. Fig. 22 shows the elemental distribution over a large particulate cluster. Presence of higher percentage of Al infiltrated into the dispersoid cluster is very evident in this case. The Reaction zones reveal (Fig. 23) higher peaks for Mg and Ti, quite possibly due to the presence of $MgTi_2O_5$. XRD analysis of the extracted particulates has confirmed the presence of TiO_2 and $MgTi_2O_5$ in the composite.
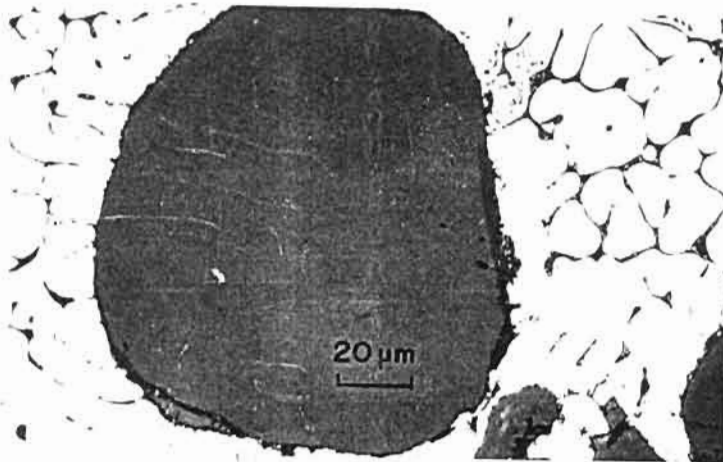
73
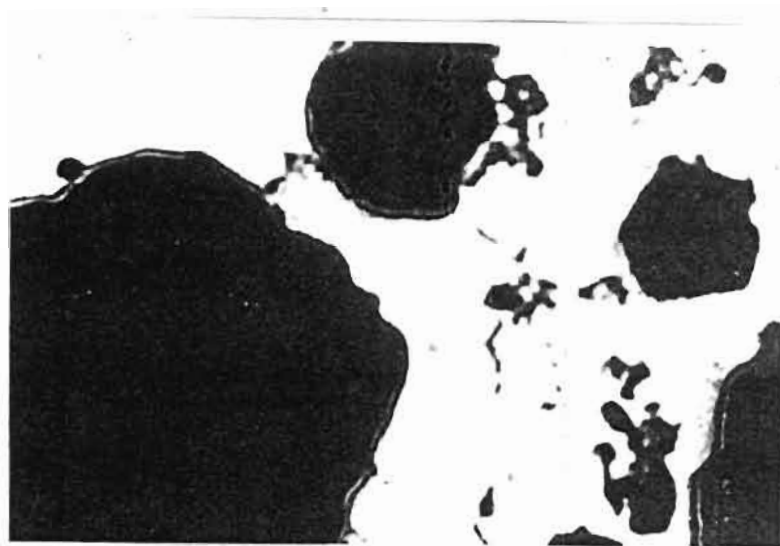
60 um

Fig.18 : SEM picture of LM cast billet. Indicates reaction
zone around the dispersoid.
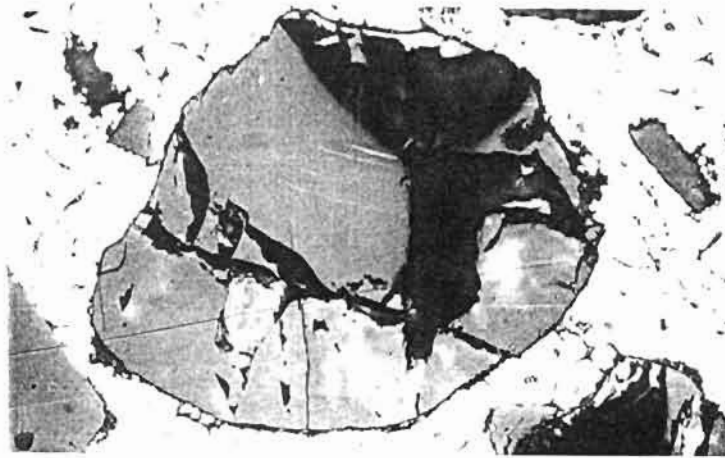
60 μm

Fig.19 : SEM picture of RC billet. Indicates cracked particle
        -agglomerates and thin reaction zone around the
         dispersoid

20 μm

30 μm

Fig.20 : Same as above at higher magnification

SERIES II METALLOGRAPHY SECTION   TUE 24-OCT-89   14:10
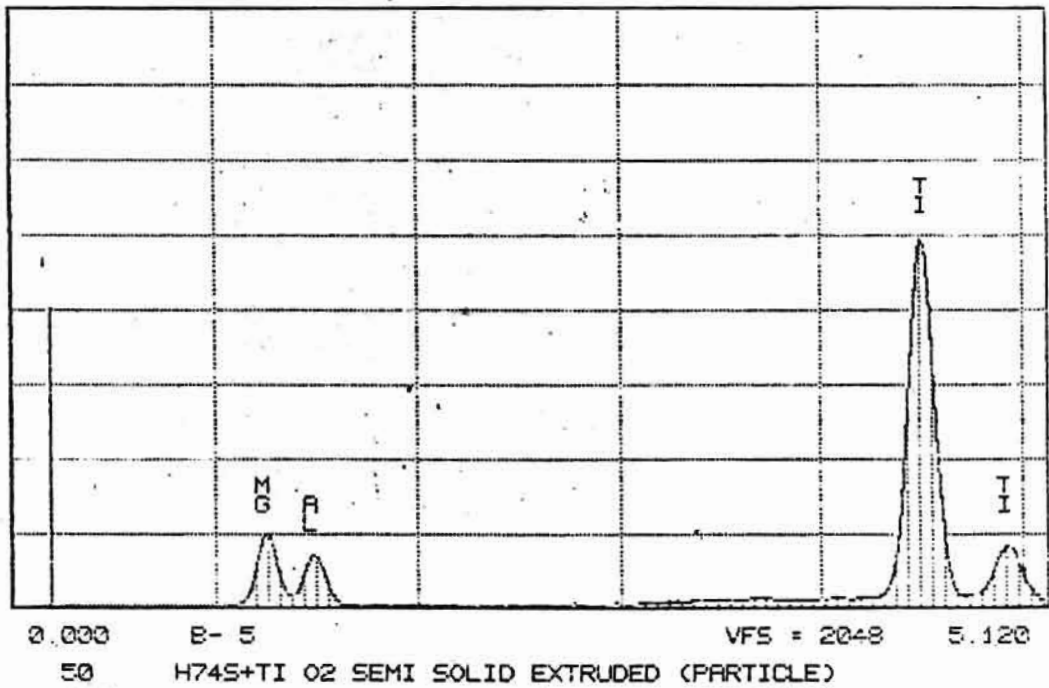Cursor: 0.000keV = 0   ROI   (0) 0.000: 0.240

0.000   B- 5   VFS = 2048   5.120
50   H74S+TI O2 SEMI SOLID EXTRUDED (PARTICLE)

Fig. 21.   EDAX intensity count on a particle.
           Graph indicates elemental analysis.
           Ti and Mg peaks are due to TiO_2 and $MgTi_2O_5$.

0.000   B- 5   VFS = 512   5.120

50   H74S+TIO2 SEMI SOLID EXTR.(PARTICLE CLUSTER)
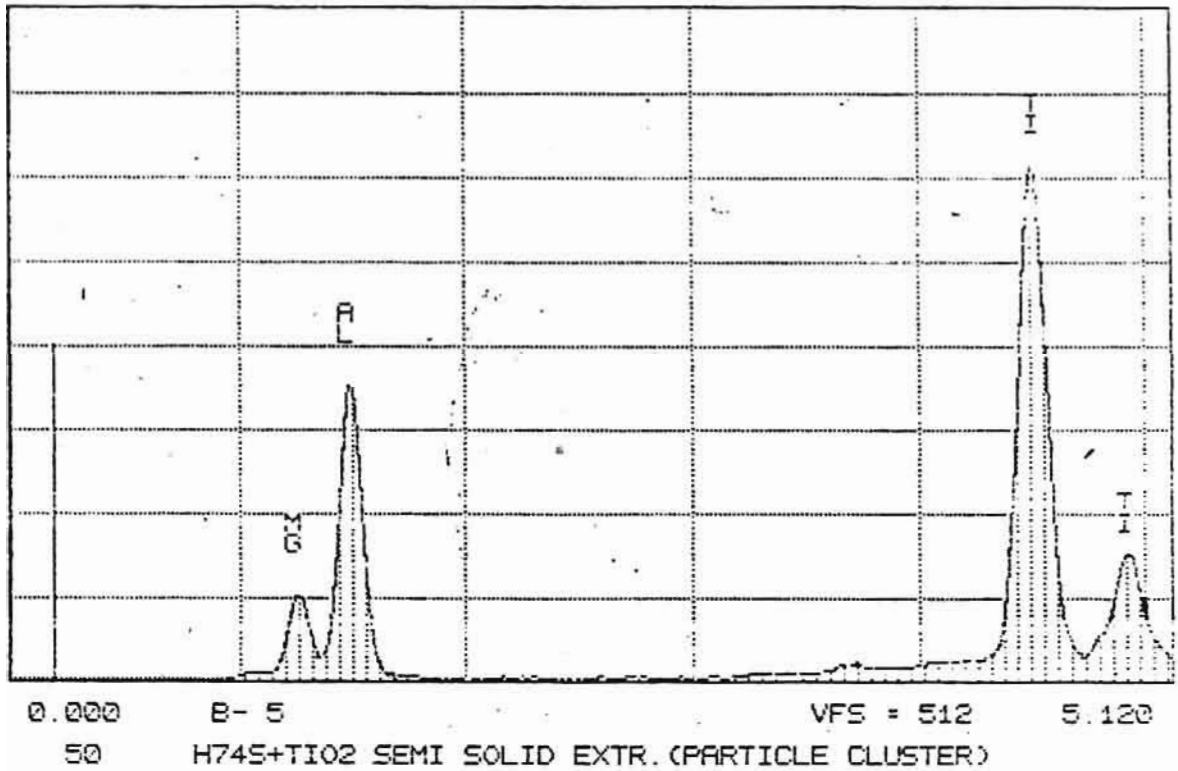
Fig. 22. EDAX intensity count on a particle cluster.
         Ti and Mg peaks are due to TiO_2 and $MgTi_2O_5$.
         Higher peak for Al indicates infiltration of
         Al into the particle interface region.

0.000   B- 5   VFS = 2048   5.120
   50   H74S+TI02 (REACTION ZONE)

Fig. 23.   EDAX intensity count on the reaction zone.
           Higher peak for Mg indicate larger amount
           of $MgTi_2O_5$ than TiO_2 in the reaction zone.

III.2. **Forgings:**

Forging operations were discontinued with the formation of cracks on the composite after the initial 30% reduction. It must be mentioned here that the base alloy is highly forgeable and that heavy forging reductions are practised by hot working process. Apparently dispersion of TiO_2 particles in this alloy system reduces the forgeability of the alloy, irrespective of the casting route, i.e. LM or RC route.

The SEM observation (Fig.24) on the fractured surface from the cracked portion of the forged sample has shown very poor bonding between the matrix and the dispersoid. Particle agglomerations and porosities were also observed in the same sample. Particle fall out from the cracked surface (Fig.24) is also observed to be creating pores on the surface. The matrix is found to have ductile flow during forging as observed by the presence of dimples and microvoid formations (Fig.25). Particle separation from an agglomerate into several platelets within a large dimple (Fig.25) probably indicate that the forging cracks develop from these areas due to coalescence of microvoids on press forging. Microvoids on the matrix alloy without TiO_2 may however get closed up during press forging, and that is why, heavy forgings reductions are found possible on the base alloy systems. Henceforth, it may be concluded that the forging is not likely to improve the properties of the composite containing agglomerates of dispersoids. On the other hand, if dispersoids are not clustered but dispersed individually in
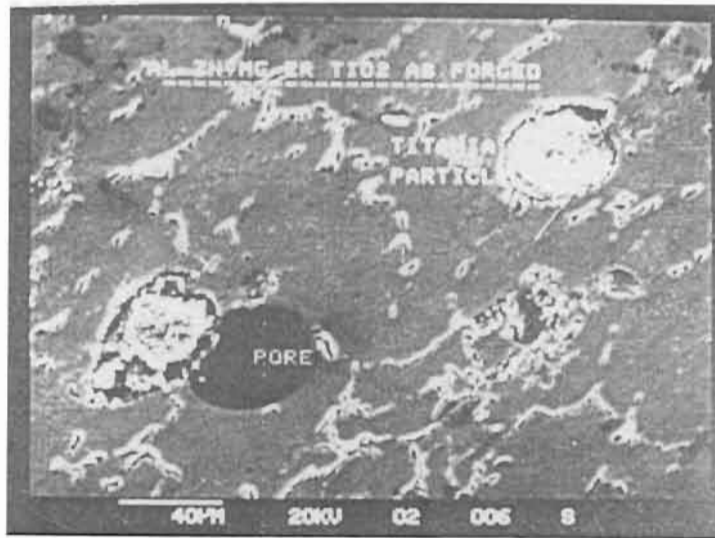
74

Fig.24 : SEM picture of the forged composite. Shows poor
bonding between matrix and the dispersoids.
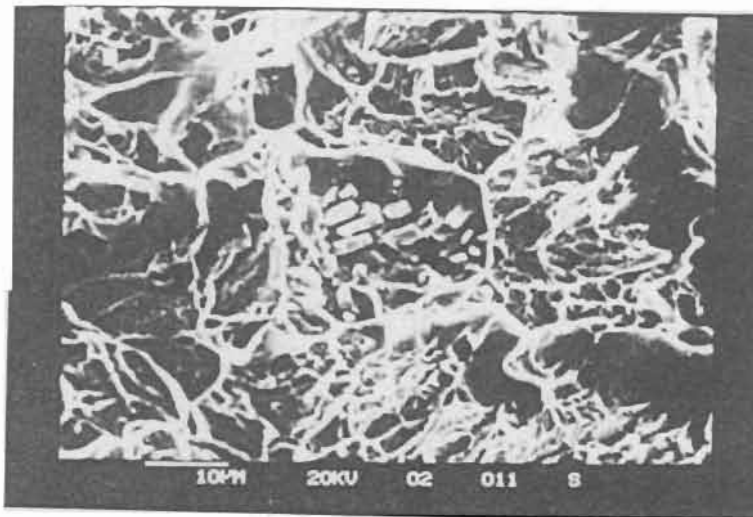Agglomerates and pores are also seen.

Fig.25 : Fractograph of the forging crack. Shows
disintegration of a particle cluster into several
platelets within a dimple. Matrix is ductile.

the composite, while forging, pull out of particles will not take place during forging but improvements in the mechanical properties will take place depending upon forging conditions (165). In a very recent study (128), Al-Mg alloy AA 5083 composite reinforced with SiC particulates of particle size varying from 0.5 μm to 5.0 μm by powder metallurgy technique was successfully hot forged to a reduction ratio of 3 : 1. In short, the choice of the route for mechanical working of the composite depends upon the type and nature of distribution of dispersoids in the matrix.

III.3. Extrusions:

The results under this section are discussed in two sub-sections : (i) extrusion characteristics and (ii) heat treatment of extruded sections.

III.3.1. Extrusion Characteristics:

The surface features of the extruded composite samples are shown in Fig.26. Solid extruded (SE) rods exhibited good surface finish compared to semi-solid (SSE) or semi-liquid (SLE) extruded rods, which exhibited surface cracks. A very recent study (128) on semi solid extrusion of 7178 Al alloy (Al-Zn-Mg-Cu) with 15 vol % Al_2O_3 short fibres, also reported surface cracks.

The surface cracks of the SSE and SLE rods were of size 2mm x 2mm. The surface machined extruded rods of both SSE and SLE are shown in Figures 27 and 28. Unlike in earlier studies (146,128) which exhibited cylindrical surface cracks (perpendicular to the extrusion direction) (Fig.29), in the present study, it is observed that the discontinuity is in the longitudinal direction, (parrellel to the direction of extrusion). This could probably be due to the particle abrasion effect on the die wall and material shrinkage effect on solidification of the partially liquid billet during the extrusion process. This is confirmed by particle segregation over the surface of the SSE and SLE rods, compared to the absence of such segregation in the SE rods (Fig.26). It was

76

SEMI-LIQUID EXTRUSION

SEMI-SOLID EXTRUSION

SOLID EXTRUSION

Fig.26 : Surface features of the three types of extrusions.
All the rods are of 17 mm diameter. Surface cracks
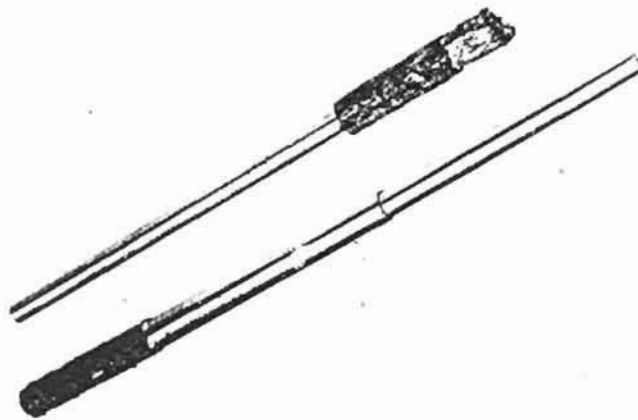are seen on semi-solid and semi-liquid extrusions.

Fig.27 : Machined surface of the semi-solid and semi-liquid
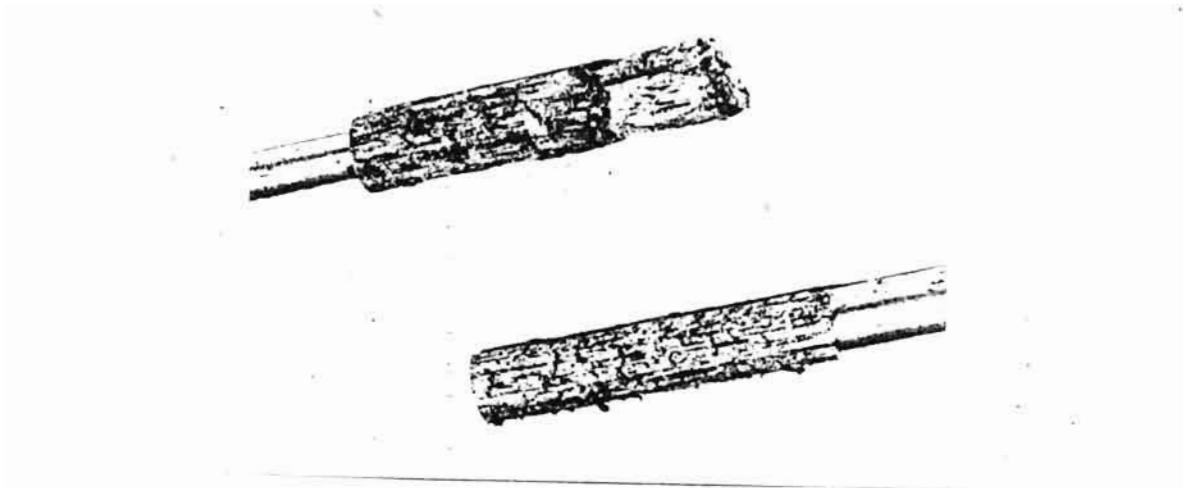extrusions. Shows that cracks are not deep.

Fig 28 : Close-up view on the nature of surface cracks of
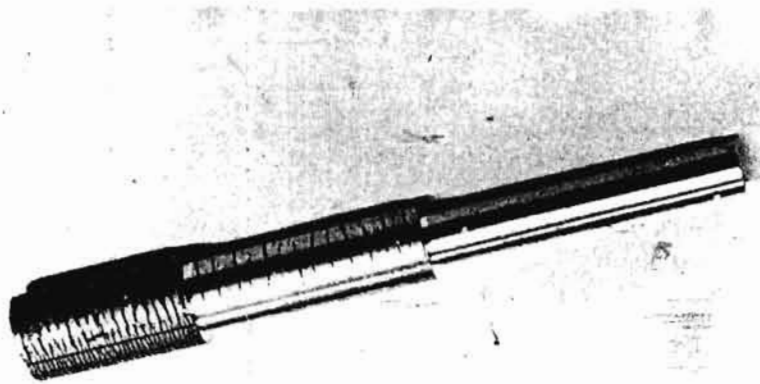both SSE and SLE rods. Cracks are of longitudinal
nature and parallel to the direction of extrusion.

Fig.29 : Surface cracks on a base alloy during high
temperature extrusion. Cracks are circular
and perpendicular to the direction of extrusion.

reported in an earlier study that (128) aluminium cladding on the composite (SiC short fibre re-inforced 7178 Al alloy composite) has totally eliminated the surface cracks of the semi-solid state extrusion. Therefore, it can be said that the particle abrasion on the die wall is the prime criterion for the longitudinal cracks during the slurry state extrusion of this composite. Particles are free to move during the slurry state extrusion and thereby segregate towards the die wall favouring abrasion on the die walls causing surface cracks. However, particle segregation is not possible during the solid state extrusion and it is observed that no surface cracks are formed during such extrusion. This composite is also hot extruded in the same temperature range as that of the base alloy (723 - 753 K) and the surface features of the extruded products are found to have no surface defects. The optical microstructure (Fig.30) of the solid extruded rod indicate streaks of TiO_2 particles aligned in the extrusion direction. Agglomerates are found to be partly separated and got aligned in streaks in the direction of extrusion.

The extrusion results on composites clearly suggest that, during SE process, both the matrix and the agglomerated dispersoids are getting deformed. The weakly bonded TiO_2 particles in the agglomerate are getting sheared and separated into partly individual particles and partly into smaller agglomerates. They also get aligned in the direction of extrusion. The measured size of the particles in the streak is about one micron, nearer to the dispersed particle

77
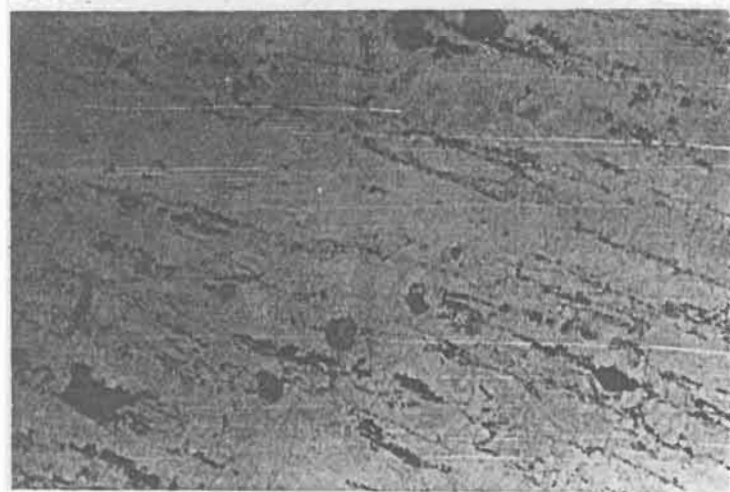
100μm

Fig.30 : Optical microstructure of solid extruded rod.
Few particles are deagglomerated and aligned
in the direction of extrusion.

size.   However, all the agglomerates may not get separated
like this   as evident in the microstructure (Fig.30). A
suitable die design may have to be considered in the
extrusion process to overcome this problem. IN SSE and SLE
processes, since the matrix is in a slurry state and very
soft, the deformation process is not able to shear or break
the agglomerate. Hence the agglomerates mostly remain as
such after extrusion.

These extrusion studies suggest that, conventional hot
extrusion of the base alloy is applicable to this composite
and most of the dispersoids get aligned in the direction of
extrusion. Some of the dispersoids in the weakly bonded
agglomerates also get sheared and separated into individual
particles.

III.3.2. **Heat Treatment and mechanical properties**
   **of Extruded sections:**

The optical microstructure (Fig.31) of the heat treated (T6) SE composite revealed coarse grained structure with both streaked and agglomerated dispersoids. The particulate distribution has not been changed from their extruded condition by the heat treatment. Fig.32 shows the optical microstructure of the base alloy extruded structure, in T6 heat treated condition. The structure reveals subgrain formation and uniform distribution of precipitates.

Typical mechanical properties of the composites extruded under different conditions and then heat treated to T6 condition are compared with the base alloy G74S (148,159) (Also extruded and heat treated to T6 condition) in Table XIX.   The base alloy had UTS of 360 MPa, YS of 290 MPa, and percentage elongation of 13, whereas SE composite had UTS of 250-300 MPa, YS of 170-210 MPa, and percentage elongation of 14. Considering the UTS value of TiO_2 as 56 MPa and using the basic rule of mixture for composite, the strength of the composite is theoretically calculated as 340 MPa. Though the experimental value is not far below the theoretical prediction , the decrease in strength level is quite possibly due to the fact that the particulates are not finely dispersed and the smaller size agglomerates are still present in the structure. TiO_2 dispersion has neither enhanced the mechanical properties by dispersion hardening

79
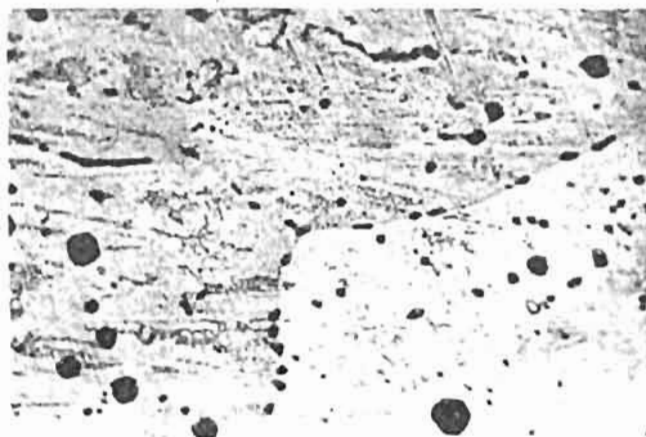
50 μm

Fig.31 : Optical microstructure of heat treated SE rod.
Coarse and elongated particles are dispersoids
uniformly distributed. $MgZn_2$ precipitates are fine.
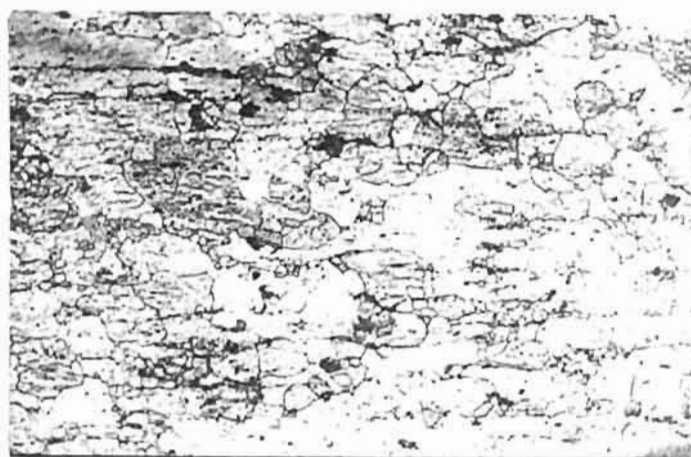
100 μm

Fig.32 : Optical microstructure of heat treated base alloy.
Shows typical structure of the alloy in heat treated
condition and formation of sub-grains.

TABLE-XIX

Comparison of the Mechanical Properties

of the Base Alloy G74S and the Composites.

(Both in Extruded and T6 Heat Treated Condition)

Material	U T S MPa	Y S MPa	% E	Hardness B H N

| G74S(extrusion) Al-4.5Zn-2.2Mg | 360 | 290 | 13 | 100 |
| H74S / AA7005 Al-4.5Zn-1.4Mg (extrusion) | 360 | 280 | 12 | 100 |

Al-3.9Zn-1.2Mg-4.7 TiO_2 Composite				
Solid Extrusions	250-300	170-210	14	76-81
Semi-Solid Extrusions	110-130	70-90	4	57-58
Semi-Liquid Extrusions	140-150	80-100	5	52-53

<u>Observation</u>: Tensile strength of the composite in solid extruded and heat treated condition is close to the theoretical prediction (340 MPa, annexure 3)

effect since the dispersoids are not finely and individually dispersed and are mostly in agglomerated form. The controlling factor for strengthening these particulate dispersed composites is the size and distribution of the particles., Though the particles selected for dispersion were of fine size (average size 0.37 µm), the particles were not dispersed finely due to agglomeration during the synthesis. Thus a better condition for composite synthesis to disperse the particles finely and separately, avoiding any agglomeration and a modified die design to obtain better dispersion of particles during extrusion might result in better mechanical properties in these composites.

Both SSE and SLE composites have exhibited poor mechanical properties viz., nearly half of that of SE composite. Better strength and higher elongation of the solid extrusions over semi-solid or semi-liquid extrusions are obviously due to the nature of the worked matrix structure of the SE rods. The structure is partly eutectic (cast) in semi-solid extruded sections and mostly eutectic in semi-liquid extruded sections. This greatly attributes to the lower mechanical properties in these two systems. In the case of solid extruded sections, the matrix alloy is not in its cast structure but is in the hot worked and heat treated condition giving rise to better mechanical properties. The SEM analysis of the tensile fracture of the SE composite showed (Fig.33) multiple modes of fracture viz., both transgranular and intergranular. The bonding between the
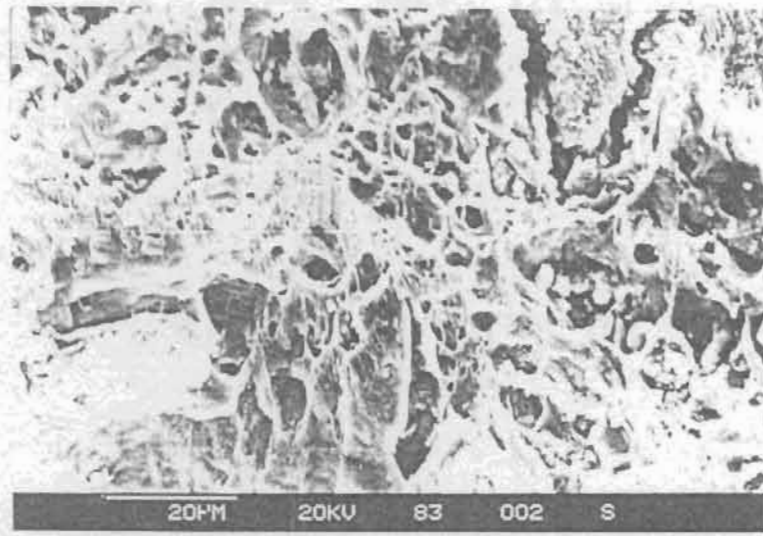
80

Fig.33 : Fractograph of tensile fracture on SE rod. Shows
formation of microvoids and dimples and particle
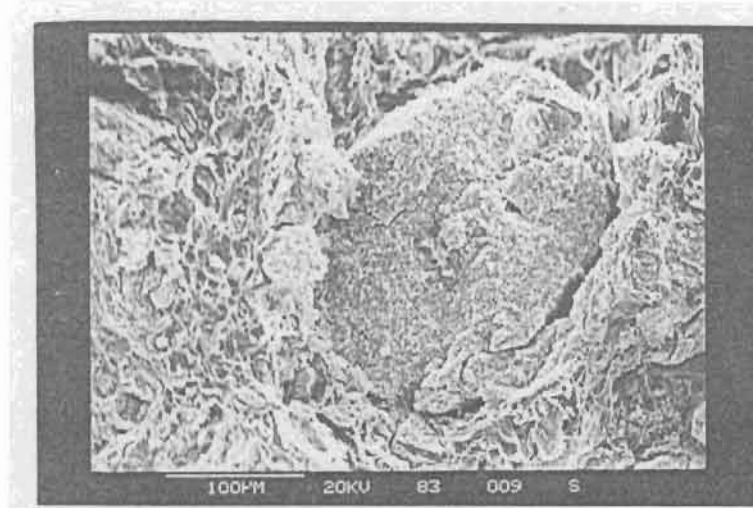debonding within the dimples.

Fig.34 : Same as above focussed on a particle cluster.
Shows particle fracture and debonding from
the matrix.

particles/agglomerates seems to be poor and a crack is seen on the agglomerate as shown in Fig.34. The agglomerates seem to have broken during extrusion process. The tensile fracture of SSE composite (Fig.35) shows larger defects corresponding to larger size agglomerates. Similar observations are made from the fractured surface of SLE composites also. It is clearly seen from Fig.36 that the particles are agglomerated and that they might have got weakly bonded during composite synthesis. The microhardness of these dispersoids ranged between 130-190 VPN as against the specified values of 700 VPN for TiO_2 particles (150). This once again indicates that the dispersoids are wekly bonded aggregates of the particles.
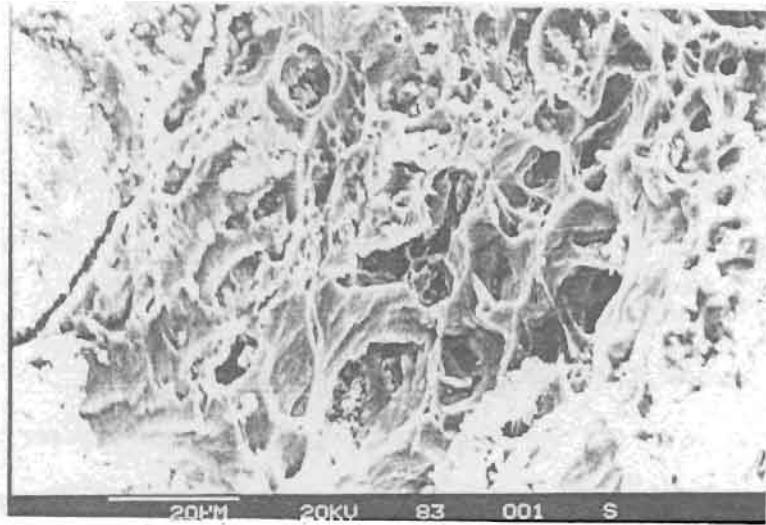
Fig.35 : Fractograph of tensile fracture of SSE rod.
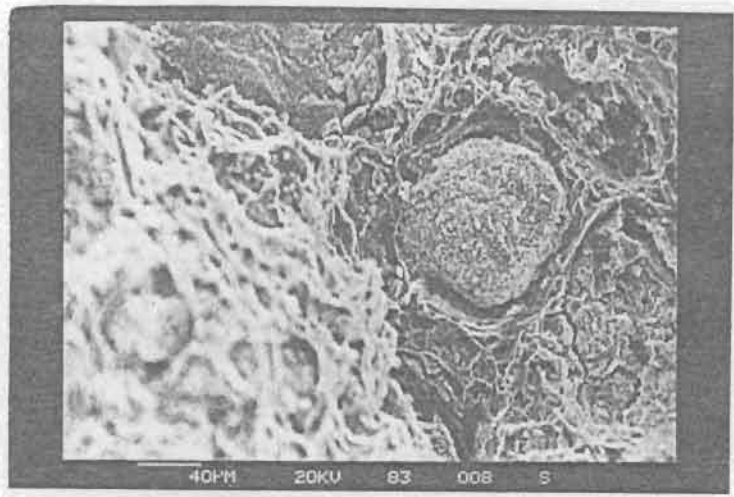   Reveals deep dimples and particulates within.

Fig.36 : Same as above on a particle cluster.
          Particle debonding is evident.

III 4. **ROLLING**

The composite was found to exhibit good workability on hot rolling which is evident from the hot rolled sheet indicating no rolling defects such as side cracks, surface fissures etc. Fig.37 shows the microstrucre of the hot rolled sheet of thickness 3.8 mm after a total reduction of 89%. The particles were observed to have mostly deagglomerated to much smaller sizes (2.4 µm) from their initial large size (14.54 µm) in the cast stage, and realigned in the rolling direction. Tensile strength of the composite in the hot rolled state (Table XX) is also on the lower side with higher percentage elongation, and is comparable to the properties of the base alloy in the similar condition. It may be noted here that the base alloy is an age-hardenable system and that the strength in the hot rolled condition is very insignificant. The strength of the composite in the hot rolled condition was evaluated to estimate the dispersion hardening effect, if any, of the TiO_2 dispersoids in the composite. The results indicate that the dispersion hardening is not effective after hot rolling in this composilte, quite possibly because the dispersoids are still in smaller agglomerates (size ranging upto 2.4 µm) and submicron size dispersion is required for any positive dispersion hardening effect.

Heat treatment has practically doubled the composite strength (Table XXI)from 140 MPa to 276 MPa by retaining the

TABLE XX

Mechanical Properties of "hot Rolled" Composite Sheets

(reduction in thickness from 35 mm to 3.8 mm)

(Reduction Percent 89)

S.No.	UTS (MPa)	YS (MPa)	% E
1.	139	96	23.2
2.	140	108	20
3.	140	--	21.2
4	138	80	23.2

Observation: Strength values are very low, but comparable to
that of the base alloy in annealed condition.
Properties indicate, there is no dispersion
hardening effect on this composite system.

TABLE XXI

Comparison of Mechanical Properties of composite and base alloy sheets in hot rolled and heat treated condition

Heat treatment	UTS (MPa)	YS (MPa)	% E
1. ST + 413 K / 36 hrs. (3.8 mm sheet)	231	175	14
	231	180	13
	235	188	--
2. ST + 378 K / 4 hrs.+ 413 K / 24 hrs.	241	176	14.8
	241	176	16.8
	238	173	17.2
3. ST +378 K / 4 hrs.+ 393 K / 20 hrs.	263	208	17.9
	278	210	18.7
	267	206	19.3
	276	203	19.7
4. Base alloy (condition as in 2)	310	260	7

<u>Observation</u>: Tensile strength values are comparable to that of the base alloy. Heat treatment under serial No. 3, is found to be better than others.
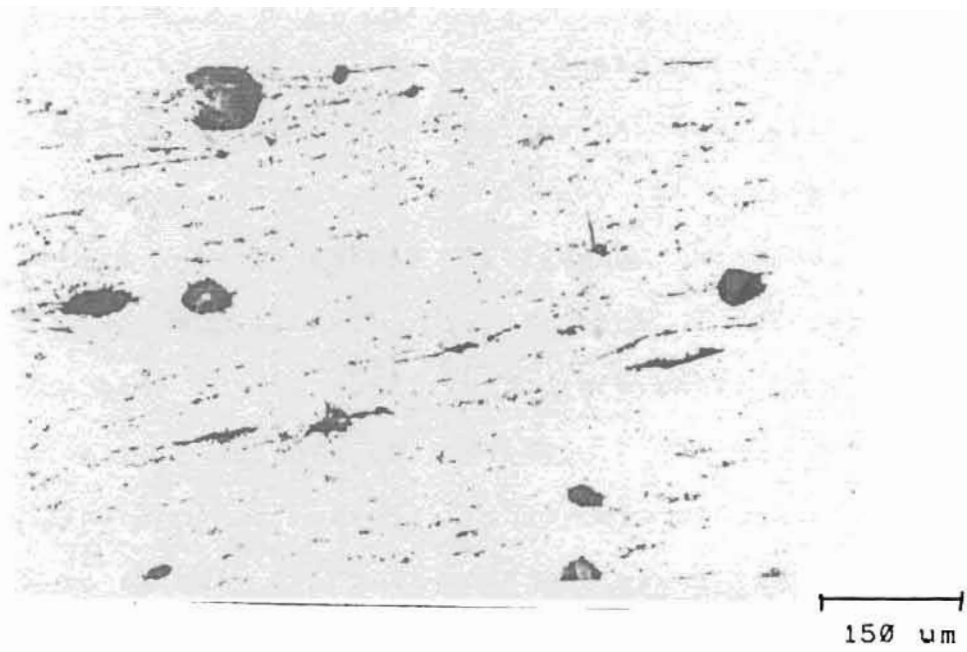
150 um

Fig.37 : Optical microstructure of hot rolled composite sheet
Indicates vast deagglomeration and particle realign-
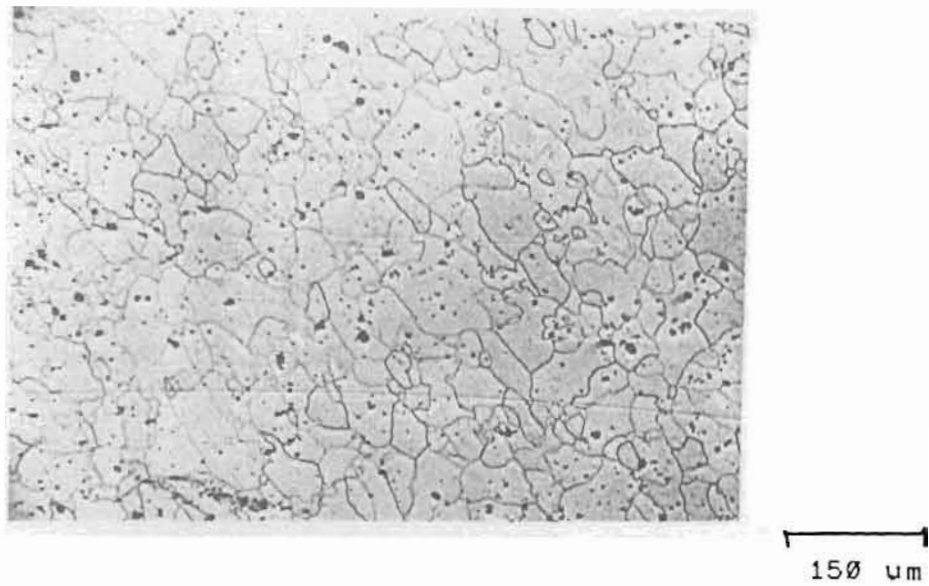mênt along the direction of rolling.

150 um

Fig.38 : Optical microstructure of the heat treated composite
sheet. Shows formation of sub-grains and good
distribution of particles and dispersoids.

percentage elongation at 19%. This strengthening is assumed to be due to conventional precipitation hardening of the alloy system. Fig.38 shows the optical microstructure of the composite heat treated to maximum strength level (S.No. 3 of Table XXI). The grains are fairly uniform with average grain size ranging between 30 and 50 μm. The precipitates and dispersoids are very uniformly distributed throughout.

Figures 39 and 40 show the distribution of dispersoids / precipitates both in the matrix and preferentially along the grain boundary. Precipitates formed on Al-Zn-Mg alloys are basicaly $MgZn_2$ and are normally finely distributed. It may be difficult to distinguish between $MgZn_2$ precipitates and the particulates of the same size in a microstructure. However, the coarser particles are essentially the particulate agglomerates since such large size precipitates are not possible in this alloy system. Since TiO_2 is basically very malleable, its presence in the grain boundary adds to the enhancement of the elongation of the composite. The particulate dispersoids vary in size from 0.4 to 2.4μm.

Figures 41 and 42 show the SEM fractographs of the as-rolled sheet in two different magnifications and figures 43 and 44 show that of the heat treated sheet. The material flow is very ductile in both cases. The dimples are very deep in both the cases, with the diameter ranging from 2 to 8 μm. Bimodal distribution of dimple sizes is seen to exist (e.g. there are small dimples located between the larger ones). Particle fracture (marked f in Figs. 41 & 44) and particle pull out (marked p in Figs. 42 & 43) are seen in both the rolled and
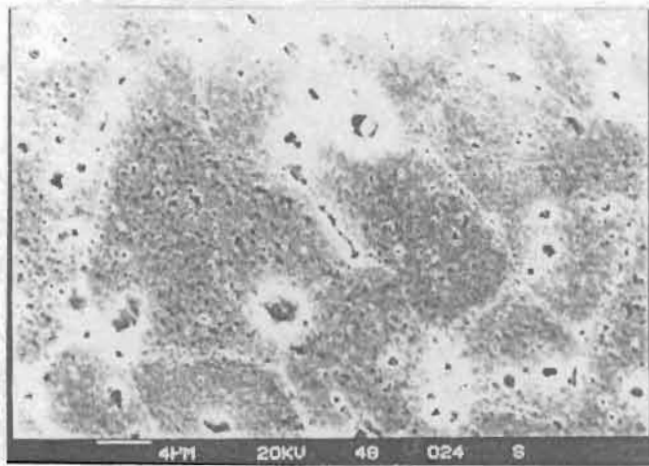
Fig.39 : SEM picture of heat treated composite sheet.
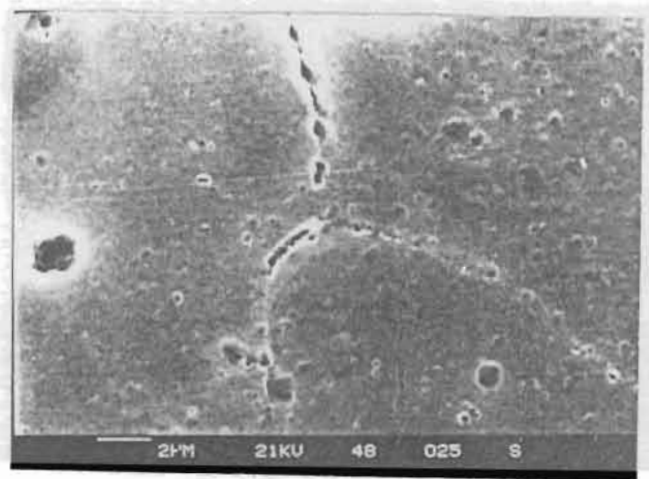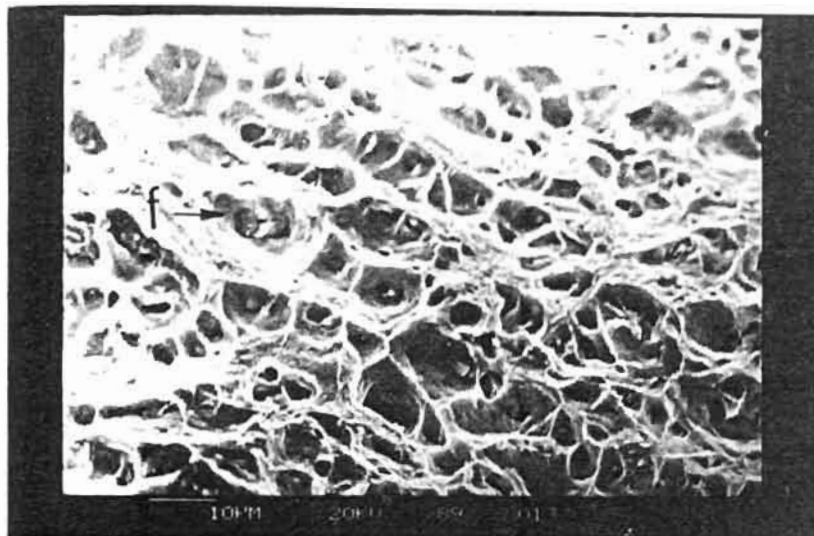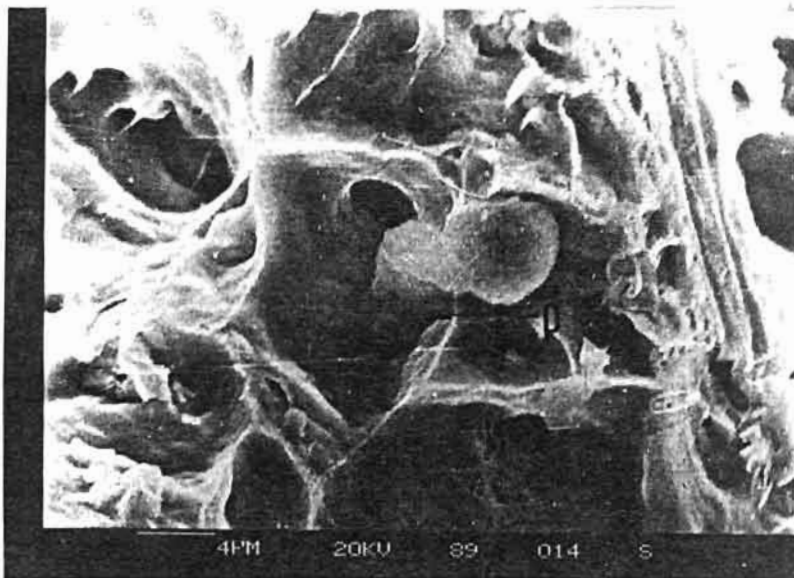Shows particle over the matrix and the grain
boundary.

Fif.40 : Same as above at higher magnification.
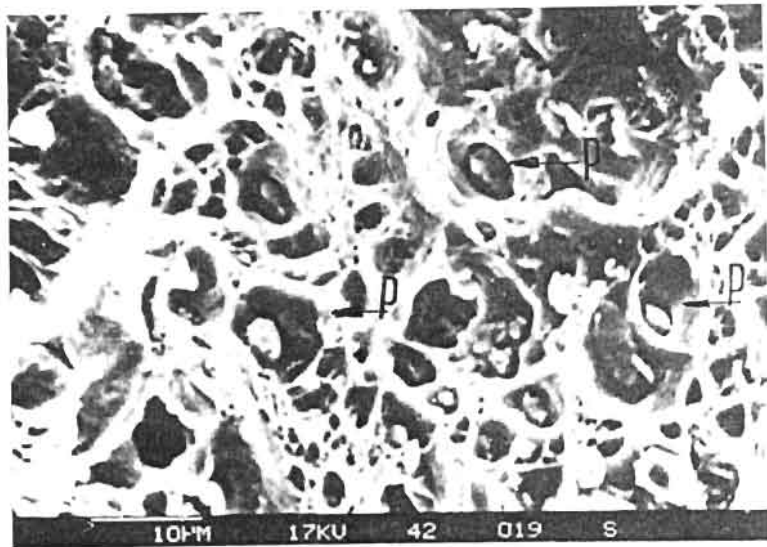Shows three grain joint and the particle
distribution.

20 um

Fig.41 : Fractograph of tensile fracture on hot rolled
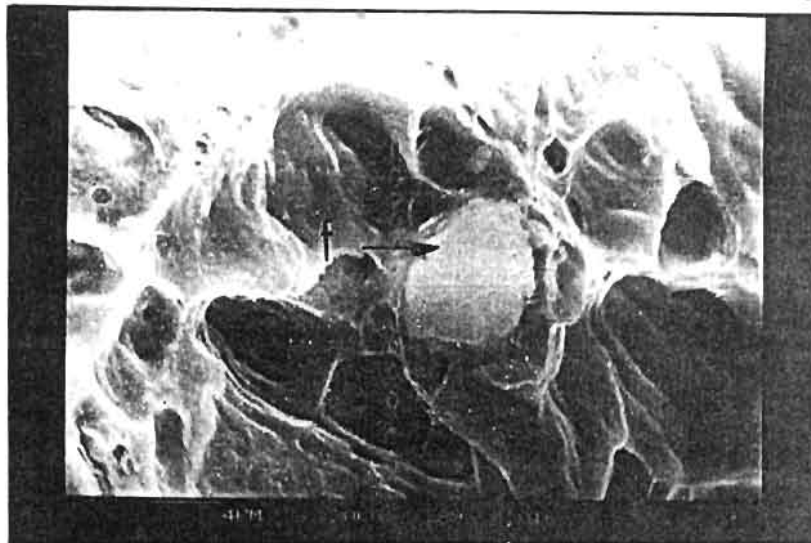composite sheet. Reveals deep dimples and
particles inside.

6 um

Fig.42 : Same as above at higher magnification. Shows a
particle, pulled out of a dimple.

20 um

Fig.43 : Fractograph of tensile fracture on heat treated
composite sheet. Structure similar to Fig.41.

6 um

Fig.44 : Same as above at higher magnification. Shows a
particle positioned between several dimples.

heat treated sheets. It is reported in an earlier study (165) that loss of adhesion of SiC and SiO_2 particles take place in the Al-Zn-Mg alloy matrix (AA 7091) on heat treatment due to seggregation of Mg and Zn at the interface. In this composite, decohesion is not due to heat treatment, but probably due to the poor bonding and also thermal mismatch. Since the basic strength of the TiO_2 particles is low unlike SiC particles, decohesion probably does not affect the strength of the basic alloy. The differential thermal expansion coefficients of TiO_2 and the base alloy, as recorded in the tables V and VII as 8×10^{-6} and 23.5×10^{-6} respectively. This differential thermal expansion results in a thermal mismatch strain ϵ according to the relation (9)

$$\epsilon = \delta\alpha \times \delta T \qquad -- \qquad (14)$$

where $\delta\alpha$ is the difference in α between the particle and the matrix and δT is the temperature change . The thermal mismatch strain on heat treatment for this composite is calculated to be 6.71×10^{-3}. This ϵ is expected to strengthen a particulate MMC (167), however, there was no strengthening effect in this composite system due to the decohesion of the particles.

Final thermomechanical treatment with upto 10% cold reduction in thickness by rolling after solution treatment was found very effective to enhance the properties of the Al-Zn-Mg base alloy in the earlier study by the investigator(160). However, TMT on the TiO_2 dispersed Al-Zn-Mg alloy composite did not

show any improvement in mechanical properties. The dislocations introduced by TMT influenced the ageing kinetics and morphology of the of the hardening precipitate in the base alloy system thereby enhancing the mechanical properties. However in the composite system, the dislocations preferably interacted with the dispersoids and did not act as preferential sites for nucleation of precipitates, thereby not responding to TMT. Similar results are reported in the earlier studies also (9).

Hot rolled and warm rolled sheets were subjected to very severe cold rolling operations to as much as 94% reduction in thickness to produce foils of thickness 0.10 mm. The composite was very malleable with fine surface finish and without any rolling defects. The base alloy cracked severely on 75% cold reduction without an intemittent annealing treatment. The photograph on Fig.45 shows the surface features of the base alloy and the composite sheets. It may be noted that the base alloy system is normally cold rolled to foils with an intermittent annealing treatment. This excellant cold workability of this composite without an intermittent annealing is possibly because of the basic nature of the particulates. The particulates are weakly bonded and flow easily on rolling by de-agglomeration. Mechanical properties of the cold rolled sheets are compared with that of the base alloy in Fig.46. It is observed that 75% cold reduction in thickness has the maximum strengthening level in this composite system with a tensile strength value

85

MATRIX MATERIAL (H74S)
THICKNESS - 0.80mm
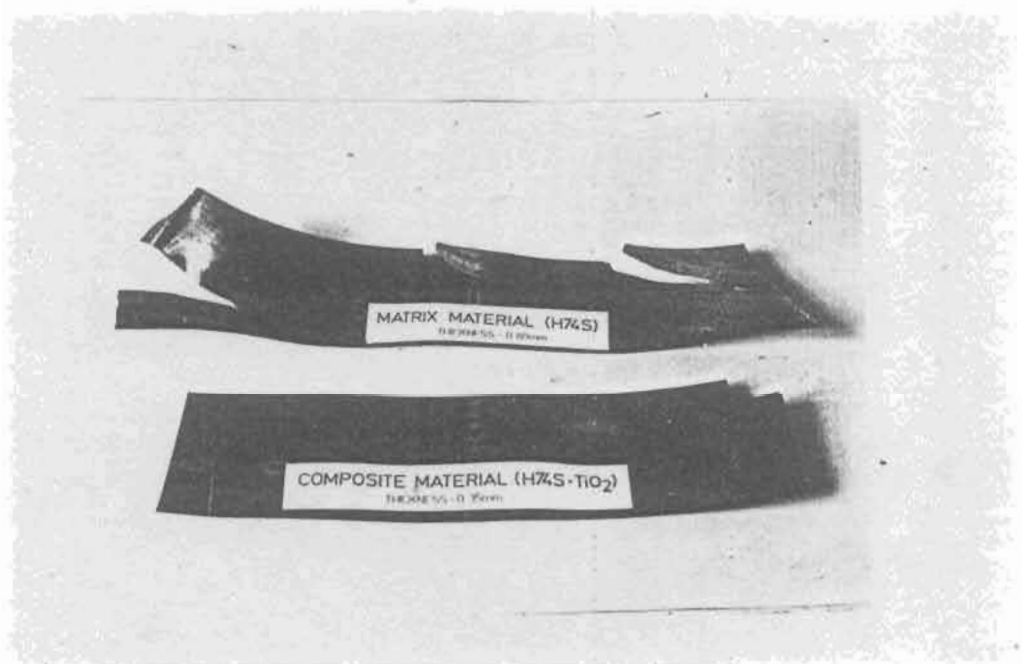
COMPOSITE MATERIAL (H74S-TiO2)
THICKNESS - 0.75mm

Fig.45 : Photograph of the cold rolled sheets of both
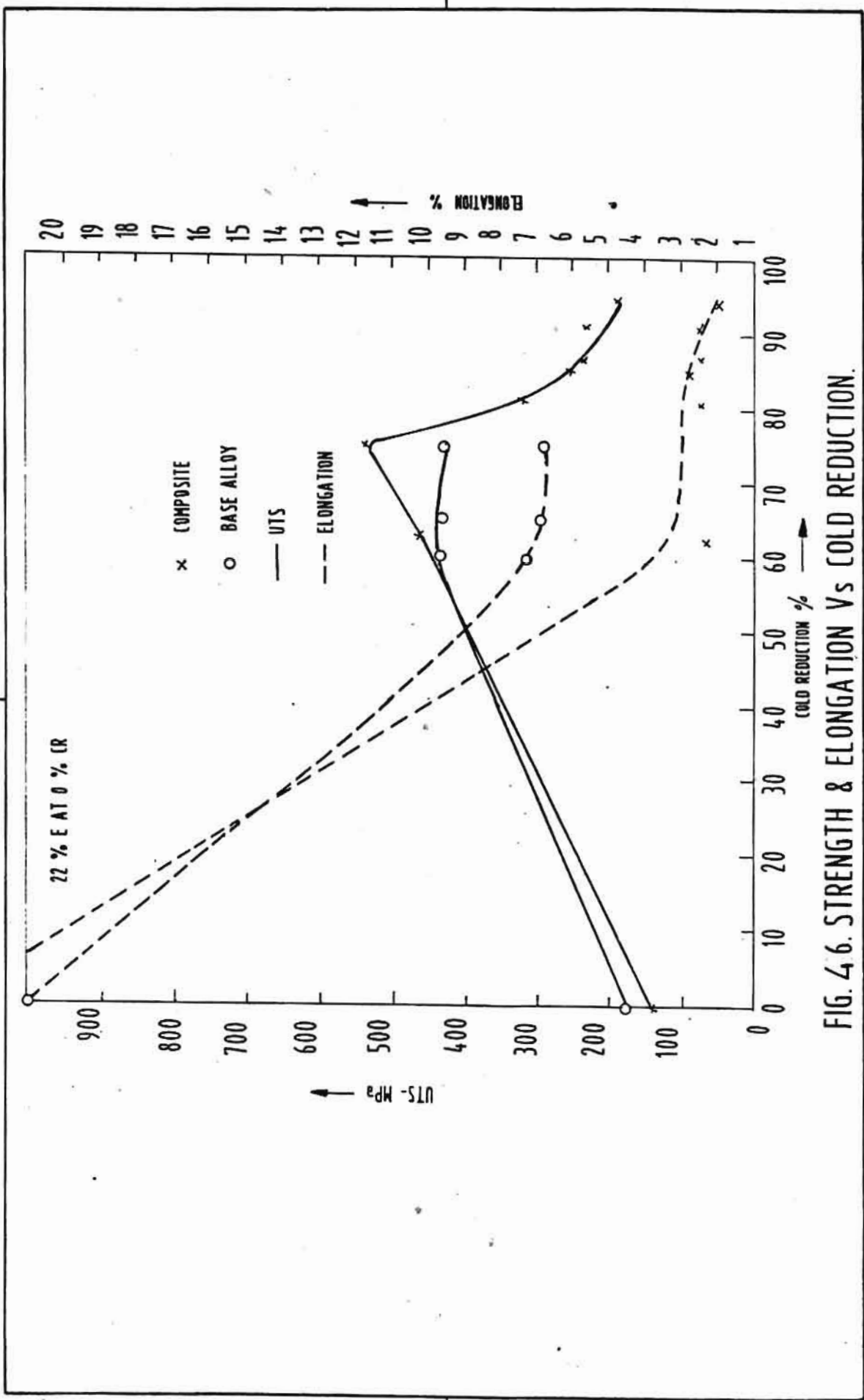base alloy and the composite.

FIG. 4.6. STRENGTH & ELONGATION Vs COLD REDUCTION.

of 540 MPa, about 26% higher than the theoretical prediction of 427 MPa and 22% higher than that of the base alloy (440 MPa) in the cold worked condition. However the percentage elongation also has drastically reduced to a very low value of 2%. Further reduction in thickness by cold rolling upto 94% has reduced the strength level to the least value of 182 MPa with further reduction in percentage elongation to 0.8%. Similar results were observed (168) in an Al-Ni system also which was reported to be due to dynamic recovery at quite a low temperature and high strain rates (169). The base alloy strength of 180 MPa with 22% elongation in hot rolled condition (values corresponding to annealed condition, since in the hot rolled condition, the base alloy is considered to be in fully recrystalised condition) has significantly increased to above 440 MPa with a drastic reduction in the percentage elongation to 6% on 60% cold rolling. Further cold reduction upto 65% and 75% did not change the properties of the base alloy. The strength of a crystalline solid is determined by the stress required to either generate or move dislocations in the material. Dislocation motion is controlled either by dislocation-dislocation interactions, direct dislocation-particle interactions or indirect dislocation-particle interactions (some matrix structure defined by the presence of dispersoids). The strengthening mechanisms in MMC have been related to high dislocation density in the matrix originating from differential thermal expansion (170), geometrical constraints (171) and plastic

86

deformation during the processing. Thermal mismatch strain is not a factor to be considered during cold working. Dislocation due to geometrical constraints are generally caused during the deformation of ductile matrix containing a hard dispersoid. Since TiO_2 did not form a hard dispersoid due to preferential agglomeration, it can be said that the strengthening mechanism in this composite is preferentially due to plastic deformation.

Considering the micro-mechanism approach on deformation processing, a material yields when applied stress is able to cause large scale movement of dislocations. Barriers for this large scale movement are introduction of further dislocations produced by many sources like particle dispersoids, thermal mismatch between particle and the base alloy, grain and sub-grain boundaries, work hardening etc. Cold rolling is essentially a work hardening process, which introduces large scale dislocations. It may be noted here that, the mechanical properties of MMCs are also affected by the residual stresses which form as a result of thermal mismatch between the matrix and the dispersoid. It was observed that (173,174) although the average residual stress in MMC is relatively small, there can be relatively substantial compressive stresses at the matrix-dispersoid interface boundary. In addition, the state of stress in the matrix region adjacent to the dispersoid may be either tensile or compressive, depending on the strengthening phase. Also that, in the matrix region, between the dispersoids, the

87

residual stress will be tensile, and plastic deformation is likely to initiate in this region since it contains fewer dislocations when compared to the dispersoid - matrix interface.This is expected to result in the fragmentation of the grains and formation of sub-grains in the matrix giving rise to strengthening effect. The higher strength of this composite at 75% cold reduction is due to the combined effect of dislocation hardening and sub-grain formation. Dislocation hardening however results in heavy pile up of dislocations at the grain boundary and particle-matrix interface boundary leading to reduced ductility. As deformation proceeds, the stress induced at the particle matrix interface by dislocation tangles leads to the relaxation of the dislocation loops. This reduces the strength level at higher deformations. Deagglomeration of particulates also result in relaxation of dislocation density at the interface boundary effecting a reduced strength, as deformation proceeds. This reduced strength due to relaxation of dislocation loops and particulate deagglomeration helps in the easy flow of the composite even at low ductility, as measured by percentage elongation in a tensile test. This phenomena of better formability in the cold rolled condition has been reported (171) in certain non-heat treatable wrought Al alloys also like Al-1.2Mn (AA 3003) alloys. .

Fig.47 shows the SEM picture of 1.4 mm thickness sheet in the cold rolled condition. The structure shows the fragmentation of the agglomerates of TiO_2 particles on cold roling.
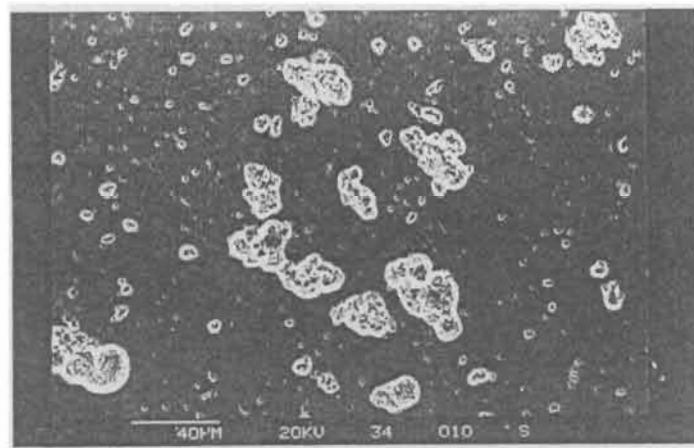
88

Fig.47 : SEM picture of cold rolled composite sheet of
         thickness 1.4 mm. Reveals deagglomeration and
         distribution of the dispersoids.

Fig.48 shows the optical metallograph of the 0.65 mm thickness sheet which has given the highest strength level in the composite. It is a very massive structure exhibiting some more TiO2 agglomerates. The fractograph of the above is shown in Fig. 49. The fracture is of highly brittle nature. The crack initiation is probably from the voids adjacent to the particles. Fig.50 shows the TEM picture of the 0.65mm sheet with severe particle-dislocation tangles. The particles are of size varying from $0.2\mu m$ to 0.7 μm with the largest inter particle spacing at 2 μm. Fig.51 shows the dislocation tangles responsible for dislocation hardening effect. The particles observed in the structure is of size $0.17\mu m$. Fig.52 shows the optical microstructure of 0.35 mm cold rolled sheets. This reveals the effect of cold rolling in breaking up the agglomerates of TiO_2 particles in the matrix. Fig.53 shows the fractograph of the tensile tested specimen. The fracture is of mixed mode indicating both ductile and brittle shear.

Fig.54-56 show the TEM picture of the sheet from where it is noted that dislocation tangles are much more relaxed from what was observed earlier in 0.65 mm rolled sheet (Fig.50 & 51).The particle sizes were of the order of 0.2 μm with the largest inter particle spacing at 1.4 μm. The fractograph of the tensile tested sheet of size 0.2mm is shown in Fig. 57 which reveals a massive brittle failure.

Fig.58 shows the optical microstructure of 0.15mm as rolled sheet. The elongated grain boundaries are clearly revealed

89
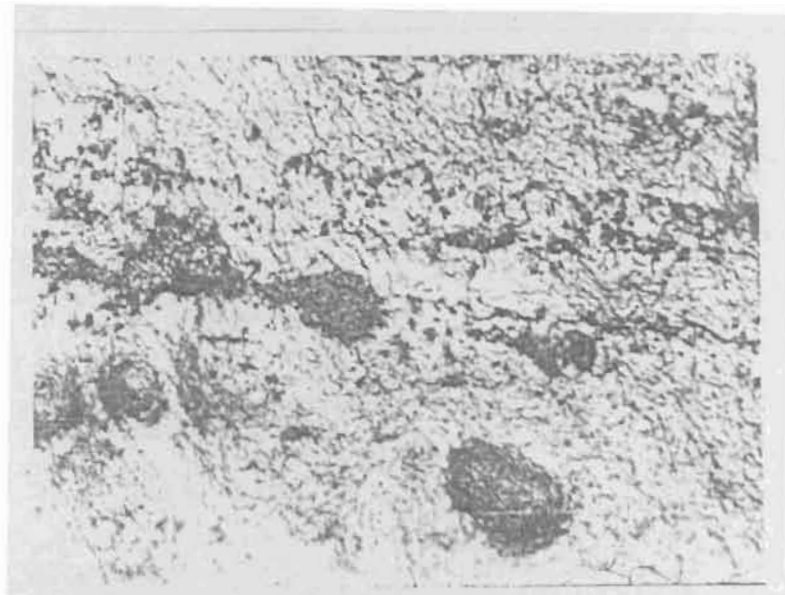
100μm

Fig.48 : Optical microstructure of cold rolled composite
sheet of thickness 0.65 mm. Shows massive structure
and particle alignment along the direction of
rolling

Fig.49 : Fractograph of tensile tested cold rolled composite
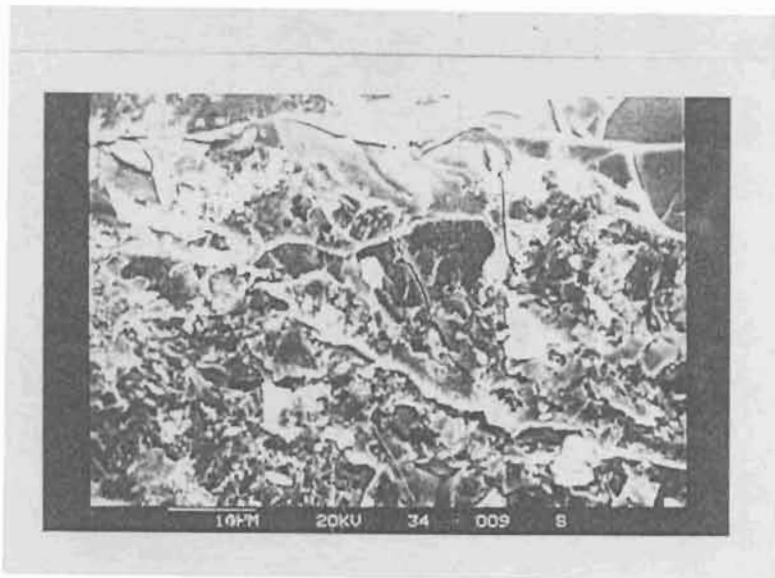sheet of thickness 0.65 mm. Shows brittle fracture &
initiation of cracks from voids adjacent to particle

1 .um
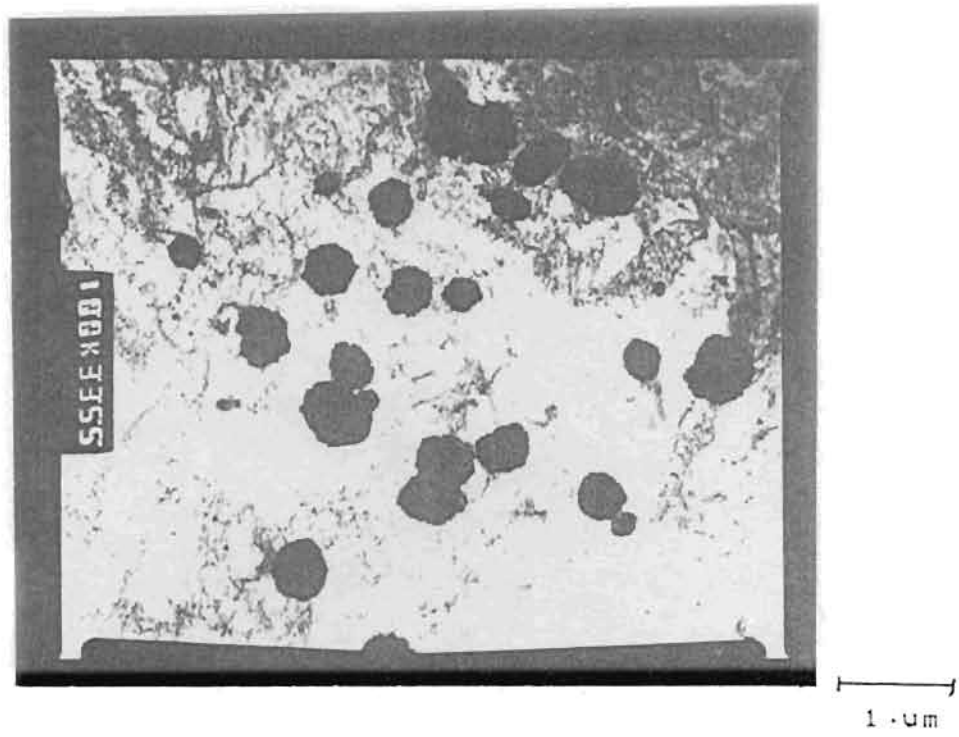
Fig.50 : TEM picture of cold rolled composite sheet (∅.65 mm)
        Shows good distribution of particles and formation
        of dislocation tangles.

∅.2 uM
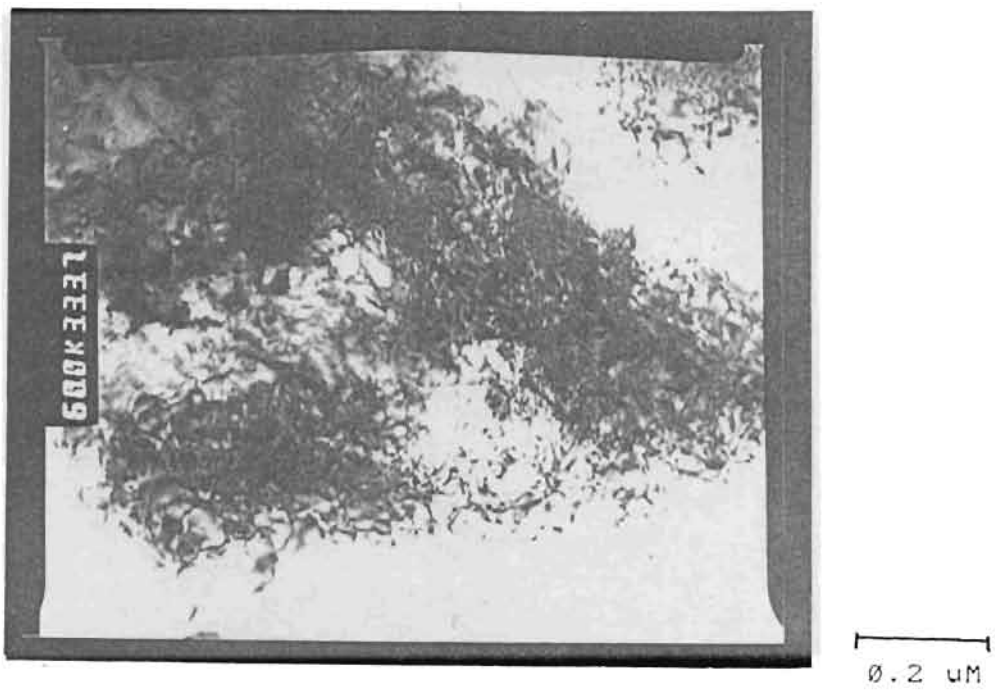
Fig.51 : Same as above at higher magnification. Shows
         dislocation tangles. (UTS 54∅ MPa).
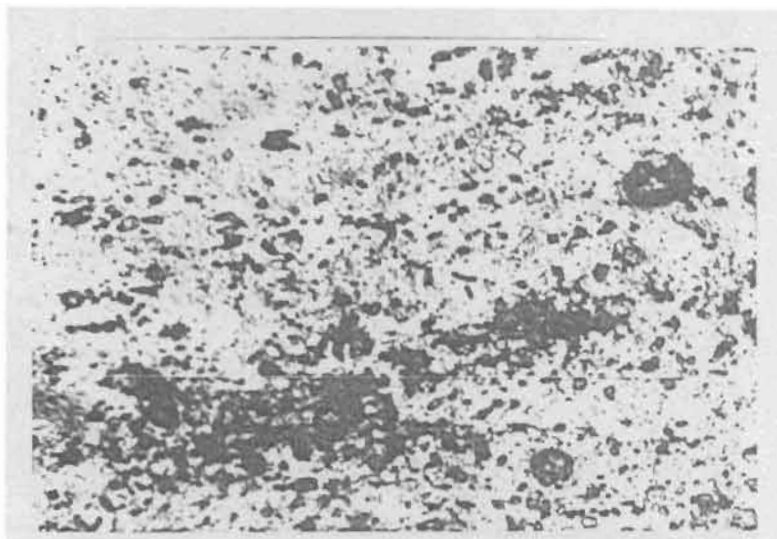
100 um

Fig.52   Optical microstructure of cold rolled composite
sheet (thickness 0.35 mm). Reveals disintegration
of particle cluster and realignment along
direction of extrusion
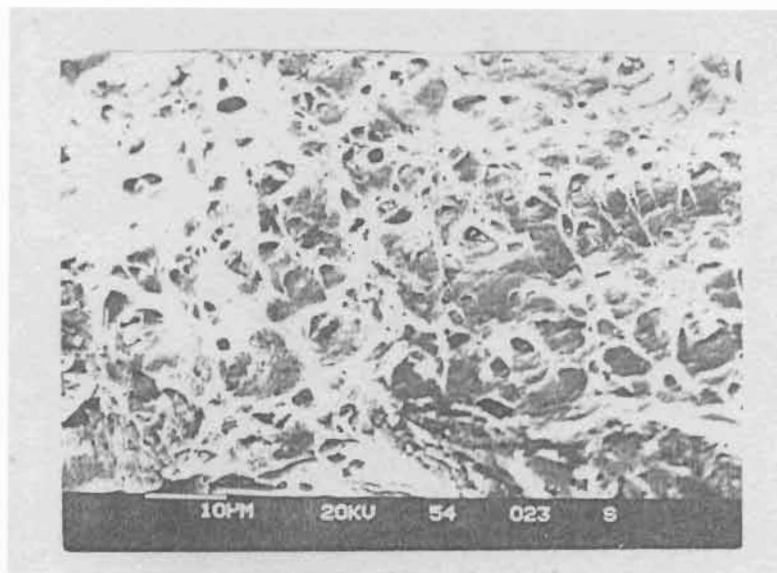
Fig. 53 : Fractograph of the tensile fracture of the sample
at Fig.52. Reveals formation of microvoids over
the matrix and failure by brittle shear.

1 um
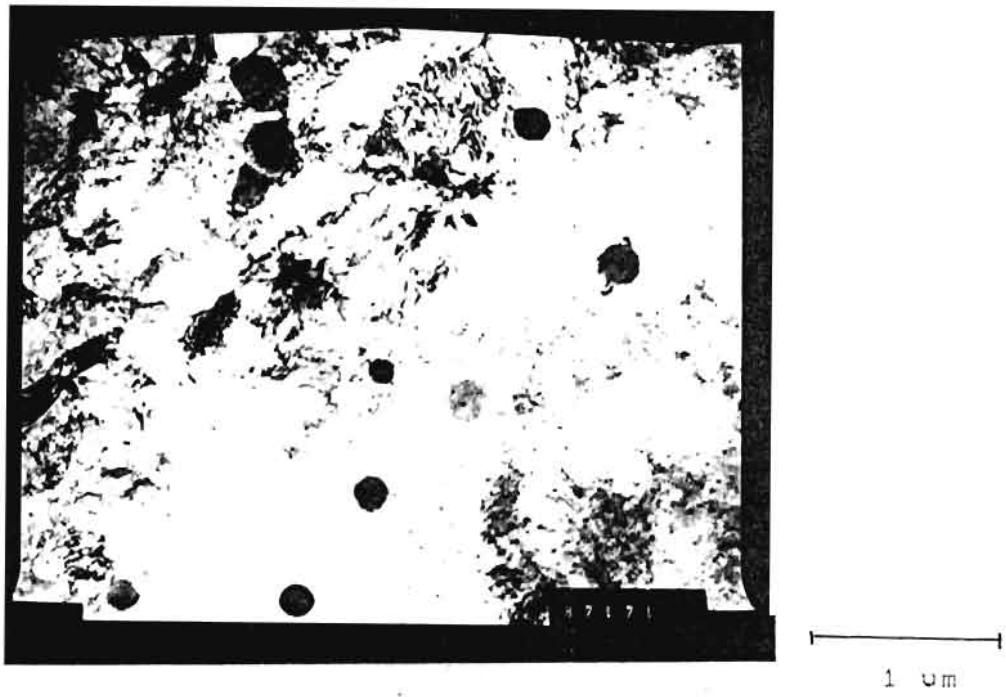
Fig.54 : TEM picture of cold rolled composite sheet
(thickness 0.2 mm). Agglomerate sizes are small
compared to that in Fig.50. Dilsocation tangles are
more relaxed .

0.4 um
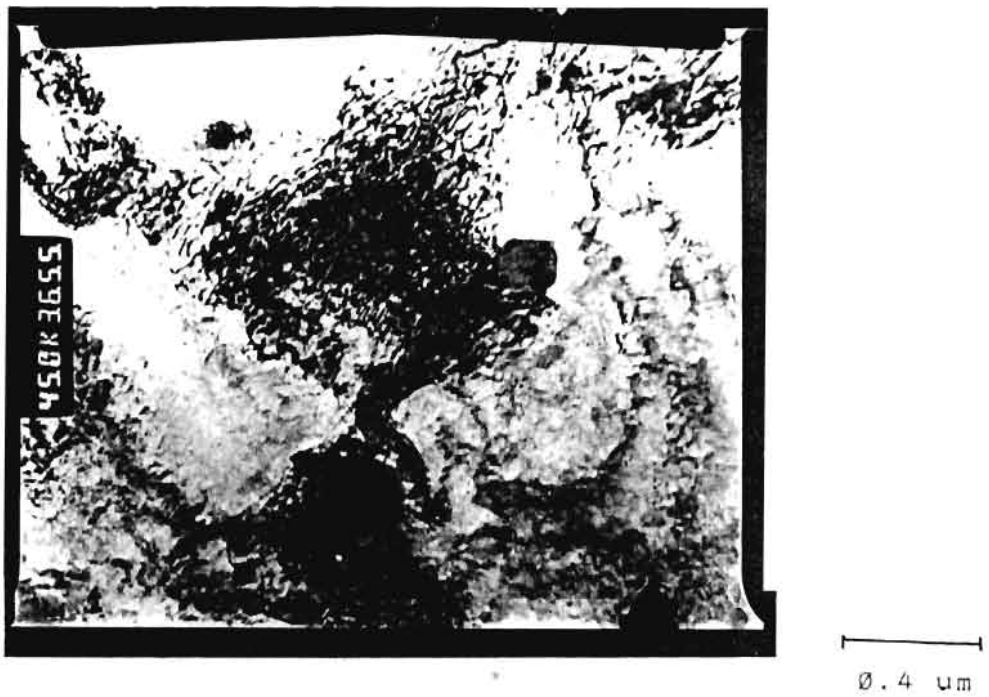
Fig.55 : Same as above showing relaxed dislocation tangles.

1 um

Fig.56 : Same as in Fig.54, showing dislocations at grain
boundaries
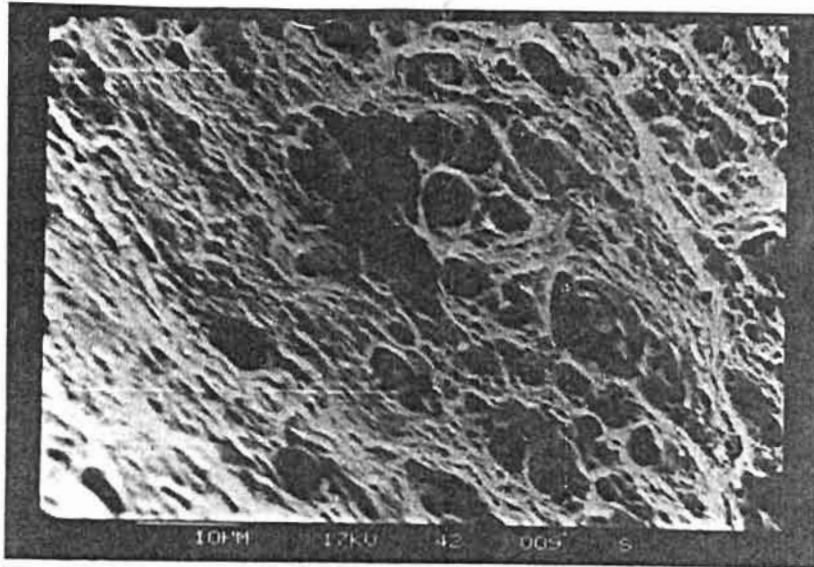
Fig.57 : Fractograph of tensile fracture of cold rolled
composite sheet (thickness Ø.2 mm). Reveals massive
brittle fracture.

100 um

Fig.58 : Optical microstructure of cold rolled composite
sheet (thickness 0.15 mm). Reveals elongated grains
along rolling direction and fine distribution of
dispersoids.

good particulate dispersion. However, this has not resulted in the expected dispersion strengthening. This may be due to one or more of the following effects:-

i)   Presence of cracked particles

ii)   highest triaxial tensile stress

iii) lower work hardening rate leading to work softening

iv)   formation of voids and

v)   cross slip and other slip systems are operative reducing the effective flow stress for the fracture

Fig.59 shows the TEM picture of a large single particle of size 0.5μm in the 0.15mm cold rolled sheet. The SAD on this particle is shown in Fig.60 which is a complicated diffraction pattern corresponding to the TiO_2 and $MgTi_2O_5$ Fig.61 is the SAD on the particle free matrix of the structure shown in Fig.63. This corresponds to the Al-Zn-Mg alloy structure.

Fig.62 is the TEM picture of 0.1mm rolled foil. SAD on the particle agglomerate is shown in Fig.63 which is similar to Fig,60. Fig. 64 shows the dislocation pile up at the grain boundary which reduces the ductility of the composite in the cold rolled condition.

Fig.65 shows the optical microstructure of the heat treated sheet of 0.65 mm thickness. The structure reveals the formation of very fine grains and sub-grains during the deformation process. The grain size vary in size from 25μm to 35μm with several sub grains. From the tabulation of mechanical properties (Table XXII), it is observed that

TABLE - XXII

Comparison of Mechanical Properties of base alloy and
composite sheets in cold rolled and Heat Treated Condition
(sheet thickness 0.65 mm)

S.No.	Heat treatment	UTS (MPa)	% E
1.	ST + 378 K / 4 hrs.+ 393 K / 20 hrs.	331	12
		328	12.3
		333	12.8
		339	12.1
		327	13.1
2.	ST + 378 K / 4 hrs. + 393 K / 30 hrs.	257	13.2
		248	14.2
		322	13.8
		317	12.8
3.	ST + 378 K / 4 hrs. + 393 K / 40 hrs.	251	14.7
		278	13.2
		298	13.9
4.	ST + 378 K / 4 hrs. + 413 K / 24 hrs.	263	11.8
		317	14.3
		276	14.7
5.	Base alloy (condition as in 4)	325	7

NOTE   ST = Solution Treatment at 733 K + Water Quench.

Observation: Properties after heat treatment (S.No.1) is better
and is higher than that of the base alloy.
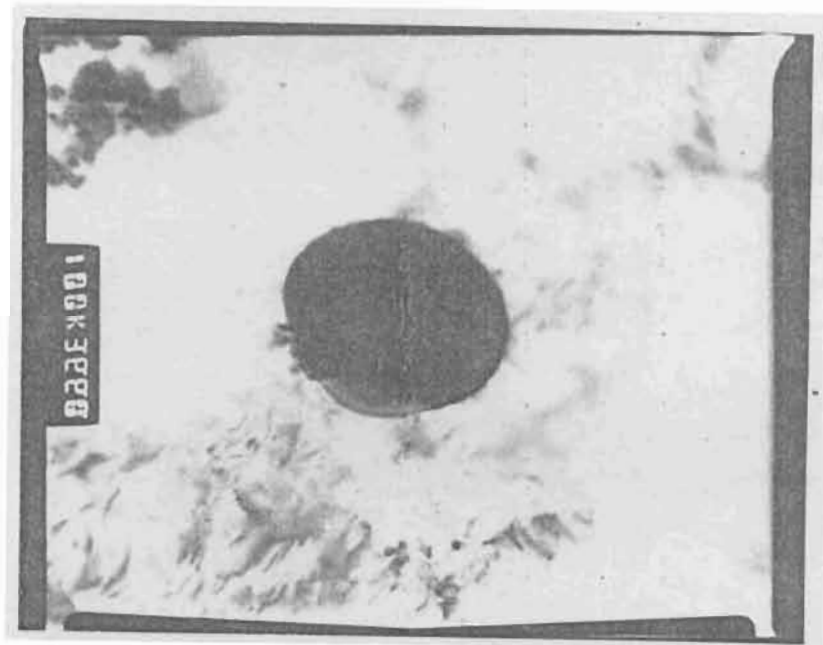
0.2 um

Fig.59 : TEM picture of the sample as in Fig.58. Shows a large single particle of size 0.5 um.
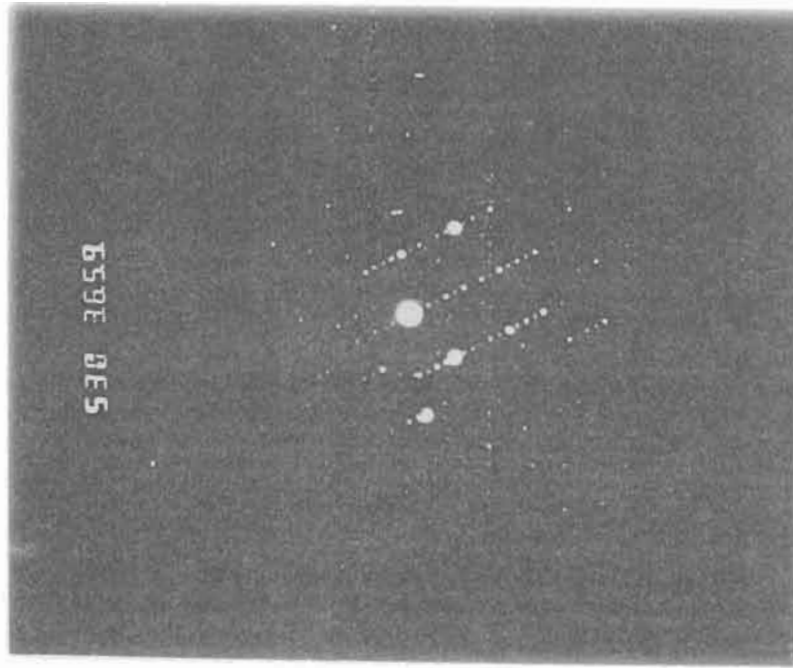
Fig.60 : Selected area diffraction over the particle shown in
Fig.59. Diffraction pattern corresponds to TiO_2 and
$MgTi_2O_5$.. (Lamda = 0.0335A, Camera L = 530 mm).
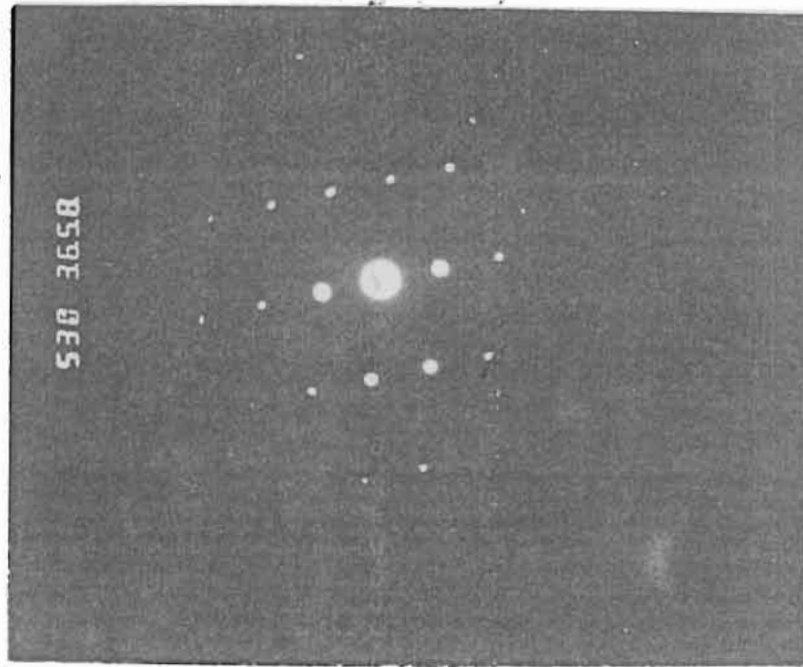
Fig.61 : SAD over the matrix area of Fig.59. Diffraction
pattern is typical of FCC Al base alloys.
(Lamda = 0.0335A, Camera length = 530 mm)

0.4 um

Fig.62 : TEM picture of cold rolled composite sheet (thickness 0.1 mm). Reveals deagglomeration of dispersoids. A few particles are also seen over grain boundary.
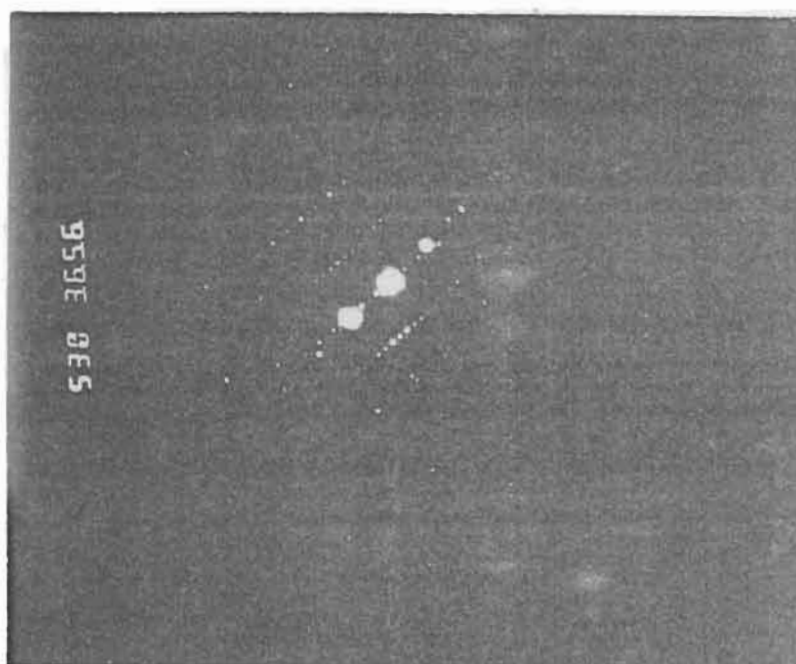
Fig.63 : SAD over the particle on the sample at Fig.62. Diffraction pattern similar to Fig.60.
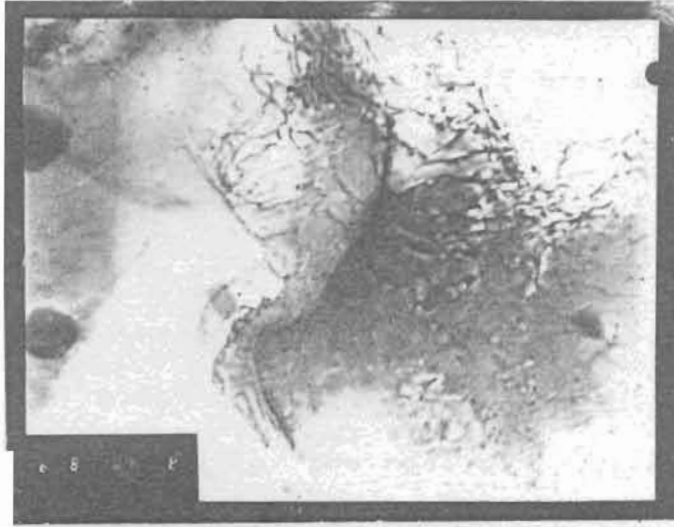
0.2 μm

Fig.64 : TEM picture of sample as in Fig.62. Reveals severe
         segregation of dislocations over the grain boundary.
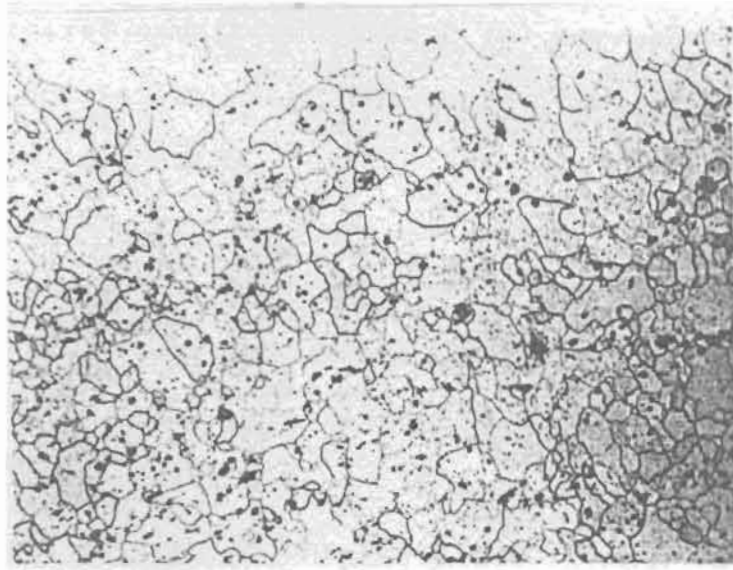
100 μm

Fig.65 : Optical microstructure of heat treated composite
          sheet sample (thickness Ø.65 mm). Reveals
          uniform precipitation and dispersion, and
          formation of sub-grains.

conventional ageing cycle that was adopted for the base alloy has given the optimum properties for the composite sheet also. This is in agreement with the recent study (118) where it is reported that in AA 2014-Al_2O_3 composite system, the optimum properties are obtained at 16 hrs. ageing at 433K and the base alloy is also aged for 18 hours at the same temperature. However in AA 6061-Al_2O_3 system it is reported (118) that ageing time is reduced from 18 hours to 10 hours at the same ageing temperature and that in the case of SiCw reinforced 2124 Al alloy composite, the ageing time at 450 K was reduced from 10 hours for the base alloy to about 4 hours for the composite (19).

Heat treatment of the cold rolled sheet drastically reduced the strength level of 540 MPa to 333 MPa with the regain of the ductility level from 2% to 12%. This strength level in the heat treated condition is well in agreement with the theoretical prediction for the composite. The regain of ductility is primarily because of the relaxation of dislocation at the grain boundaries due to heat treatment. This also attributes to the reduction in strength level. The fractograph of the tensile tested samples are shown in Fig.66 and 67., The failure mode is ductile with bimodal dimple size distribution. Particle pull out within some of the dimples can be seen in the fractographs. A compilation of mechanical properties of the sheet samples at various stages, is given in Table XXIII.

High temperature mechanical properties of 0.65 mm sheets in
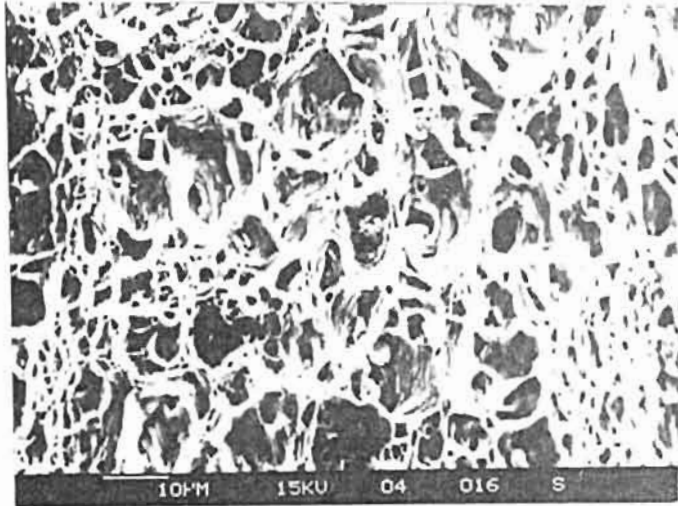
Fig.66 : Fractograph of tensile fracture of smaple at Fig.65. Reveals formation of microvoids and deep dimples typical of ductile fracture.
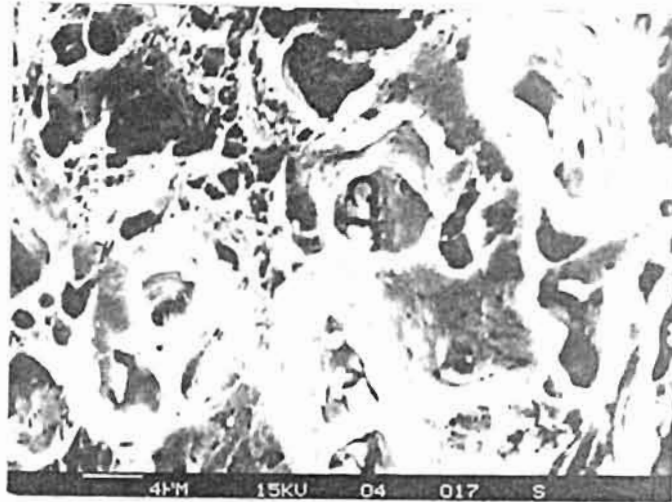
Fig.67 : Same as in Fig.66 at higher magnification. Shows dimples and particles positioned within.

TABLE - XXIII

Mechanical Properties of the Composite Sheet Samples

at various Stages at Room Temperature

(from Tables XX - XXII)

S.No.	Condition	Sample Thickness mm	No.of Samples	UTS MPa	YS MPa	% E
1.	As Hot Rolled	3.8	4	130-140	80-110	20-23
2.	HR + ST +					
a)	aged 413 K/36H	3.8	3	230-240	170-190	13-14
b)	378K/4 +413k/24	2.3	3	230-240	170-180	16-17
c)	378K/4 +393K/30	2.6	4	260-280	200-210	18-20
3.	As Cold Rolled					
a)	60-70% Reduction	1.4	3	460-470	--	1.4
b)	70-80 ''	0.65	4	480-550	--	1.8
c)	80-90 ''	0.5-.35	8	250-360	--	1.6
d)	90-95 ''	0.2-.10	4	180- 230	--	1.2
4.	CR + ST +					
a)	378k/4 +393k/20	0.65	5	330-340	--	12-13
b)	378K/4 +393K/30	''	4	250-320	--	13-14
c)	378K/4 +393K/40	''	3	250=300	--	13-15
d)	378K/4 +413K/24	''	3	260-320	--	12-15

NOTE   ST = Solution Treatment at 733 K + Water Quench

Observation: Composite strength at 70-80% cold work (S.No.3b) is superior but at low elongation. Properties at S.No. 4a are optimum.

heat treated condition with 20 hours reageing at 393K are shown in Table XXIV. It is observed that the tensile strength of the base alloy reduces drastically from 390 MPa at room temperature to 100 MPa at 473K whereas the alloy composite retain its strength above 200 MPa at 473K, an increase of more than 100% from that of the base alloy. From the base alloy strength it is noted that the strengthening precipitate $MgZn_2$ dissolves in the matrix at temperature above 400 K. As such the strength of the base alloy reduces above this solvus temperature. In the composite system particle strengthening is effective at higher temperatures. Strengthening associated with equiaxed particulates at high temperatures is due to the suppression of the natural creep mechanism that can occur in the monolithic material (9), i.e. dislocation glide may be prevented by the particulates , thus requiring dislocation motion to occur by slower climb around the particulates. This results in higher tensile strength for the composite. The strength level of TiO_2 composite is comparable to that of Al_2O_3 dispersed liquid forged 2024 composite system (36). It is also superior to the high temperature aluminium alloy AA 2618 as shown in Table VI.

Young's Modulus was determined on the 0.65mm sheet in cold rolled condition. Loading was done on INSTRON 100T UTM by gradual tensile loading and the strain data was recorded at equal intervals of load. The stress strain curve is shown in Fig.68. The Young's Modulus was experimentally found out to be 69.17 GPa as against 71 GPa for the base alloy. This

92

TABLE - XXIV

Comparison of Mechanical Properties of Base Alloy and
Composite Sheets at elevated temperatures

Alloy Systems	Room Temp			373K			423K			473K		
	UTS MPa	YS MPa	E %	UTS MPa	YS MPa	E %	UTS MPa	YS MPa	E %	UTS MPa	YS MPa	E %
G74S (base alloy)	390	340	15	300	280	20	170	150	35	100	80	60
G74S + TiO_2 0.65 mm Sheet T6 Condition: (composite)	330	--	12	290	210	14	230	200	17	210	200	22
Liquid Forged Composite(36)												
2024	390	270	8	--	--	--	260	--	10	--	--	--
2024 + Al_2O_3	340	250	3	--	--	--	240	--	2	--	--	--
2014	320	210	7	--	--	--	230	--	9	--	--	--
2014 + Al_2O_3	320	220	5	--	--	--	210	--	3	--	--	--

Observation: Composite properties are much superior to that
of the base alloy at temperatures above 423 K.
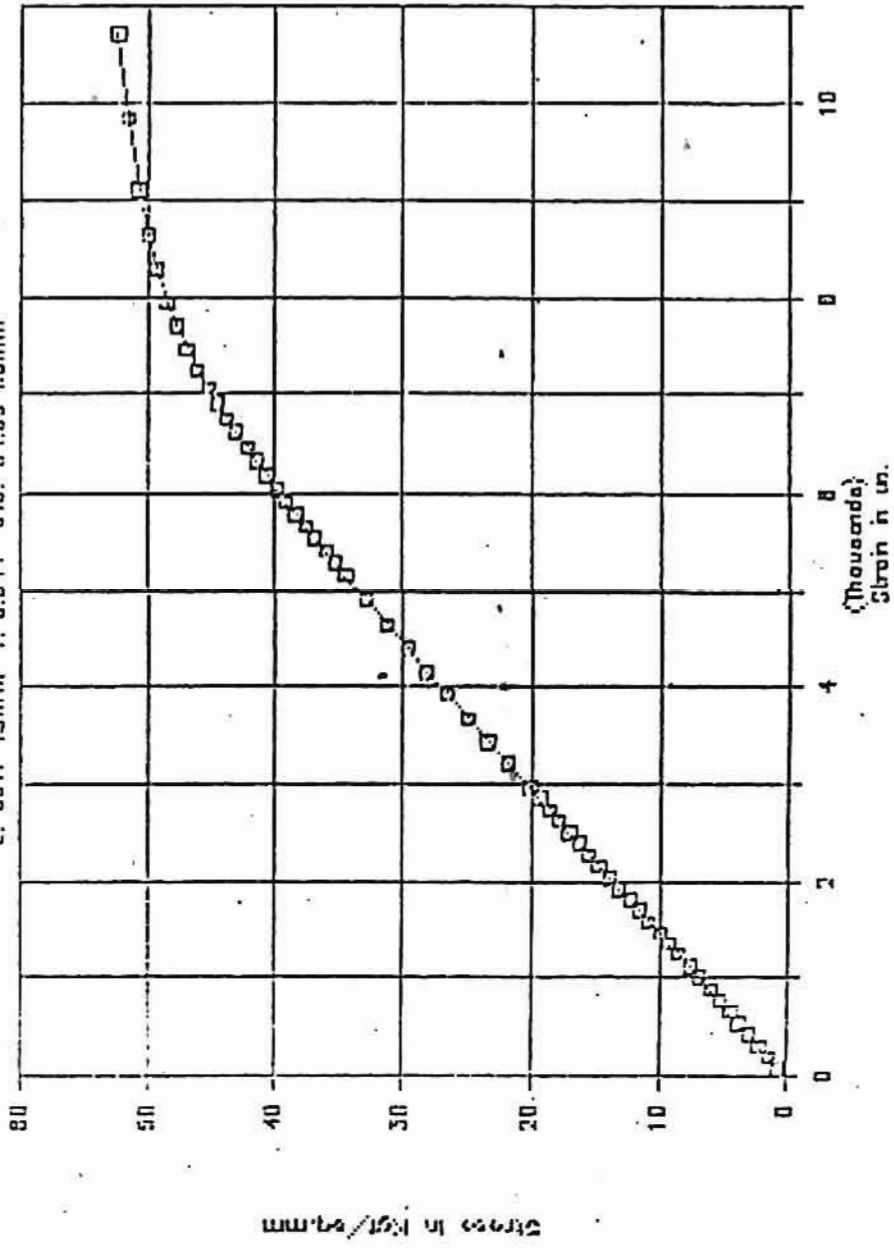
Fig.68. Stress – Strain Curve of a Cold Rolled
Composite Sheet (thickness 0.65 mm).

indicates that TiO_2 dispersion has only a marginal influence on the modulus properties. Theoretical calculation of Young's Modulus of the composite could not be carried out for want of modulus values for TiO_2 which is not reported in a wide spectrum of literatures scanned through during this investigation. Poisson's Ratio for the composite is calculated to 0.335 in the cold rolled condition at the UTS value of 540 MPa.

Density of the composite was measured at various stages. Density was 2.63 gm/cc in the cast stage, 2.76 gm/cc in the solid extruded sections and 2.80 in the rolled sheets. This shows the compaction of the composites at each stage. Density values of the composite in the extruded and rolled sections are in good agreement with that of the theoretical prediction. The composite in the cast stage is more porous than the secondary processed composites.

Thermal conductivity of the composite in the cast condition was experimentally determined to be 74.035 W/m.K (0.17 cals/cm.s.K) as against 0.29 cals/cm.s.K for the base alloy. Both density and thermal conductivity of the composite have been theoretically calculated using the rule of mixture for composites, considering the available values of the particulate TiO_2 and the matrix alloy AA 7005 (Tables V & VII) and found to be 2.82 gm/cc and 0.281 cal/cm.s.K respectively. The experimental value for thermal conductivity of the composite (in billet form) is only about 60% of that of the theoretical prediction. This shows that the billets are not sound and contains large number of porosities, as

93

indicated by the density values also, which decreased the thermal conductivity value. Thermal conductivity of the solid extruded rod was measured to be 122.7W/m.K (0.29 cals/cm.s.K). this value is practically the same as predicted by theoretical calculation and within the experimental error of measurements. Thermal conductivity on the rolled sheet could not be evaluated because of the restrictions on the dimensions of the specimen for the available instrument.

94

CHAPTER IV
CONCLUSIONS

IV CONCLUSIONS

The following conclusions are drawn from this investigation:

IV.1. Casting and synthesising the composite.

5 wt% TiO_2 particles of average particle size 0.37μm were dispersed in Al-Zn-Mg alloy matrix, using both liquid metallurgy and rheocasting techniques.

The macrostructure over the entire cross section revealed that, in LM cast billets, the peripheral region of about 64% of the surface area contained chilled zone with very fine grains, a middle zone of about 27% contained columnar grains and the core region of about 9% contained equiaxed grains. In RC billets, the chilled zone was practically about 85% and the core region of about 15% contained equiaxed grains. There was no columnar grains in the RC billets.

Particles were found to be agglomerated in both the castings produced by either liquid metallurgy or rheocasting routes. In RC composite, the TiO_2 particle cluster sizes ranged upto 150 μm, but most of the clusters (about 48%) were in the range of 5 to 10 μm and practically 96% were of size below 50μm. The average particle size in the RC billet was found to be 14.54 μm. In LM composite, the particle cluster size ranged upto 250 μm with about 64% in the range above 50 μm size. The average particle size in the LM cast billet was found to be 86.6 μm. This indicated that RC route leads to finer sizes of agglomerates as compared to LM route and

95

therefore it is the preferred route for dispersing fine particulates.

In RC composite, the structure of the cast matrix was refined and primarily equiaxed, with cell size ranging between 10 and 20 μm with relatively uniform dispersion of TiO_2. In LM composite, the cast structure was very coarse and dendritic, and TiO_2 was observed primarily in the interdendritic regions. Evidence of gross particle pushing effect by the growing dendrite fronts into the centre of the castings was also observed in the case of LM castings.

During the synthesis of composites, the melt temperature was found to increase from 993 K to 1073 K in the case of LM route and from 873 K to 923 K in the case of RC route. This temperature increase was positively due to the exothermic reactions between TiO_2 and Mg present in the composite. The reaction products were analysed by XRD and found to contain TiO_2 and $MgTi_2O_5$. The thickness of the reaction zone in LM cast billets was measured to be 3 μm and that in RC billets was only 1 μm. Anatase grade TiO_2 that was added to the composite was also found to have transformed to rutile grade TiO_2 during the composite synthesis.

More than 94% of the dispersoids added to melt during the synthesis have been recoverd as particulates. XRD analysis of the particulates extracted from the billets has shown the presence of $MgTi_2O_5$ (Magnesium di-titanate) and rutile grade TiO_2. About 43 wt% of the magnesium originally added to the

96

melt was lost during the synthesis of the composites by both LM and RC routes due to oxidation reactions.

Microhardness testing on the particle clusters revealed that the particulates did not get sintered during the composite synthesis, but got weakly bonded forming agglomerates.

These studies indicated that, sub-micron size TiO_2 can be dispersed in Al alloy matrix by rheocasting technique. The exothermic nature of reaction between TiO_2 and Mg, keeps the melt at high enough temperature to enable addition of larger quantities of dispersoids.

IV.2. FORGINGS

During forging of the composite, the TiO_2 clusters break up and decohesion of particles from the matrix take place. Further forging operation with the processing sequence used in this study, resulted in cracks in the material. This apparently shows that dispersion of TiO_2 particles reduces the forgeability of the base alloy.

IV.3. EXTRUSION

The composites were extruded at 3 temperature ranges : i) At conventional hot extrusion temperature, (ii) temperature just above the solidus of the matrix alloy and (iii) temperature just below the liquidus of the matrix alloy. In the later two temperature ranges, the composite was in a slurry form.

During conventional hot extrusion, the cluster of TiO_2 got deagglomerated and the particles were aligned in the direction of extrusion. However during slurry state extrusion, the clusters did not get sheared and the matrix structure also resulted in partly cast structure at the grain boundaries, the cast structure being more predominant in the extrusions processed near the liquidus temperature.

Surface features of the conventional solid extrusions were smooth and defect free. However, slurry state extrusions exhibited very rough and cracked surface. The surface cracks on the composites after high temperature (above solidus temperature)extrusion were of size 2 x 2 mm and longitudinal in nature parallel to the direction of extrusion. This indicated that the surface cracks are due to the abrasion effect of the dispersoids on the die walls during extrusion in addition to the material shrinkage on solidification from its slurry state. Ultimate tensile strength of the solid extrusions in T6 heat treated condition ranged upto 300 MPa, not far below the theoretical prediction. Percentage elongation of the composite in the extruded and heat treated condition was very much comparable to that of the base alloy in the similar condition. In conclusion it can be said that Al-Zn-Mg -TiO_2 cmposite can well be extruded in the solid state using similar extrusion parameters as that of the base alloy and that the properties of the extruded composite is in agreement with the properties predicted theoretically by the rule of mixture for composites.

98

IV.4.**ROLLING**

Hot rolling was done in the temperature range of 733 - 693 K. Upto 95% reduction in thickness could be effected by hot rolling. TiO_2 particles were found to be largely separated from their cast stage agglomerates and were aligned in the rolling direction.

Hot rolled composite sheets were heat treated to T6 condition using the same parameters applicable to the base alloy. The thermomechanical treatment involving about 10% cold reduction after solution treatment and prior to ageing, enhanced the mechanical properties of the base alloy system, but did not have any effect in this composite system. This is probably because , the dislocations introduced by cold reduction after solution treatment interacted with the particulates and were not available as the potential nucleation sites for the precipitation for effecting any change in the kinetics or morphology of precipitation.

Cold rolling was carried out upto 94% reduction in thickness, making a foil of thickness 0.1 mm. The highest tensile strength of 540 MPa, 26% higher than the theoretical prediction and 22% higher than that of the base alloy in the cold rolled condition, was obtained at 75% reduction in thickness and further cold reduction decreased the strength level and also the elongation level. The higher strength level at 75% cold reduction is attributed to combined effect of dislocation hardening and sub-grain formation. The reduced ductility is due to the pile up of dislocations at the grain

99

of dislocation hardening and sub-grain formation. The reduced ductility is due to the pile up of dislocations at the grain boundaries and at the metal-particle interaface regions. At higher deformations above 75%, the stress induced at the particle-matrix interface by dislocation tangles leads to the relaxation of the dislocation loops. This results in reduced strength at above 75% cold deformation. However, dislocation tangles at the grain boundaries keep the percentage elongation at low level.

TiO_2 dispersions have significantly enhanced the cold workability of the base alloy. In the case of base alloys, the flow stress does not decrease at higher deformations and the material gets work hardened and ultimately develops cracks. But in the case of composites, the strength decreases as cold deformation proceeds above 75% reduction and that the particulates continues to deagglomerate during cold working. This enables easy flow of the composite during cold rolling even upto 94% reduction in thickness. This will eliminate the need of an intermittent annealing treatment during cold rolling operations.

Heat treatment of cold rolled sheets drastically reduced the effect of dislocation strengthening. The strength of the composite is in good agreement with the theoretical prediction made based on the basic rule of mixture for composite. Heat treatment also resulted in regaining the ductility of the composite from the cold rolled level, by the relaxation of the dislocation tangles at the grain boundary.

100

range 0.2μm to 0.7μm with the largest interparticle spacing at 2.0 μm, and in 0.2 mm sheets the particles were found to be of size 0.2 μm with interparticle spacing of 1.4μm.

TiO_2 dispesion has enhanced the high temperature strength of the alloy considerably. At the test temperature of 473 K, the composite exhibited tensile strength of about 210 MPa as compared to below 100 MPa for the base alloy at the same test temperature, an increment of above 100%.

These studies indicatd that TiO_2 dispersoids have beneficial effect on the malleability of the base alloy system. The tensile strength, in heat treated condition, at room temperature is well in agreement with the theoretical prediction. The strength in the cold rolled condition is enhanced significantly by an order of 26% more than the theoretical prediction, by the addition of TiO_2 to the alloy system. Effect of TiO_2 addition to the base alloy in retaining the strength at higher temperatures is also very significant. An increase in tensile strength of more than 100% compared to the base alloy has been obtained in the composite at a test temperature of 473 K.

IV. 5. HIGHLIGHTS OF THE INVESTIGATION.

IN SUMMARY, THE HIGHLIGHTS OF THIS INVESTIGATIVE WORK ON THE DISPERSION OF TiO_2 PARTICULATES OF AVERAGE PARTICLE SIZE 0.37 μm, IN Al-Zn-Mg WROUGHT ALLOY MATRIX, ARE LISTED BELOW :

*   While synthesising the composite, the melt temperature increases, due to exothermic reaction between TiO_2 and Mg. This will enable simultaneous addition of larger amounts of other particulates as well.

*   Rheocasting method is the preferred route for dispersing finer size particulates.

*   Extrudability and the properties of the extruded composite are comparable to that of the base alloy.

*   Malleability of the composite on both hot rolling and cold rolling is much superior to that of the base alloy. No intermittent annealing is required on cold rolling this comoposite. Composite has been successfully cold rolled into foils of thickness 0.1 mm.

*   Tensile strength in the cold rolled condition at 75% reduction in thickness, is 26% higher than the theoretical prediction and 22% higher than that of the base alloy in the similar condition.

*   Tensile strength of the composite at 473 K is more than 100% above that of the base alloy at the same test temperature.

102

CHAPTER V

SUGGESTIONS FOR FUTURE WORK

SUGGESTIONS FOR FUTURE WORK

The strength of the Al-Zn-Mg alloy depends basically on the Zn : Mg ratio and higher this ratio, higher is the strength level of the alloy. Similarly, addition of copper to the Al-Zn-Mg alloy increased the strength to the highest level. It is therefore suggested that Al-Zn-Mg-Cu system may be selected as the matrix alloy for dispersing TiO_2 with higher Zn : Mg ratio to see the effect on strengthening. The alloy combination may be similar to AA 7075 or AA 7178. However, for applications involving welding, it is required to select weldable high strength Al-Cu alloys (2000 series) as the matrix material.

Only 5 wt% of TiO_2 dispersion was used in this investigation, and it is suggested that the effect of dispersion upto 25% may be studied . This may have significant influence on the high temperature properties.

It is also suggested that studies may be formulated to study the effect of simultaneous additions TiO_2 and other dispersoids like SiC and Al_2O_3 in high strength alloy systems.

A more detailed study should be carried out on the deformation mechanisms on the new composite system and analyse the results with Transmission Electron microscopy.

103

REFERENCES

VI. REFERENCES:

1. T.W.Chou, A.Kelley and A.Okura ; Composites,16 (1986) 187.

2. S.G.Fishman ; J.of Metals,38 (1986) 26.

3. Y.Flom and R.J.Arsenault ; J.Metals,38 (1986) 31.

4. Idem ; Mat. sci.Eng.,77 (1986) 191.

5. A.H.M.Hoves ; J.Metals,38 (1986) 28.

6. A.Mortensen, M.N.Gangur, J.A.Cornie and M.C.Flemings ; J.Metals,38 (1986) 30.

7. A.Mortensen,J.A.Cornie and M.C.Flemings ; J.Metals,40 (1988) 12.

8. V.C.Nardone and K.W.Prewo ; Scripta Met.,20 (1986) 43.

9. I.A.Ibrahim, F.A.Mohamed and E.J.Lavernia ; J.Mat.Sci.,26 (1991) 1137.

10. M.M.Schwartz ; Composites Materials Handbook, Ed. H.B.Crawford and E.Richardson, McGraw Hill,New York,1984.

11. A.K.Dhingra ; J.Metals, 38 (1986) 17.

12. I.J.Polmear, Light Alloys-Metallurgy of light metals, Edward Arnold, London, (1989) 162.

13. J.R.Carrol,Jr.; Dispersion strengthened Al alloys,Ed. Y.W.Kim, The Mat.Soc.,Warrandale,Pa.(1987).

14. A.Mortensen, J.A.Cornie and M.C.Flemings ; Met.Trans.19A (1988) 709.

15. G.Elkabir, L.K.Rabenberg, C.Persad and H.L.Marcus,Scripta Met.,20 (1986) 1411.

16. A.L.Geiger and M.Jackson ; Adv.Mat.Process.,7 (1989) 23.

17. H.J.Rack ; Proc.6th ICCM. Elsevier Applied Sci.,London, (1987) 2.382.

18. W.H.Hunt,Jr.,C.R.Cook,K.P.Amanie and T.B.Gurganus ; Powd. Met.Comp.,Ed.P.Kumar, A.Ritter, and K.Vedula ;The Met.Soc. Warrendale,Pa.,(1987).

19. H.J.Rack ; Dispersion Strengthened Al alloys, Ed.Y.M.Kim and W.Griffith, The Mat.Soc.,Warrendale,Pa. (1988) 649.

20. S.Krishnamurthy, Y.W.Kim, G.Das and F.H.Froes ; Metal-ceramic matrix composites, Ed. R.B.Bhagat, A.H.Claver, P.Kumar and A.M.Ritter ; The Min.Metals and Mater.Soc., Warrendale, Pa. (1990) 145.

21. C.Persad, S.Ranganathan, B.H.Lee, D.L.Bourell, Z.Eliezr and H.L.Marcus ; Mater.Res.Soc.Sym.Proc.120 (1988) 23.

22. T.C.Willis ; Metals and Materials, 4 (1988) 485.

23. J.White, I.G.Palmer, I.R.Hughes and S.A.Court ;Al-Li alloys, Ed.T.H.Sanders.Jr. and E.A.Starke.Jr.,MCE Pub. Williamsburg,VA (1989) 1635.

24. M.Gupta, F.A.Mohamed and E.J.Lavernia ; Mater.Manuf. Process, 5 (1990) 165.

25. B.P.Krishnan, N.Raman, K.Narayanaswamy and P.K.Rohatgi; Wear 60 (1980) 205.

26. P.K.Rohatgi, N.Murali, H.H.Shetty and R.Chandrasekhar; Mat.Sci.Eng. 26 (1976) 115.

27. M.K.Surappa, N.Seshan and P.K.Rohatgi; Pro.All Ind.Sem. on Al Metallurgy 46 (1978) 1.

28. V.Agarwala and D.Dixit; Tran.Ind.Inst.Metals 22 (1981) 521

29. A.R.E.Suiger; Int.J.Powd.Met. 21 (1985) 219

30. M.K.Surappa, S.V.Prasad and P.K.Rohatgi; Wear 77 (1982)295

31. K.J.Bhansali and R.Mehrabian; J.Met. 34 (1982) 30.

32. A.Sato and R.Mehrabian; Met.Trans. 7B (1976) 443.

33. R.Mehrabian, R.G.Reik and M.C.Fleminge; Met.Trans.5 (1974) 1899-1905.

34. M.K.Surappa and P.K.Rohatgi; J.Mat.Sci. 16 (1981) 983-993.

35. F.A.Girot, J.M.Quinisset and R.Naslain; Comp.Sci.& Tech. 30 (1987) 155-184.

36. F.M.Hosking, F.F.Portillo, W.Wundewrlin and R.Mehrabian; J.Mat.Sci. 17 (1982) 477-498.

37. P.K.Ghosh and S.Ray; Ind.J.Tech. 26 (1988) 83-94.

38. A.A.Das and S.Chatterjee; Met.Mat.Tech. 13 (1981) 137.

39. P.K.Rohatgi, B.C.Pai and S.C.Panda; J.Mat.Sci. 14 (1979) 2277-2283.

40. A.Banerjee, M.K.Surappa and P.K.Rohatgi; Met.Trans. 14B (1983) 273.

41. A.Banerjee and P.K.Rohatgi; J.Mat.Sci. 17 (1982) 335-342.

42. P.K.Rohatgi, R.Asthana and S.Das; Int.Metals Review 31 (1986) 115.

43. M.Ruble and A.G.Evans ; Mater.Res.Symp.Proc.120 (1988)293.

44. T.Young; Phil.Trans.R.Soc. 95 (1805) 65.

45. F.Delannay, L.Froyen and A.Deruyttere; J.Mat.Sci. 22 (1987) 1-16.

46. K.V.Prabhakar and P.K.Rohatgi; Pro.Int.Symp.on the Quality Control and Role of Metal Sci. Delft, The Netherlands (1977) 215.

47. A.Mortensen and J.A.Cornie; Met.Trans. 18A (6) (1987) 1160-1163.

48. A.Banerjee, P.K.Rohatgi and W.Reif; Metall 38(7) 1984 656-661.

49. B.P.Krishnan, M.K.Surappa and P.K.Rohatgi; J.Mat.Sci. 16 (1981) 1209-1216.

50. M.F.Amateau; J.Comp.Mat. 10 (1976) 279.

51. A.G.Kulkarni et al; J.Mat.Sci. 14 (1979) 592.

52. B.C.Pai and P.K.Rohatgi; Mat.Sci.& Eng. 21 (1975) 161.

53. J.P.Rocher, J.M.Quinisset and R.Naslain; J.Mat.Sci.Lett. 4 (1985) 1527-1529.

54. A.Banerjee; MSc Thesis, Uni.Kerala, India (1982)

55. Y.Kimura et al; J.Mat.Sci. 19 (1984) 3107.

56. C.G.Levi, G.J.Abbaschian and R.Mehrabian; Met.Trans. 9A (1978) 697-711.

57. D.A.Mortimer and M.Nicholas; J.Mat.Sci. 5 (1970) 149.

58. A.D.Macquillan and M.L.Macquillan; Titanium, Butterworths, London (1956) 6.

59. A.R.Champion, W.H.Krueger, H.S.Hartmann and A.K.Dhingra; Proc.Int.Conf.on Comp.Mat. ICCM 2 AIME (1978) 883.

60 W.H.Hunt;Inter Faces in Metal Matrix Composites, Ed: A.K.Dhingra and S.G.Fisherman; Conf.Proc. New Orleans TMS-AIME (1986) 3-25.

61. B.P.Krishnan, M.K.Surappa and P.K.Rohatgi; J.Mat.Sci.16 (1981) 1209-1216.

62. Y.V.Naidich and G.A.Kolesnichenko; Soviet Powd.Met.& Metal Ceramics, 1 (19) (1964) 191.

63. F.A.Badia and P.K.Rohatgi; Trans.AFS.77 (1969) 402.

64. M.K.Surappa and P.K.Rohatgi; Met.Tech. 7 (1980) 378.

65. R.J.O'Malley, C.E.Dremann and D.Apelian; J.Metals, 31 (2) (1979) 14.

66. Deonath, R.T.Bhat and P.K.Rohatgi; J.Mat.Sci.15(5) (1980) 1241.

67. P.K.Rohatgi, B.C.Pai and S.C.Panda; J.Mat.Sci.14(1979)227.

68. B.F.Quigley, G.J.Abbaschian,R.Wunderlin and R.Mehrabian; Met.Trans.13A (1982) 93.

69. B.C.Pai, S.Ray, K.V.Prabhakar and P.K.Rohatgi; Mat.Sci.& Eng. 24 (1) (1976) 31.

70. B.C.Pai and P.K.Rohatgi; J.Mat.Sci. 13 (1979) 329.

71. J.Sugishita, S.Fujiyoshi and T.Imura; Wear, 81 (1982) 209

72. D.M.Karpinos, P.M.Asakarov and O.V.Abramov; Sov.Powd.Met. & Ceramics, 21 (3) (1982) 213.

73. S.Biswas, V.Sreenivasa, S.Seshan and P.K.Rohatgi; Trans. AFS. 88 (1980) 71.

74. M.K.Surappa and P.K.Rohatgi; Met.Trans.12B (1981) 327.

75. Deonath and P.K.Rohatgi; J.Mat.Sci.15(11) (1980) 2777.

76. M.K.Surappa and P.K.Rohatgi; Met.Tech.7 (1980) 378.

77. M.C.Flemings, R.G.Reik and K.P.Young; Mat.Sci.& Eng. 25 (1976) 103.

78. B.P.Krishnan, H.R.Shetty and P.K.Rohatgi; Trans.AFS. 84 (1976) 73.

79. Deonath and P.K.Rohatgi; J.Comp. 12(2) (1981) 124.

80. B.Zanfout, A.A.Das and J.R.Franklin; Metallurgy of light alloys, Inst.Metallurgists,London, (1983) 215.

81. D.G.Gdelderloos and K.R.Karsek; J.Mat.Sci.Lett.3(3) (1984) 232.

82.F.A.Girot, L.Albingre, J.M.Quinisset and R.Naslain;
   J.Metals,(Nov.1987) 18-21.

83.F.A.Badia, D.F.McDonald and J.R.Pearson; Trans.AFS.
   79-(1971) 269.

84.A.M.Patton; J.Inst.Metals, 100 (1972) 197.

85.M.K.Surappa and P.K.Rohatgi; Met.Tech.5 (1978) 358.

86.B.P.Krishnan, H.R.Shetty and P.K.Rohatgi; Trans.AFS.
   84 (1976) 73.

87.R.T.Pepper and R.A.Penty; J.Comp.Mat.8 (Jan.1974) 29-37

88.M.H.Richman, A.P.Levitt and E.S.Dicessare; Metallography
   6 (1973) 497.
89.E.F.Fascetta, R.G.Riek, R.Mehrabian and M.C.flemings ;
   Trans.AFS, 81, (1973) 81.

90.A.Sato and R.Mehrabian; Met.Trans.7B (1976) 443.

91.C.G.Levi, G.J.Abbaschian and R.Mehrabian; "Rheocasting"
   Ed: R.D.Frenels and F.S.Modi; Columbs,Ohio (1979)

92.B.Kujur, A.K.Roy, C.B.Raju and M.Patel; J.Mat.Sci.
   22 (1987) 962-964.

93.T.P.Murali, M.K.Surappa and P.K.Rohatgi; Met.Trans.
   13B (1982) 485.

94.M.C.Flemings; Solidification Processing,McGraw Hill(1974).

95.Y.Abe, M.Nakatani, K.Yamatsuta and S.Horikiri;
   "Developments in the Sci.Tech.Of Comp.Mat.ECCM I.
   Bordeaux,France (Sept.1985) 604-609.

96.L.J.Masur, A.Mortensen, J.A.Cornie and M.C.Flemings;
   Pro.6th Int.Conf.Comp.Mat. Ed:Elsevier Applied Sci.
   London,(1987) 2320-2329.

97.K.C.Russel, J.A.Cornie and S.Y.Oh; Interfaces in Metal
   Matrix Comp.Ed: A.K.Dhingre and S.G.Fisherman; Conf.Proc.
   New Orleans,(1986) 61-91.

98.N.I.Abdul Lateef, A.Razaq, I.Khedar and S.K.Goel;
   J.Mat,Sci. 22 (1987) 466-472.

99.M.A.Bayoumi and M.Suery; Proc.6th Int.Conf.Comp.Mat.
   Ed: Elsevier Applied Sci. London,(1987) 2481-2490.

100.A.R.T.deSilva and G.A.Chadvick; J.Mech.Phy.& Solids,
    17 (1969) 387-403.

101. J.K.Lee, Y.Y.Eaemme, H.I.Aaronson and K.C.Russel;
     Met.Trans. 11 A (1980) 1837-1847.

102. H.P.Cheskis and R.W.Heckel; Met.Trans.1 (1970) 1931-1942.

103. R.W.Heckel,   R.J.Zaehring and H.P Cheskis; Met.Trans.
     3 (1972) 2507-2513.

104. M.Vogelsang, R.J.Arsenault and R.M.Fisher; Met.Trans.
     17 A (1985) 379.

105. R.J.Arsenault; Mat.Sci.& Eng. 64 (1984) 171.

106. R.J.Arsenault and R.M.Fisher; Scripta Metallurgica,
     17 (1983) 67-71.

107. Y.Flom and R.J.Arsenault; Mat.Sci.& Eng. 75 (1985) 161-167

108. J.T.Hartman, K.H.Keene, R.J.Armstrong and A.Wolfenden;
     J.Metals, (April1986) 33-35.

109. J.C.Williams and G.Garmong; Met.Trans.6A (1975) 1699-1709

110. T.Imai, Y.Nishiida, M.Yamada, H.Matsubara and I Shirayangi
     J.Mat.Sci.Lett.6 (1987) 343-345.

111. J.Dinwoodie, E.Moore, C.Langman and W.R.Symes; Proc.ICCM V
     Met.Soc.AIME,(1985) 671-685.

112. G,B,Kenbergs; J.Australian Metals,4 (1969) 236-241.

113. B.F.Quickley, G.J.Abbschian, R.Wunderlin and R.Mehrabian;
     Met.Trans. 13 A (1982) 93-100.

114. T.W Clyne, M.G.Bader, G.R.Cappelman and P.A.Hubert;
     J.Mat.Sci. 20 (1985) 85-96.

115. D.Webster; Met.Trans. 13 A (1982) 1511-1519.

116. D.L.McDanels; Met.Trans.16 A (1985) 1105-1115.

117. J.A.Papazian and P.N.Adler, Met.Trans.A,21A (1990)401-410.

118. T.F.Klimowicz and K.S.Vecchio,,"Fundamental Relationship
     between Microstructure and Mechanical Properties of MMC,
     Ed. M.N.Gungor and P.K.Liaw, TMS Pub.,USA (1990) 255-267.

119. M.Manoharan and J.J.Lewandowski, Acta Met.38(1990)489-496.

120. J.A.Papazian,Met.Trans.A, 19A(1988) 2945-53.

121. A.H.Nakagawa and M.N.Gungor, as in Ref.97. 127-144.

122. T.E.Johnson and T.D.Selnaesi, abid, 557-580.

123. D.L.McDanel, Mat.Trans.A, 16A(1985) 1105-15.

124. H.M.Ledbetter and M.W.Austin,Mat.Sci.Engg.,89(1987)53-61.

125. W.J.Clegg, Acta Met.,36 (1988) 2141-49.

126. A.P.Divecha, S.G.Fishman and J.Foltz; SAMPE,2 (1979) 1433-1450.

127. B.Zantout, A.A.Das and J.R.Franklin; Inst.Metallurgists, 20 (1983) 215-221.

128. I.Dutta, C.F.Tiedemann and T.R.McNelley, Scripta Met. 24 (1990) 1233-38.

129. A.Banerjee, S.V.Prasad, M.K.Surappa and P.K.Rohatgi; Wear, 82 (1982) 141-151.

130. U.T.S.Pillai,R.K.Pandey and K.D.P.Nigam; Proc.ICCM V Met.Soc.AIME (1985) 895-911.

131. C.R.Crowe, R.A.Gray and D.F.Hasson; abid, 843-865.

132. D.Webster; Proc,ICCM III,Pergamon Pres,France,(1980) 1165-1170.

133. A.P.Divecha, C.R.Crowe and S.G.Fishman; Failure Modes in Comp,IV, AIME (1978) 406-417.

134. A.P.Divecha, S.G.Fishman and S.D.Karamkar; J.Metals,9 (1981) 12-17.

135. D.F.Hasson, S.M.Hoover and C.R.Crowe; J.Mat.Sci.,20 (1985) 4147-4154.

136. L.Ackwemnn, J.Charbonnier, G.Desplanches and H. Koslowski; Proc. ICCM V, Met.Soc.AIME(1985) 671-685.
137. R.G.Schierding and O.Des Deex; J.Comp.Mat. 3 (1969) 619-629.

138. R.L.Mehan; J.Comp.Mat.4 (1970) 90-101.

139. H.J.Rack, T.R.Baruch and J.L.Cook; Proc.ICCM IV, Japan Soc.Comp.Mat.(1982) 1465-1472.

140. M.Y.Wu and O.D.Sherby; Scripta Metallurgica, 18 (1984) 773-776.

141. D.Webster; SAMPE; 2 (1979) 1433-50.

142. J.T.Staley; Mat.Eng.Quart. 16 (1976) 8.

143. S.J.Ceislak, R.M.Hart, P.L.Mehr and L.N.Mueller; Proc.17th Int.Tech.Conf.New York (1985).

110

144. K.R.Van Horn; Aluminium, Vol.1, ASM, Ohio (1967).

145. P.K.Balasubramanian and B.K.Sarkar; Trans.Ind.Inst.Metals 32 (1979) 170-171.

146. P.K.Balasubramanian; Mat.Sci.&Tech. 1 (1985) 470-474.

147. H.Kambe and P.D.Garm; Thermal Analysis - Comparative Studies on Materials, Halsted Press; Tokyo (1974) 51.

148. Metals Handbook; 10th Edn., Vol.II, ASM, Ohio, (1990).

149. Handbook of Lattice spacings and structure of metals and alloys, Ed: W.B.Pearson, Pergamon Press; 2 (1967) 486.

150. Handbook of Materials and Techniques for Vacuum devices, Ed; W.H.Kohl, Reinhold Publishing Co (1967) 69.

151. Materials Data book, Ed: E.R.Parker, McGraw Hill Book Co. New York (1967) 263.

152. Materials Hand book, Ed: George S.Brady, McGraw Hill Book Co., New York (1971) 816.

153. Encyclopedia of Minerals, Ed: Willard Lincoln Roberts et al, Van Nostrand Reinhold Co., New York (1974) 21.

154. Titanium, Ed: A.D.McQuillan and M.K.McQuillan, Butterworth Scientific Publication, London, (1956), 252.

155. P.K.Joy and Gopalakrishnan, Tranvancore Titanium Products India (Private Communication) (1988).

156. D.S.Robert and A.P Joseph,J.Amer.Cer.Soc.48(1965)391-398.

157. INDAL, Alupuram, Inspection Report No.1075/86. (1986).

158. INDAL, (Private Communication) 1987.

159. INDAL DATA SHEET (1976).

160. R.M.Pillai et al; Proc. of Indo-US Workshop on Solidification and Processing of Materials, DMRL, Hyderabad, India, Ed: R.K.Trivedi, Transtech Publications (1988).

161. P.K.Balasubramanian and B.K.Sarkar ; Trans.IIM,30,No.3, (1977) 172.

162. O.Kubaschewski and C.B.Alcock, Metallurgical Thermochemistry, Pergamon Press, Oxford, 42 (1979) 267-386.

163. B.Fredenberg and A.Mocellin, J.Am.Ce.Soc. 71(1988) 22.

111

164.Comprehensive Inorganic Chemistry,Vol.1,Ed.A.F.trotman-Dickenson ; Pergamon Press,Oxford,(1973) 651.

165.B.C.Pai, B.N.Kesavaram, K.Sukumaran, S.G.K.Pillai and K.G.Sathyanarayana; Proc.Conf. High Strength Aluminium Alloys for Defence and Industry, R&D Engineers, Pune (1984).

166.R.S.Haaland, G.M.Michal and G.S.Chottiner, abid,779-791.

167.M.Taya, K.E.Lulay and D.J.Llyod ; Acta Met. 39, No.1 (1991) 73.

168.Larry M.Morris ; Dispersion strengthening of Al alloys, Ed.Y.W.Kim and W.Griffith,The Minerals, Metals and Mater. Soc.Warrendale,Pa. (1988) 397.

169.N.Blake and M.A.Hopkins ; J.Mat.Sci.20 (1985) 2861.

170.R.J.Arsenault and R.M.Fisher,Scripta Met. 17 (1983) 67.

171.I.J.Polmear, Metallurgy of light metals, Edward Arnold London, (1989) 72.

172.W.S.Miller and F.J.Humphrey, abid, 517-541.

173.J.D.Eshelby ; Proc.Roy.Soc. A 241,(1957) 376.

174.R.J.Arsenault and M.Taya ; Acta Met.35 (1987) 651.

175.A.R.E.Singer; Int.J.Powd.met; 21(3)(1985) 219.

176.T.G.Nich and D.J.Chellman, Scripta Met; 18(1984) 925-928.

177.B.Sartor, H.Staats and H.J.Seeman; Metall. 28(8) (1974) 771.

178.P.K.Rohatgi, Unpublished work (1984).

179.P.Niskanen and W.R.Mohn; Adv.Mat.and Proc. Metal Progress; 133 (1988) 39.

180.Aluminium Standards and Data, ASM,(1972-73).

181.Al alloys-Gen.Properties data ; Cegedur Pechiney,T.01B France (1979).

182.Powder Diffraction File-Inorgarnic, from Micro Fiche Housing Frame, MP 138-32-1 Muscatine, Iowa.

===

ANNEXURES

ANALYSIS OF TIO$_2$ IN ALUMINIUM ALLOY MATRIX COMPOSITE MATERIAL

Solutions required:

(1) Acid mixture: H$_2$SO$_4$ (18.9 ml) + HNO$_3$ (30 ml) + HCl (30 ml) + H20 (70 ml).

(2) 26 to 30% NaOH solution.

(3) HNO$_3$ + HCl mixture 1:2

(4) NaOH (5%)

(5) HCl (5%)

Flow Diagram of Treatment

Acid treatment » residue treatment » Washing treatment.

Procedure

1. Acid Treatment

Weigh 10 gm of Al+TiO$_2$ chips and dissolve in the acid mixture. Dissolution of these chips evolves moderate amount of heat and hence it should be added slowly and carefully to the acid mixture. Entire Al matrix alone will be dissolved in the acid mixture whereas, TiO$_2$ powder will be precipitated at the bottom of the beaker. Since the precipitates would be very fine, filter the precipitate using the finest filter paper available.

2. Residue Treatment

Treat the precipitate with 10 ml of 25 to 30% NaOH solution followed by addition of HNO$_3$ + HCl mixture 1:2 (This facilitates removal of silicon precipitate along with the TiO2 by the formation of monometric silicic acid).

113

3. Washing Treatment

The final step in this analysis is the washing treatment. Wash the filter paper along with the residue successively with:

> (a) Water
> (b) NaOH - 5%
> (c) Water
> (d) HCl - 5%

Weigh the residue.

CALCULATIONS

$$\text{The percentage of } TiO_2 \text{ powder in the Composite} = \frac{\text{Weight of residue}}{\text{Weight of sample}} \times 100$$

If any precipitate sticks to the filter paper which causes difficulty in removing the residue for weighing, heat the filter paper in weighed crucible until no residue of the filter paper is left behind.

$$\text{Weight of the precipitate} = (\text{Weight of the crucible with precipitate}) - (\text{Weight of the crucible})$$

In the present investigation, precipitates were filtered out through whatman make filter paper of grade 41. The precipitates along with the filter were then ignited at 1173K for 2 hours which ensured complete absence of residue from filter paper. The powder weight was then measured. The weight of the residue is reported as 4.7% .

114

X-RAY DIFFRACTION STUDIES

Unit	:	Philips X-Ray generator PW 1729 with vertical goniometer.
		Philips diffractometer control PW 1710. Holland make.
Facility	:	Metallography facility, Materials Testing and Energy Systems Division, Metallurgy and Materials Group, VSSC.
Samples	:	1. TiO_2 powder procured from M/s. Travancore Titanium Products Ltd., Trivandrum.

Experimental	:	Radiation	:	Cu Kα with Ni filter.
Details	:	Accelerating Voltage	:	35 KV
		Tube current	:	20 mA.

Programme Details	:	(Starting angle) SAN	:	10°
		(Speed of goniometer) SPE	:	0.05°/min.
		(Recorder speed) RSP	:	10°/min.
		(Recorder full scale) RFS	:	1 E 3 (1000)
		(Recorder time constant) RTC	:	5
		(Recording time interval) INT - Seconds	:	6
		(Continuous scanning programme with scanning range 10° to 90°) CSP	:	80

Process

Compacted powder was taken in a nylon specimen holder and Cu-Kα radiation of wave length = 1.54 A was applied on to the sample, using a nickel filter. Ni filter filters out Kα radiations. A diffractogram of intensity Vs characteristic of the constituents of the sample is obtained on the recorder. The diffractogram and the diffraction analysis

115

giving details of incident angle, d spacing and intensity are printed out by the recorder. These values are compared with standard JCPDS (182) data (Joint committee of powder diffraction system) for the possible sample identification.

The possible chemical compounds which have been screened for the diffraction analysis are listed below:

Al_2TiO_5 $MgTi_2O_5$ $MgTi_2O_4$ $MgTiO_3$

Mg_2TiO_4 $ZnTiO_3$ $Zn_2Ti_3O_8$ Zn_2TiO_4

$ZnTiO_3$ $ZrTiO_4$ Fe_2TiO_4 $Fe_3Ti_3O_9$

$FeTi_4O$ $Fe_2(TiO_4)3$ $Fe_2(TiO_3)3$ Fe_5TiO_8

Mn_2TiO_4 $Fe_2MgTi_3O_{10}$ $(FeMg)Ti_2O_5$ $FeMgTi_4O_{10}$

$Mg_2Al_6Ti_7O_{25}$ $Mg_3Al_4Ti_3O_{25}$ $Mg_4Al_2Ti_9O_{25}$ $MgAl_8Ti_6O_{25}$

$MgAl_2Ti_3O_{10}$ $(ZnMnFe)(TiFe)O$ Ti_2O_3, TiO_2, Mgo, Al_2O_3

$2MgOTiO_2$ $Al_2O_3TiO_2$

The diffractogram of the TiO_2 powder (both calcined stock and milled stock) is shown in figures A1 to A4 and the corresponding comparison of data with JCPDS values are given in AT-1.

TiO_2 has a tetragonal crystal structure and the lattice parameters are calculated using the formula for tetragonal structure as given below:

$$\frac{1}{d^2} = \frac{h^2 + k^2}{a^2} + \frac{l^2}{c^2} \qquad ------ \qquad (1A)$$

substituting the values of d, h, k and l in the above said equation, the lattice constants a and c for TiO_2 (anatase grade) are calculated. Considering the hkl plane (200),

116

TABLE-AT I.

Diffraction Data (TiO_2)

Peak No.	Incident Angle	d Value	Intensity Count	JCPDS DATA d Value	I/I_1	(hkl) Value

Calcined TiO_2 Anatase Grade

Peak No.	Incident Angle	d Value	Intensity Count	d Value	I/I_1	(hkl) Value
1	29.430	3.52	1627	3.52	100	(101)
2	43.719	2.40	137	2.43	10	(103)
3	44.270	2.38	287	2.38	20	(004)
4	45.166	2.33	138	2.33	10	(112)
5	56.417	1.89	599	1.89	35	(200)
6	63.463	1.70	324	1.70	20	(105)
7	65.048	1.67	310	1.67	20	(211)

Milled TiO_2 Anatase Grade

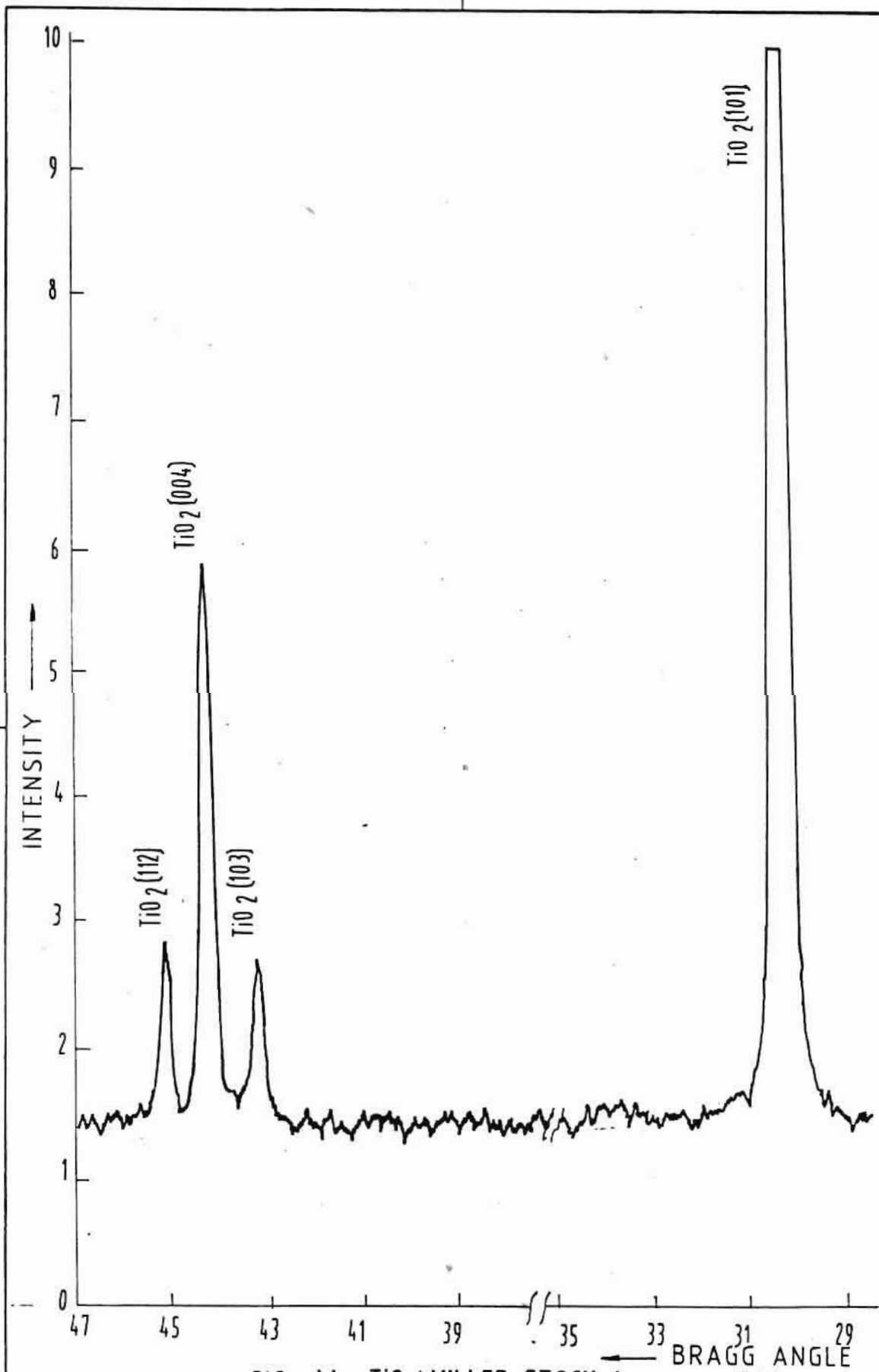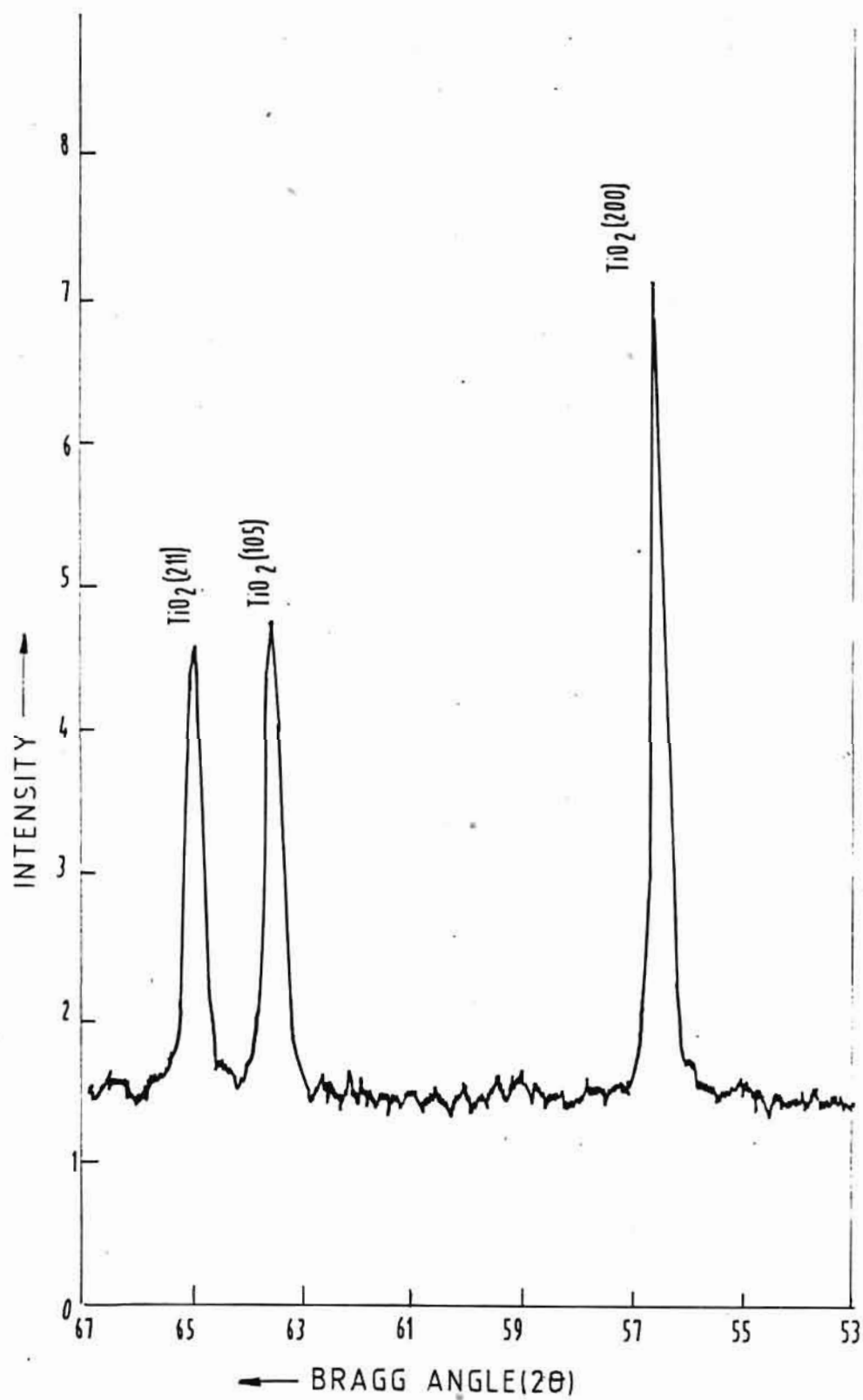| Peak No.	Incident Angle	d Value	Intensity Count	d Value	I/I_1	(hkl) Value
1	29.619	3.50	2117	3.52	100	(101)
2	43.242	2.43	156	2.43	10	(103)
3	44.353	2.37	452	2.38	20	(004)
4	56.596	1.89	595	1.89	35	(200)
5	63.634	1.70	416	1.70	20	(105)
6	65.106	1.66	383	1.67	20	(211)

FIG. A1. TiO₂ MILLED STOCK-1
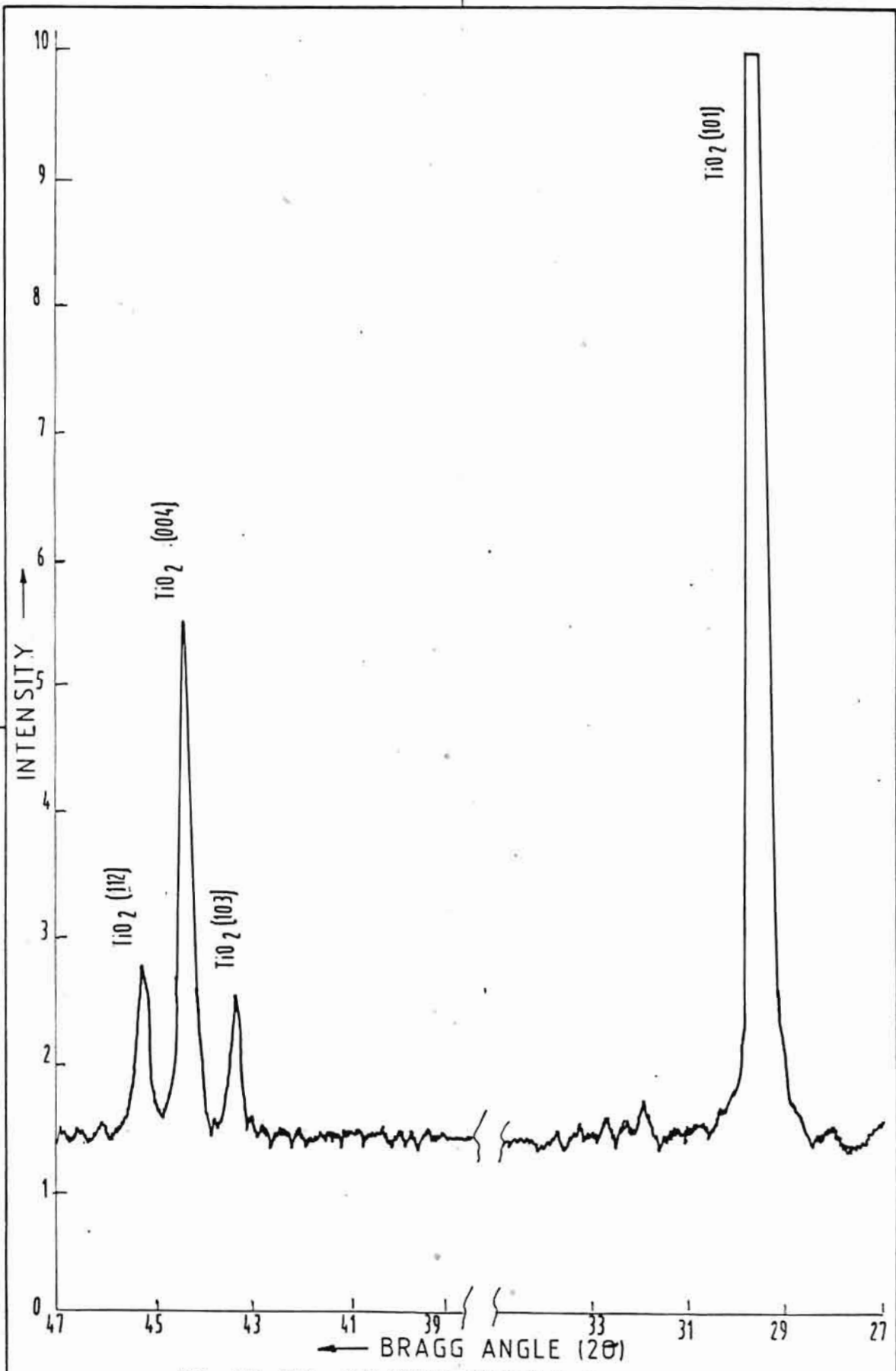(XRD DATA)

FIG. A2. TiO₂ MILLED STOCK -2
(XRD DATA)

FIG. A3. TiO₂ CALCINED STOCK-1 (XRD DATA)
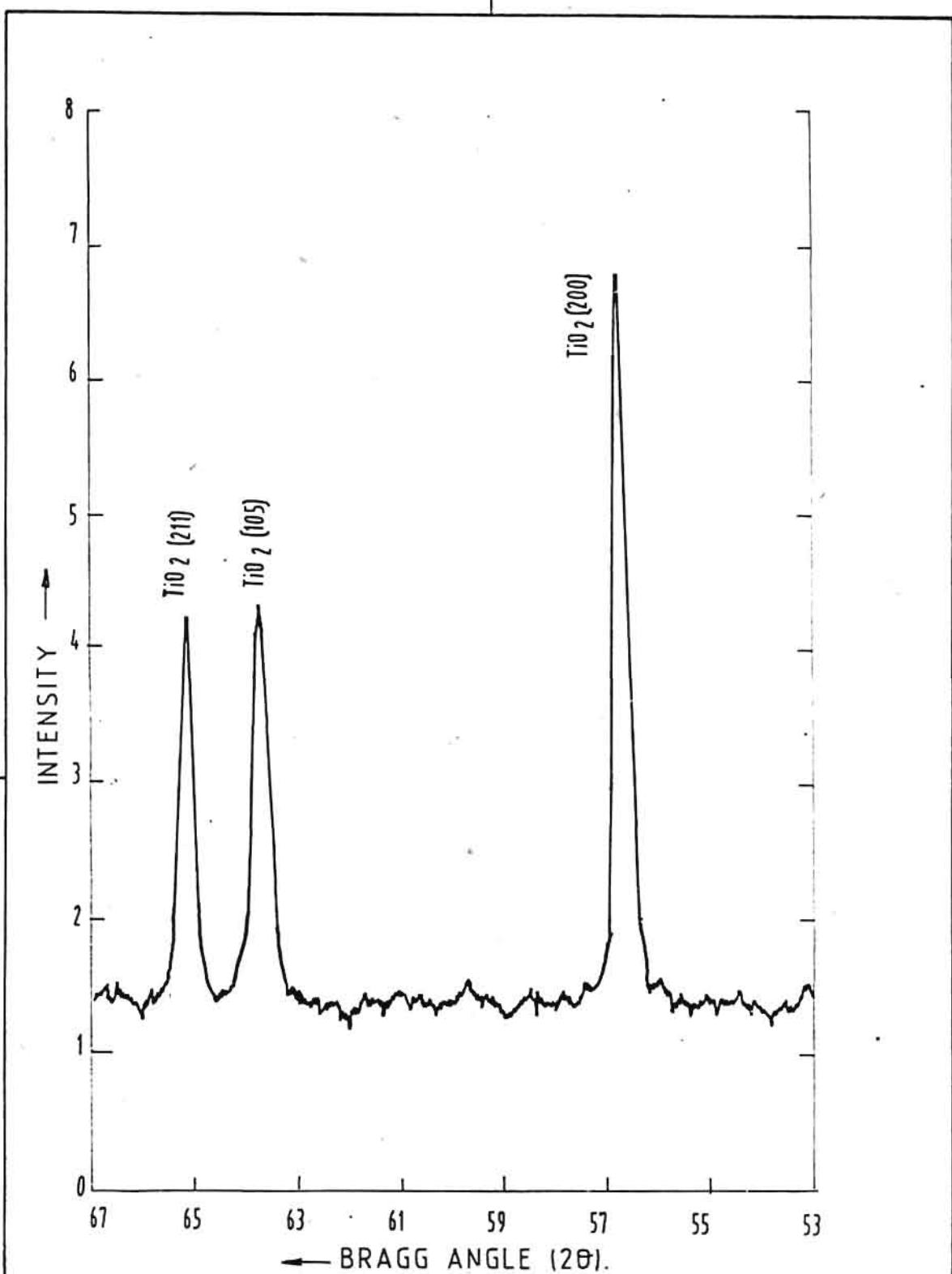
FIG. A4. Ti O₂ CALCINED STOCK-2
(XRD DATA)

values of "a" is calculated using the following values:

d = 1.89,   h = 2,   K = 0 and   l = 0

The value of 'a' is calculated as 3.78 against the JCPDS value of 3.7852 for the anatase grade.

Considering the 'a' value as 3.78 and using other hkl values, 'C' value has been calculated and shown below:

hkl	'C' Value	'C' Average	JCPDS Values
(004)	9.520	9.5153	9.5139
(112)	9.509		
(105)	9.517		

The lattice constants thus confirms the anatase grade for the TiO2 powder.

The diffractogram of the extracted powder from the composite is shown in figures A5 to A7. The corresponding comparison of data with JCPDS values is given in Table AT-2.

From the Table, it is observed that the extracted powder contains only TiO_2 and $MgTi_2O_5$. The crystal structure for TiO_2 is tetragonal and the lattice constants are calculated from the same equation viz. equation (1A).

Considering the 'd' values for (hkl) planes (110), (200) and (210), the average 'a' value has been calculated. Substituting the value of 'a' for (hkl) planes (211), (002), (221) and (202), the average value of 'C' has been calculated. The results are shown below:
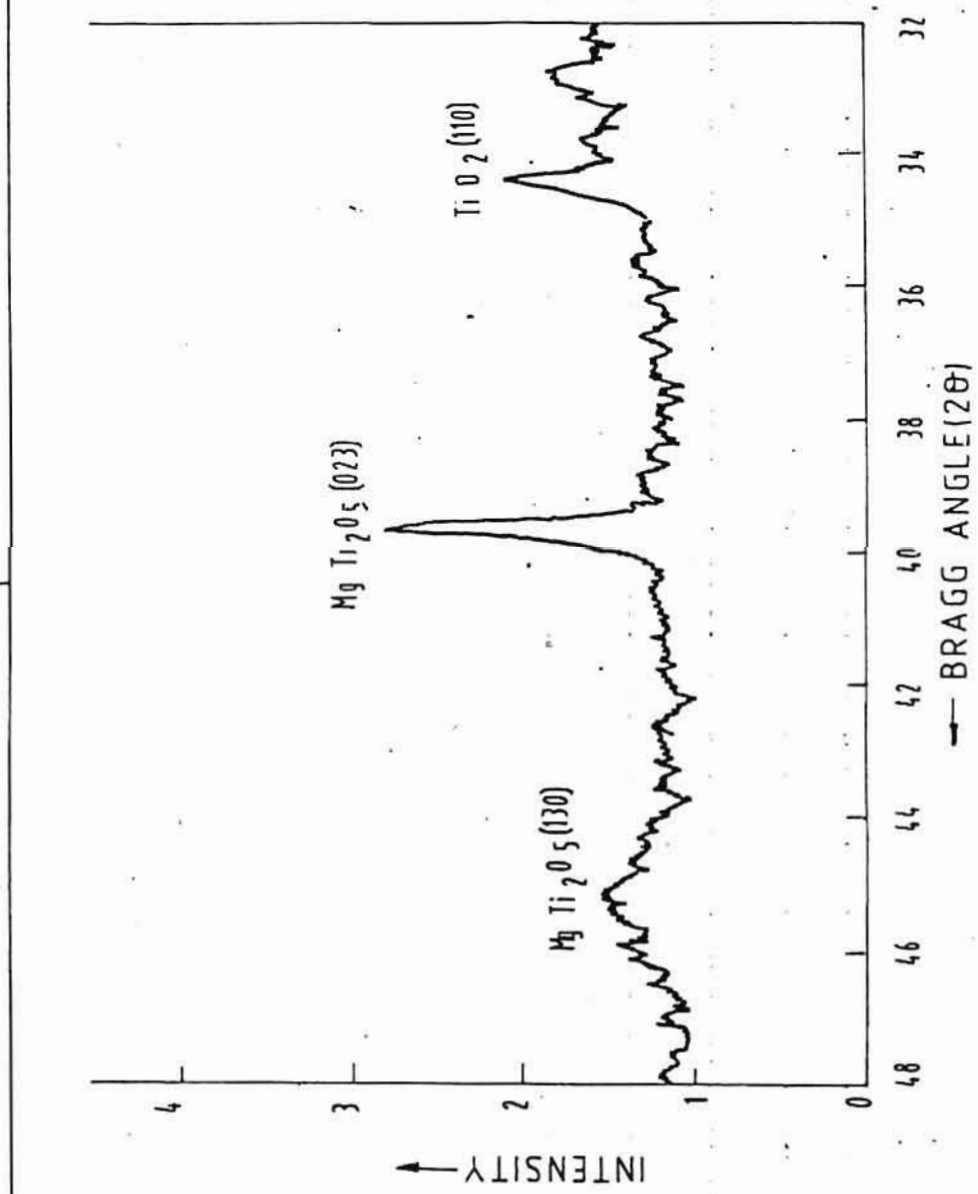
117

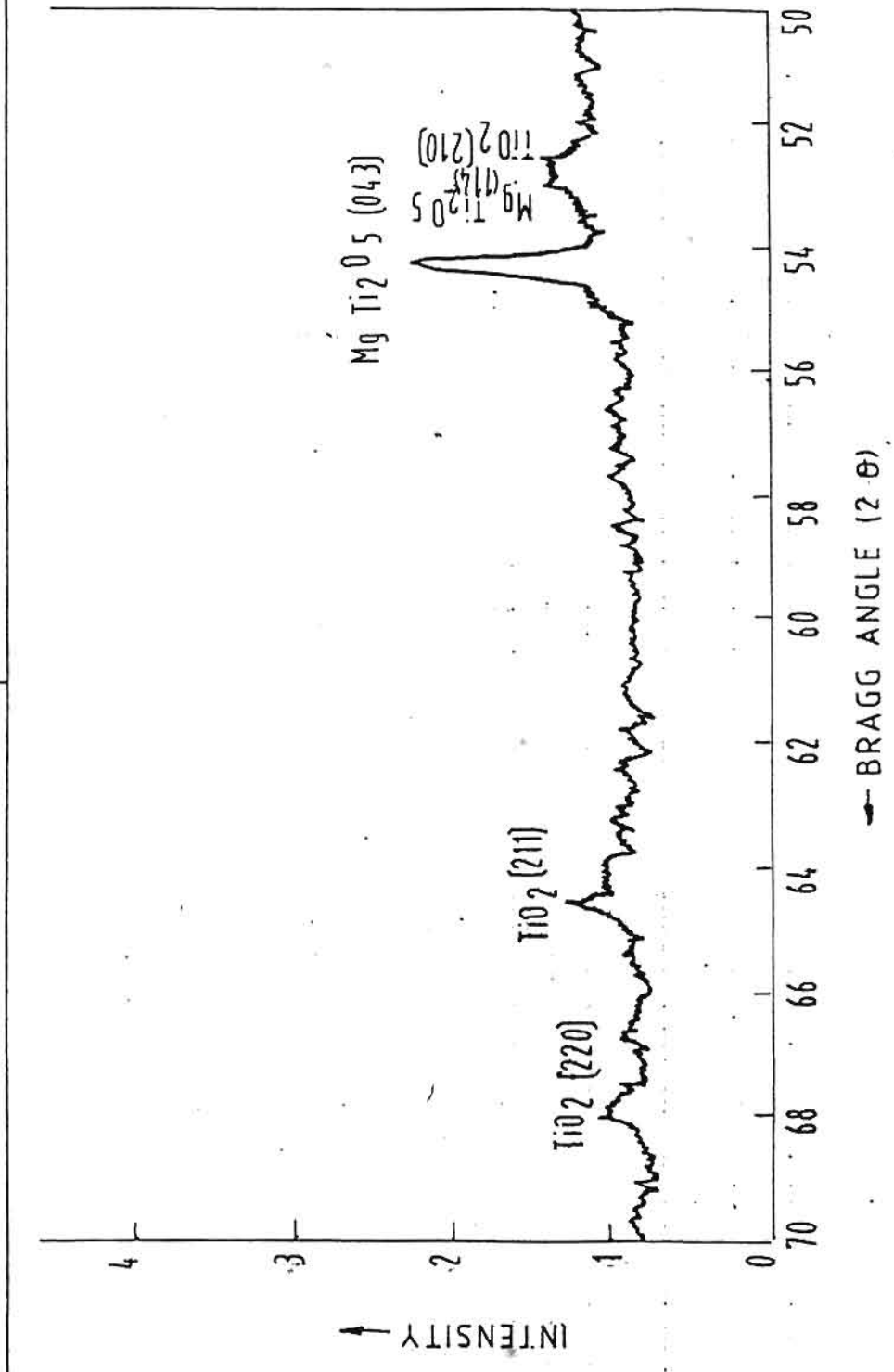FIG. A5. EXTRACTED PARTICLE-1 (XRD DATA)
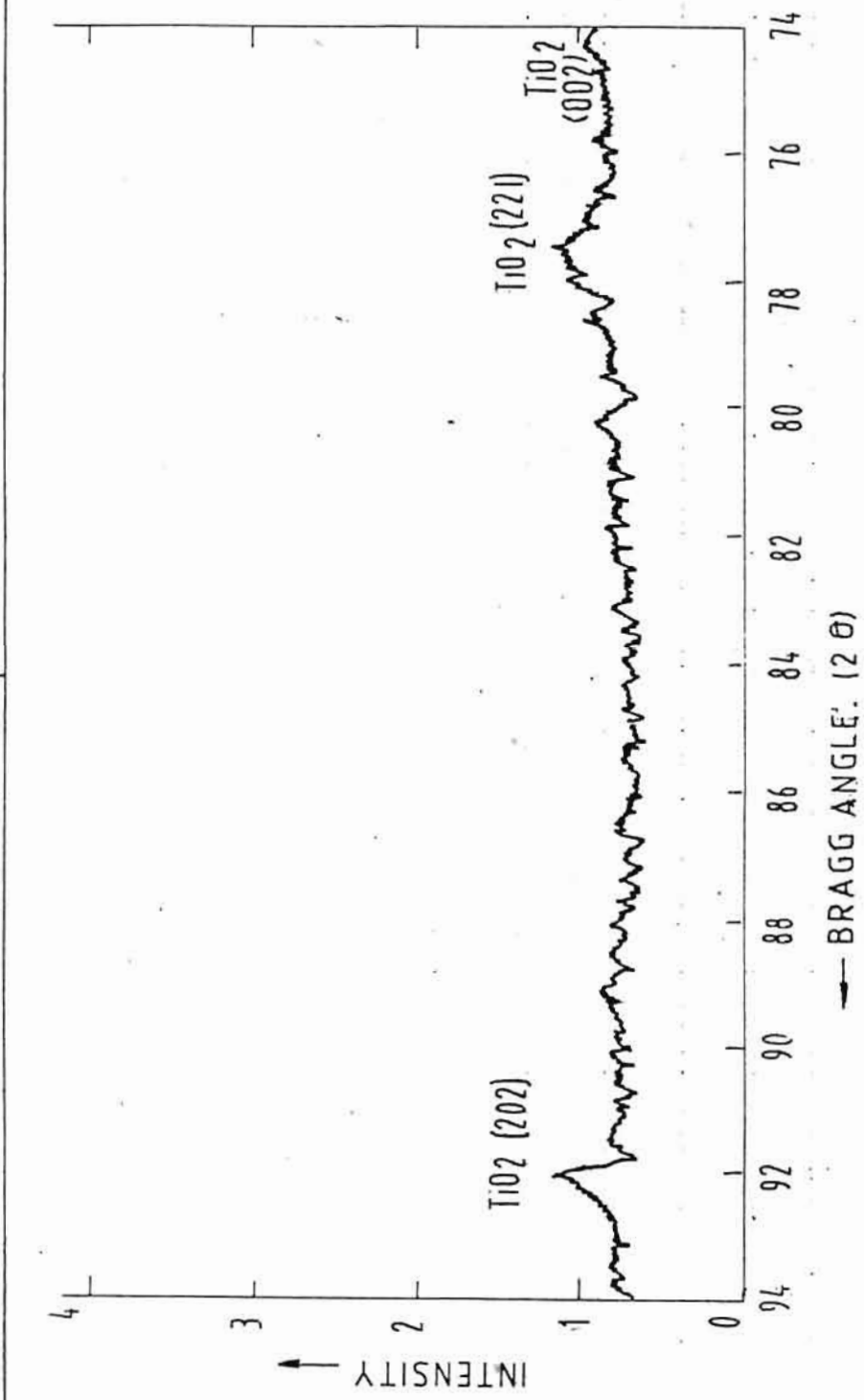
FIG. A6. EXTRACTED PARTICLE-2 (XRD DATA)

FIG. A 7. EXTRACTED PARTICLES -3 (XRD DATA)

TABLE-AT 11

Diffraction Data (Extracted Powder)

Peak No	Incident Angle	d Value	Intensity Count	<------ JCPDS d Value	DATA-----> (hkl)	Compound
1	32.189	3.2288	145	3.25	(110)	TiO2
2	37.588	2.7784	232	2.75	(023)	MgTi2O5
3	43.125	2.4355	128	2.45	(130)	MgTi2O5
4	46.150	2.2838	114	2.297	(200)	TiO2
5	52.683	2.0173	116	2.05	(210)	TiO2
				2.03	(114)	MgTi2O5
6	54.149	1.9666	193	1.964	(043)	MgTi2O5
7	64.369	1.6805	91	1.6874	(211)	TiO2
8	67.912	1.6025	84	1.60	(061)	MgTi2O5
9	74.199	1.4839	75	1.4797	(002)	TiO2
10	77.632	1.4280	90	1.4243	(221)	TiO2
11	92.354	1.2406	79	1.2441	(202)	TiO2

Lattice Constant	Calculated Value (Average)	JCPDS Value for rutile grade
a	4.5639	4.5933
c	2.9589	2.9592

These lattice constants show that the TiO_2 in the extracted powder is rutile grade.

The crystal structure of $MgTi_2O_5$ is orthorhombic and the lattice constants are calculated from the equation:

$$\frac{1}{d^2} = \frac{h^2}{a^2} + \frac{K^2}{b^2} + \frac{l^2}{c^2} \quad ------ \quad (2A)$$

Using the 'd' values for the (hkl) planes (023), (043) and (061), the average value for 'b' is calculated. Using this value of 'b' for the plane (130), the value of 'a' is calculated and the value of 'c' is obtained by substituting for 'a' and 'b' in the equation for the plane (114). The lattice constants so calculated are given below as compared to the JCPDS values.

$MgTi_2O_5$ - Orthorhombic structure.

Lattice Constants	Calculated Values	JCPDS Value
a	3.6731	3.744
b	9.7255	9.736
c	9.9881	9.980

ANNEXURE 3

CALCULATIONS OF THEORETICAL PROPERTIES

Material	σ_{UTS} MPa	K cals/cm.s.K	Density(δ) gm/cc
Matrix alloy (7005)			
Heat treated :	350	0.29	2.78
Cold rolled :	440	0.29	2.78
TiO_2	56	0.009	4.24

TiO_2 addition   =   5 wt%

Base alloy   = 95 wt%

Volume of TiO_2 = 5/4.24 = 1.18

Volume of base alloy = 95/2.78 = 34.17

Total volume   = 35.35

Vol % of TiO_2 = 1.18/35.35 = 3.3

Vol % of base alloy = 34.17/35.35 = 96.9

Basic rule of mixture for composite = α_c = $\alpha_m V_m + \alpha_p \alpha_p$

where, α = any property

        c = composite, m = matrix, and p = particulate.

Accordingly,

σ_c (heat treated) = 340 MPa, σ_c (cold rolled) = 427 MPa

K_c = 0.28 cals/cm.S.K. and δ_c = 2.83 gm/cc.

119